Al-Farabi Kazakh National University

UDC: 539.17

NASSURLLA MAULEN

Effects of cluster structure of stable boron and lithium isotopes to form the outputs of nuclear reaction in the interaction with deuterium and helium isotopes

6D060500 Nuclear Physics

Thesis is submitted in fulfillment of the requirements for the degree of
Doctor of Philosophy (PhD)

Scientific Supervisers
Doctor of Phys.-Math. Sci.
Professor Burtebayev Nassurlla

Doctor of Phys.-Math. Sci.
Professor Suzuki Takeshi

Republic of Kazakhstan
Almaty, 2020

CONTENT

NORMATIVE REFERENCES

In this dissertation, references to the following standards are used:

SOSE RK 5.04.034-2011: State obligatory education standard of the Republic of Kazakhstan Postgraduate study. Doctoral. General provisions (changes dated of August 23, 2012 No. 1080);

Rules of awarding academic degrees dated31 March , 2011 No. 127;

Interstate standards: State StandardNo. 7.32-2001 (changes dated 2006);

State Standard No. 7.1-2003. Bibliographic record. Bibliographic description. General requirements and compilation rules.

DEFINITIONS

In this dissertation, the following terms with corresponding definitions are applied:

α - particle – helium atom nucleus

Deuteron – deuteride core

Detector – device for recording secondary nuclear radiation

Scattering Chamber – vacuum volume in which the irradiated substances and detectors recording secondary nuclear radiation are placed

Ligh nuclei – atomic nuclei with mass numbers from 4 to 40

Target – irradiated substance

Cross section – the probability of interaction of an incident particle with an atomic nucleus

Angular momentum – the moment of momentum of a particle in its interaction with the atomic nucleus

Ion accelerator – nuclear facility to increase ion energy to predetermined limits

DESIGNATIONS AND ABBREVIATIONS

INP – Institute for Nuclear Physics
OP – optical potential
FP – folding potential
l.c.s. – laboratory coordinate system
c.m.s. – center of mass system
OM – theory of the optical model
DF – double folding theory
DWM – theory of the distorted wave method
CCM – theory of the method of coupled channels
MDM – theory of the modified diffraction model
ANC – theory of the method of asymptotic normalization coefficients
IRP – theory of inelastic rainbow scattering model
NR – Nuclear Rainbow
ADC – amplitude-to-digital converter
M3Y – Michigan-three-Yukawa
PA – preamplifier
CS – coencidence scheme
MeV – Mega Electron Volt
LSC – large scattering chamber

INTRODUCTION

General description of work

The dissertation is devoted to experimental and theoretical studies of interaction processes of deuterons and α particles with ^{7}Li, ^{11}B nuclei at low energies.

Experimental studies of the interaction process in nuclear reactions using accelerator technology remain the main source of direct information on the structure of nuclei and the mechanism of nuclear reactions. In this case, a special place is occupied by the simplest process in nuclear dynamics - elastic scattering. The relatively large cross-sectional value and the degree of development of the theory of this mechanism make it possible to extract information fundamentally important for nuclear physics about the value of the effective interaction potential of colliding systems. Physically reliable values of the potential are necessary for calculating the yields of the products of nuclear reactions involving different types of particles in the input and output channels of the reactions. The most developed method for its search remains the phenomenological approach based on the analysis of experimental data on elastic scattering in the framework of the optical model (OM) of the nucleus [1]. The real part of the optical potential is essentially the potential of the middle field, reflecting the fundamental properties of the atomic nucleus.

Currently it has been established, that nucleon scattering by nuclei is fairly well described by an optical model with potentials, the real part of which has a depth of $V_0 \approx$ 30-50 MeV [2]. At the same time, in the case of scattering of complex particles, the parameters of the potential extracted in its framework are subject to significant ambiguities [2, p. 35; 3]. Despite the numerous attempts made by experimenters and theoreticians, the task of determining the interaction potential of composite particles with nuclei is far from complete and belongs to one of the urgent and open problems of nuclear physics.

The Summation of accumulated data on the interaction of complex particles (hydrogen, helium and heavy ions nuclides) with light nuclei at energies above 10 MeV/nucleon indicates that scattering cross sections in the full angular range form two mechanisms: potential scattering and exchange processes (to make the main contribution to the region large angles). In this case, the contribution of metabolic processes is directly related to the structure of interacting systems. A comprehensive examination of potential scattering with metabolic processes makes it possible to use the nature of the reaction cross section at large angles to study the effects of clustering in various states of nuclei and to study their structural features. Obviously, the most favorable objects of such a study are lithium and boron nuclei, which have a pronounced cluster structure.

At present, scattering of helium ions on ^{6}Li and ^{7}Li nuclei having a pronounced cluster structure has been systematically studied. The observed “anomalous” rise in the cross section at reverse angles can be described taking into account the contribution of the exchange mechanism of cluster transfer, which is physically indistinguishable from potential scattering. Therefore, taking into account this mechanism in a number of works [4–7] allowed us not only to obtain more reliable

parameters of optical potentials, but also to extract cluster spectroscopic factors values from the analysis of cross sections at large angles. In recent studies [8–11] on the scattering of ^{3}He and α particles, the values of spectroscopic factors were obtained for the configurations "*d*+α", "^{3}He+*t*", and "*t* +α" not only for the ground, but also for the excited states of the nuclei ^{6,7}Li, where the values of spectroscopic factors for the excited states turned out to be significantly smaller than their theoretical values. In addition, the spectroscopic factor for the "d + α" configuration, extracted from the binding to the experiment on scattering of α particles on ^{6}Li nuclei, was more than one It was shown that this is due to the fact that the transfer of the α-cluster in the elastic process can be realized in two ways: both through the "d + α" configurations and through the "np + α" configuration, which can take place in ^{6}Li nuclei. In the case of deuteron scattering on this nucleus, anomalous backscattering (ABS) can be formed only through the "d + α" configurations. A systematic analysis of deuteron scattering on ^{6}Li nuclei performed in [12, 13] for a wide energy range confirmed the possibility of describing the anomalous rise in the cross section at reciprocal angles due to the elastic exchange mechanism of the deuteron cluster taking into account the channel coupling with the spectroscopic factor for the configuration "d +α" of the nucleus ^{6}Li close to one.

An additional criterion for the reliability of the obtained spectroscopic factors for the "^{3}He + t" cluster configuration of the ^{6}Li nucleus can be the extraction of these quantities from an alternative approach, namely, from the transfer of the t - cluster in nuclear reactions.

For example, the reaction (d, t) on ^{7}Li nuclei was previously studied at energies of 12 MeV [14, 15], 15 MeV [16, 17], 18 MeV [18], 20 MeV [19], and 28 MeV [20]. Only at E_d = 12 MeV [15, p. 978] were measurements performed in the full range of angles. In other cases, they were carried out in the region of the front hemisphere. A significant increase in the cross section for the reaction (d, t) at 12 MeV could be explained by the exchange of the t - cluster. The standard method of distorted waves, with both zero and finite radius of interaction, used in calculating the angular distributions in [14, p.273; 15, p. 978], does not describe experimental cross sections at large angles. At other energies (15, 20, 28 MeV), only a qualitative analysis was carried out based on the approximation of a plane wave [16, p. 1249; 19, p. 408; 20, p. 1059]. The values of spectroscopic factors were not extracted.

Of no less interest is the study of elastic and inelastic scattering of α particles and deuterons on ^{11}B nuclei [21]. This is due to the presence of "α-α-t" cluster structure of this nucleus. The study of the states of the ^{11}B nucleus, where both the cluster configuration (2α+t) and the structure of the shell model can coexist is useful for determining the characteristics of excited neutron halo states of a given nucleus. Indeed, it was suggested in a number of works that low-lying ^{11}B states mainly have a shell structure, while cluster structures are well traced in states with negative parity above or near the threshold of collapse into clusters [22–25]. In addition, in recent experiments on resonance scattering on ^{7}Li nuclei [26], a new band of negative parity was confirmed, which includes the following excited states: 8.56 MeV ($3/2^-$), 10.34 MeV ($5/2^-$), 11.59 ($7/2^-$) and 13.03 MeV ($9/2^-$).Since these states have large alpha

decay widths, this band can be formed on the basis of cluster structures. In addition, the analogy of the cluster structure of the ^{11}B nucleus with the three ^{12}C cluster structure is a fascinating task to study. In particular, in [24, p. 024302; 27], it was suggested that the $3/2^-_3$ state can have a structure consisting of three clusters in the form of the 2α+t configuration, and can be an analogue of the ^{12}C excited state with spin 0^+_2, which has a structure consisting of 3 alpha particles [28-30]. Nevertheless, in [25, p. 064315], it was suggested that the 8.56 MeV ($3/2^-$) state cannot correspond to the ^{12}C (0^+_2) state. The analogy between 8.56 MeV ($3/2^-$) and ^{12}C (0^+_2) is controversial and requires further study of this problem.

Therefore, the study of the interaction of charged particles with lithium and boron nuclei is of great interest. On the one hand, lithium and boron are one of the most important elements of the fuel cycle in the most promising projects of fusion reactors using deuterium-tritium plasma or alternative neutron-free fuel cycles. Another aspect is related to the issues of nucleosynthesis of light nuclei at an early stage of the evolution of the Universe and reactions proceeding with the formation of beryllium, lithium, and boron nuclei in a stellar enviroment.

The purpose of this thesis is an experimental and theoretical study of the influence of cluster structures of stable lithium and boron isotopes on the formation of nuclear reaction yields in interactions with deuterons and α-particles.

The objectives of the study. To achieve the goals it was necessary to solve the following tasks:

- measurement of differential cross sections for scattering of deuterons, α particles and reactions (d,t), (α,t) at ^{7}Li and ^{11}B nuclei at energies of 7-10 MeV/nucleon at the isochronous cyclotron U150M of the Institute of Nuclear Physics (Almaty, Kazakhstan);
- determination of the global parameters of the optical potentials for the nuclear systems "d+^{7}Li", "d+^{11}B" and "α+^{11}B" from the analysis of experimental data on elastic scattering;
- extraction of strain parameters for excited states of ^{7}Li and ^{11}B nuclei from analysis of experimental data on inelastic scattering;
- determination of spectroscopic factors of cluster configurations ^{7}Li→"α+t" and ^{11}B→ "2α + t".

Object of study. The processes ^{7}Li(d,d)^{7}Li, ^{7}Li(d,t)^{6}Li, ^{11}B(d,d)^{11}B, ^{11}B(d,t)^{10}B, ^{11}B(α,α)^{11}B and ^{11}B(α,t)^{12}C at energies of 7–10 MeV/nucleon.

Subject of study. Differential cross sections for scattering of d and α particles, reactions (d,t) and (α,t) on light nuclei in a beam of the U150M accelerator. Mechanisms for the formation of cross sections for elastic and inelastic scattering of ions of d and α particles, reactions (d,t) and (α,t) on ^{7}Li and ^{11}B nuclei. Parameters of the potentials of nucleus-nucleus interactions. Spectroscopic characteristics of ^{7}Li and ^{11}B nuclei states.

Research Methods. To conduct an experimental study at the U-150M isochronous cyclotron of the Institute of Nuclear Physics (Almaty, Kazakhstan), the ΔE-E technique was used to register and identify nuclear interaction products. The essence of this technique is to simultaneously measure the specific energy loss of the

products of nuclear reactions in a substance (dE/dx) and their total kinetic energy (E). Theoretical analysis was carried out using the FRESCO computer program, which allows theoretical calculations using the following models: standard optical core model, folding model, distorted wave method and coupled channel reaction method.

The main provisions to be defended:

1. Differential cross sections of nuclear reactions ^{7}Li(d,d)^{7}Li and ^{7}Li(d,t)^{6}Li at energies of 14.5 and 25 MeV, ^{11}B(d,t)^{10}B at an energy of 14.5 MeV and ^{11}B(α,t)^{12}C at an energy of 40.0 MeV and their analysis according to the optical model of the nucleus and the method of distorted waves, eliminates the discrete ambiguity of the real part of the potential for the systems "d+^{7}Li", "d+^{11}B" and "α+^{11}B" in a wide energy range.

2. The established values of the quadrupole deformation parameters of the ^{7}Li nuclei (β_2=1.1±0.3) and 11B (β_2=-0.80±0.2), taking into account the channel coupling between the ground and excited states of the studied nuclei, reduce the deviations of the calculated cross sections from experimental ones in the range of average angles to 20– 30%.

3. The established values of the spectroscopic factors of the cluster configurations ^{7}Li→“d + t” (*SF*=1.19) and ^{11}B→“2α+t” (*SF*=1.0) correctly reproduce the rise of the reaction cross sections (d, t) and (α, t) under reverse angles on the studied nuclei and justify their cluster structures.

Scientific novelty

1. For the first time, the differential cross sections for nuclear reactions ^{7}Li(d,d)^{7}Li and ^{7}Li(d,t)^{6}Li were measured at energies of 14.5 and 25 MeV, ^{11}B(d,t)^{10}B at 14.5 MeV and ^{11}B(α,t)^{12}C energies of 40.0 MeV. The analysis of these data in the framework of the optical model of the core and the distorted wave method made it possible to eliminate the discrete ambiguity of the real part of the interaction potential for the systems “d+^{7}Li”, “d+^{11}B” and “α+^{11}B”.

2. The values of the quadrupole deformation parameters of the ^{7}Li nuclei (β_2 =1.1±0.3) and ^{11}B (β_2=-0.80±0.2 with a negative sign) were determined, which made it possible to significantly improve the descriptions of the studied angular distributions in the region of average scattering angles.

3. The values of spectroscopic factors of cluster configurations ^{7}Li→“d+t” (*SF*=1.19) and ^{11}B→“2α+t” (*SF*=1.0), necessary for determining the reaction cross sections (d,t) and (α,t), are calculated at opposite angles.

Scientific and practical value of work

The results of the research are of high scientific and practical value. The obtained experimental cross sections of the ^{7}Li(d,d)^{7}Li, ^{7}Li(d,t)^{6}Li, ^{11}B(d,t)^{10}B and ^{11}B(α,t)^{12} C processes at energies of 7-10 MeV/nucleon can significantly supplement the world nuclear data bank, the IAEA library (EXFOR), because currently there are no such experimental data on the interaction of deuterons and α particles with lithium and boron nuclei over a wide angular range.

Experimental data are also needed to refine the parameters of theoretical models by comparing theoretical predictions with new experimental data in the extended energy range. The totality of the obtained data on the cross sections for the interaction

of deuterons and α particles with ^{7}Li and ^{11}B nuclei at low energies and the structural characteristics of the studied nuclear systems will be useful for model calculations of the energy balance of promising nuclear power plants, as well as in theoretical calculations of nucleosynthesis reactions in stars and interstellar spaces.

The reliability of the results

In the dissertation, well-known experimental and theoretical methods and models were used: E-E particle registration and identification technique, optical model, folding model, distorted wave method and coupled channel method. The calculations were carried out using a universally recognized, widely tested computer code: FRESCO. The achieved scientific results are in good agreement with the works of other authors in this field.

The relationship of this work with other research projects. The dissertation was carried out as part of scientific research on the following topics: "Study of the excited halo states of neutron-rich nuclei ^{9}Be, ^{11}B, ^{13}C in interactions with deuterons" №.GR 0115RK01006 (2015-2017) and "Study of radiation capture and peripheral nuclear transfer reactions of protons at energies near the Coulomb barrier caused by heavy ions for astrophysical and thermonuclear applications", AR05132062/GF(2018-2020).

Personal contribution of the author. The results presented in the dissertation by the author were obtained jointly with the staff of the SRC "Kurchatov Institute" (Moscow, Russian Federation), Saitama University (Tokyo, Japan) and the laboratory of low-energy nuclear reactions of the Institute of Nuclear Physics (Almaty, Kazakhstan) and reflected in joint publications. The author's personal contribution is to participate in the formulation of research tasks and the design of the experiment, in conducting a set of experimental studies, in processing and analyzing experimental results.

Work approbation

Materials of the thesis were reported at 6 republican and international conferences:19 th International Workshop on Radiation Imaging Detectors iWoRID, Poland, Krakov, July 2–6, 2017; XXXVI Mazurian Lakes Conference on Physics, Piaski, Poland, September 3-9, 2017;Zakopane Conference of Nuclear Physics, "Extremes of the Nuclear Landscape", August 26- September 2, 2018, Zakopane, Poland;DREB2018 - 10th International Conference on Direct Reactions with Exotic Beams4-8 June 2018, Matsue, Japan; II International Scientific Forum «Nuclear Science and Technologies» Almaty, Kazakhstan, June – 24-27, 2019; Ninth International Conference «Modern Problems of Nuclear Physics and Nuclear Technologies" September 24-27, 2019, Tashkent, Uzbekistan.

Publications

Based on the materials of the dissertation, 19 works were published (10 articles, 8 theses and one patent), 3 of which were published in journals recommended by the Committee for Control in Education and Science of the Ministry of Education and Science of the Republic of Kazakhstan, as well as 1 patent of the Russian Federation "Semiconductor detector with internal gain", 7 articles with a non-zero impact factor in journals indexed by Thomson Reuters and in Scopus.

1. Burtebayev N.,Sakuta S.B., Nassurlla Marzhan, Saduyev N., Nassurlla Maulen, Sadykov T.Kh., Trzcinska A., Wolinska-Cichocka M., Khojayev R. Mechanism of the B-11(alpha,t)C-12 reaction at an energy of 40 MeV, role of exchange processes and collective excitations // European Pysical Journal A.-2019.- Vol.55, № 3.-P.38.

2. Burtebayev N., Nassurlla Maulen,Nassurlla Marzhan; Saduyev N, Sabidolda A., Zazulin D., Sadykov T.Kh., Sakuta S.B., Trzcinska A., Wolinska-Cichocka M. Scattering of alpha-particles by ^{11}B nuclei at an energy of 40 MeV and role of the exchange mechanism with transfer of^{7}Li // International Journal of Modern Physics E. – 2018. – Vol.27, № 11. – P.1850094.

3. Chernykh A.V., Chernykh S.V., Didenko S.I., Burtebayev N., Nasurlla Maulen; Nasurlla Marzhan, Britvich G.I., Chubenko A.P., Baryshnikov F.M., Sleptsov E.V. GaAs Schottky Barrier Detectors for Alpha-Particle Spectrometry at Temperatures up to 120°C // Technical Physics Letters. – 2018. – Vol.44, №10.– P.942-945.

4. Burtebayev N.,Kerimkulov Zh.,Bakhtybayev M.,Hamada Sh., Mukhamejanov Y.S., Nassurlla M., Alimov D.,Morzabayev A., Janseitov D.M.,Trzaska W. Investigation of the elastic and inelastic scattering of ^{4}He from ^{11}Be in the energy range 29–50.5 MeV // Nuclear Physics and Astrophysics Conference. IOP Conf.Series: – Journal of Physics: Conf.Series. – 2018. – Vol.940. – P. 012034.

5. Chernykha S.V., Chernykh A.V.,Didenko S.I., Baryshnikov F.M., Burtebayev N., Britvich G.I., Chubenko A.P., Guly V.G., GlybinYu.N., Zholdybayev T.K., Burtebayeva J.T., Nassurlla M., et al. GaAs detectors with an ultra-thin Schottky contact for spectrometry of charged particles // Nuclear Instruments and Methods in Physics Research Section A: Accelerators, Spectrometers, Detectors and Associated Equipment. – 2017. – Vol. 845. – P. 52-55.

6. Chernykh A.V., Chernykh S.V., Baryshnikov F.M., Didenko S.I., Burtebayev N., Britvich G.I., KostinM. Yu., Chubenko A.P, Nassurlla Marzhan, Nassurlla Maulen, Kerimkulov Zh., Zholdybayev T., Glybin Yu. N. and .Sadykov T.Kh Characterization and simulation of fast neutron detectors based on surface-barrier VPE GaAs structures with polyethylene converter // Journal of Instrumentation. – 2016. – Vol.11. –P.C12005.

7. Burtebayev N., Kerimkulov Zh.K., Nassurlla Maulen, J.T. Burtebayeva J.T., Nassurlla Marzhan, Sakuta S.B., Suzuki T., Rusek K., Trzcińska A., Wolińska-Cichocka M. Study Of The ^{7}Li(d,t)^{6}Li Reaction At The Energy Of 14.5 MeV // Acta Physica Polonica B. – 2019. – Vol.50, № 3. – P.703-709.

8. Nassurlla Maulen, Burtebayev N., Mukhashev K.M., Nassurlla Marzhan, Khojayev R.A. Temperature dependence of the energy resolution of a gallium arsenide detector //Bulletin of KazNU, Recent Contributions to Physics. – 2018. Vol.67, № 4. - P.85-92.

9. Nassurlla Maulen, Burtebayev N., Kerimkulov Zh.K., Suzuki T., Sakuta S.B., NassurllaMarzhan, Khojayev R.Investigation of deuteron scattering on ^{7}Li nuclei at energy of 14.5 MeV // News of The NAS of RK series physico-mathematical.- 2018.- Vol.6, № 3.- P.15-22.

10. Zazulin D.M., Burtebayev N., Peterson R.J., Artemov S.V., Igamov S., Kerimkulov Zh.K., Alimov D.K., Mukhamejanov E.S., Maulen Nassurlla, Sabidolda A., Marzhan Nassurlla, Khojayev R. New results for the p-^{12}C radiative capture at low energies // News of the NAS of the RK. Phys.-math. Ser. –2019. – Vol.4, № 326. – P.5–13.

11. Пат. Российская Федерация №178710 от 17.04.2018 - Полупроводниковый детектор с внутренним усилением / Черных С.В., Черных А.В., Диденко С.И., Барышников Ф.М., Буртебаев Н, Буртебаева Д., Насурлла М.; заявитель и правообладатель Москва: Нац. Исслед. Технолог. Университет МиСИС. – № 2017146335; заявл. 27.12.2017; опубл. 17.04.2018, Бюл. № 11. – 6 с.

12. Burtebayev N., Kerimkulov Zh.K., Nassurlla Maulen, Burtebayeva J.T., Nassurlla Marzhan, Sakuta S.B.,Suzuki T., Artemov S.V., Ergashev F., Karakhozhaev A.A., Rusek K., Trzcińska A., Wolińska-Cichockae M. Study of the ^{7}Li(d, t)^{6}Li reaction at the energy of 14.5 MeV // Book of abstract Zakopane Conference of Nuclear Physics, "Extremes of the Nuclear Landscape". – Zakopane, 2018. –P.170.

13. Chernykh S.V., Chernykh A.V., Baryshnikov F.M., Burtebayev N., Britvich G.I., Kostin M.Yu., Chubenko A.P., Nassurlla Marzhan, Nassurlla Maulen, Kerimkulov Zh., Zholdybayev T., Glybin Yu.N., Sadykov T.Kh., Kazakova Yu.V.Didenko S.I. Self-biased fast neutron detector based on VPE GaAs surface-barrier sensor with polyethylene converter // Book of Abstracts of 19 th International Workshop on Radiation Imaging Detectors iWoRID. – Krakov, 2017. – P.76.

14. Burtebayev N., Nassurlla Maulen, Kerimkulov Zh.K., Burtebayeva D.T., Mukhamedzhanov E.S., Nassurlla Marzhan, Suzuki T., Sakuta S.B. Study of the deuteron scattering on ^{7}Li nuclei // DREB2018 - 10th International Conference on Direct Reactions with Exotic Beams. – Matsue, 2018. – P.18.

15. Burtebayev N., Burtebayeva J.T., Kerimkulov Zh.K., Mukhamedzhanov E.S., Nassurlla Marzhan, Nassurlla Maulen, Zholdybayev T.K., Alimov D.K., Suzuki T., Sakuta S.B. Study of the deuteron scattering on ^{11}B nuclei // XXXVI Mazurian Lakes Conference on Physics». – Piaski, 2017. – P.218.

16. Насурлла Маулен, Буртебаев Н., Сакута С.Б., Керимкулов Ж.К., Буртебаева Д.Т., Алимов Д.К., Мухамеджанов Е.С., Насурлла Маржан, Сабидолда А., Ходжаев Р. Исследование реакции (d,t) на ядрах ^{11}B при энергии 14,5 МэВ // II Международный научный форум «Ядерная наука и технологии». – Алматы, 2019. – С.43.

17. Burtebayev N., Nassurlla Maulen, Nassurlla Marzhan, Saduyev N., Sabidolda A., Zazulin D., Sakuta S.B., Trzcińska A., Wolińska-CichockaM. Рассеяние α-частиц на ядрах ^{11}B при энергии 40 МэВ и роль обменного механизма с передачей ^{7}Li // II Международный научный форум «Ядерная наука и технологии». – Алматы, 2019. – С.50-51.

18. Alimov D.K., Burtebayev N., Nassurlla Marzhan, Nassurlla Maulen, Burtebayeva J. Study of the V-W-Ambiguity when Choosing the Optical Potentials from Scattering of α-Particles on ^{10}B and ^{11}B Nuclei // Book of Abstracts of the Ninth

International Conference «Modern Problems of Nuclear Physics and Nuclear Technologies". – Tashkent, 2019. – P. 56

19. Burtebayev N., Nassurlla Maulen, Nassurlla Marzhan, Saduyev N., Sabidolda A., Zazulin D., Sakuta S.B., Trzcińska A., Wolińska-Cichocka M. Scattering of α-Particles by ^{11}B Nuclei and Role of the Exchange Mechanism with Transfer of Heavy Particle // Book of Abstracts of the Ninth International Conference «Modern Problems of Nuclear Physics and Nuclear Technologies". – Tashkent, 2019. – P. 58.

The structure and scope of the dissertation

The dissertation consists of an introduction, five sections, a conclusion and a list of used sources from 217 items. The total amount of work is 127 pages of text, including 16 tables and 51 figures.

The introduction shows the relevance, provides an overview and statement of the problem considered in this paper, formulates the goals, the novelty of the results, and substantiates their scientific and practical value. The main provisions for the defense, the personal contribution of the author, approbation and the summary of the dissertation are given.

The first section is devoted to a literary review of the data available on the topic of the dissertation.

The second section is devoted to the theory of nuclear reactions. This section describes in detail the methods of theoretical calculations that were used to describe the obtained experimental data, in particular: the optical model, folding model, coupled channel method, and distorted wave method.

The third section of the thesis presents the main characteristics of the experimental complex for studying the yields of nuclear reactions in the extracted beam of accelerated particles of the isochronous cyclotron U-150M INP. A detailed description of the system for registration and identification of nuclear reaction products, the technology of manufacturing targets and determining its thickness, a method for measuring and processing energy spectra, and calculating the differential cross sections of nuclear reactions are given. The results of testing the characteristics of a new radiation and heat-resistant semiconductor detector based on ultra-pure GaAs are presented.

The fourth section presents the results of measurements of the differential cross sections of the nuclear process ^{7}Li(d,d) ^{7}Li, ^{7}Li(d,t)^{6}Li at energies E_d = 14.5 and 25 MeV and their analysis in the framework of the optical and folding model, coupled channel method. The optimal parameters of the optical potential and potential folding in a wide energy range are found.

Specified values of the spectroscopic characteristics of the studied nuclear systems are obtained. The calculated differential cross sections were fitted to the experimental data using the FRESCO program.

The fifth section is devoted to the study of the processes of scattering of deuterons and particles on ^{11}B nuclei and ^{11}B(d,t)^{10}B and ^{11}B(α,t)^{12}C reactions at 7-10 MeV/nucleon. The main experimental regularities observed in cross-sectional structures and reactions (d,t) and (α,t) are analyzed and discussed.The optimal

parameters of the interaction potential are found from fitting experimental data on elastic scattering. Refined values of the spectroscopic characteristics of the studied nuclei were obtained from matching the experimental data with the calculated cross sections using the FRESCO program.

In conclusion the main conclusions are drawn, based on a comprehensive analysis of the obtained experimental data in the framework of the optical model and the coupled channel method.

The author expresses deep gratitude to the supervisors: doctor of physical and mathematical sciences, Professor N. Burtebayev and doctor of physical and mathematical sciences, Professor T. Suzuki for setting the task, assistance in work and useful discussion during the preparation of the dissertation.

The author is particularly grateful to the entire team of the Laboratory of Low-Energy Reactions of the Institute of Nuclear Physics, where this work was mainly performed, for the assistance and support provided at various stages of the study.

He considers it his pleasant duty to express gratitude to the faculty of the Department of Theoretical and Nuclear Physics of the Faculty of Physics and Technology of al-Farabi KazNU.

1 LITERATURE REVIEW

Of particular interest in studying elastic and quasielastic processes was the experimental discovery of phenomena that cannot be understood on the basis of the concept of strong absorption, namely, the rise of the differential cross section $d\sigma/d\Omega$ in the range of angles close to 180 ° (anomalous backscattering - ABS) two to three orders of magnitude greater than the Coulomb scattering cross section $d\sigma_R/d\Omega$.

At present, a large amount of experimental data has been accumulated on the inverse cross section maxima in elastic scattering and nuclear reactions. There are a number of review articles [4, p. 393; 5, p.669; 31-34], which describe in detail their possible methods of theoretical description. Let us dwell on the basic laws characterizing the ABS in elastic scattering.

The first experimentally established fact is the dependence of ABS on the mass number of the target nucleus: with a decrease in the mass number of target nucleus A, an increase in the absolute and relative values of ABS is observed. For example, upon scattering of α particles with an energy of 15–40 MeV on nuclei of large and medium atomic weights (for example, zirconium isotopes [35], on nuclei in the iron region [36], the differential cross sections decrease on average with increasing scattering angle. $d\sigma/d\sigma_R$ are much smaller than one at the largest angles and vary with increasing mass number from 10^{-4} to 10^{-1}. Also, the angular distributions of elastically scattered deuterons with an energy of 10-15 MeV on nuclei heavier than Al [37], ^{3}He ions with an energy of about 30 MeV on nuclei in the region of calcium and heavier [38,39], etc. As a rule, such angular distributions are well described by the standard OP model, while in elastic scattering of ^{3}He ions on lithium isotope nuclei at energies of 30 -72 MeV, a significant excess of $d\sigma/d\Omega_R$ from one is observed, which is almost impossible to describe using the standard OP model with reasonable optical potential parameters.

Given all these circumstances, a systematics of angular distributions was proposed in [40] depending on the behavior of the ratio $d\sigma/d\sigma_R$ in the range of medium and large angles. All angular distributions in it are divided into three types (figure 1.1), and the angular distributions described above on medium and heavy nuclei are assigned to the first type.

When alpha particles are scattered on the cores of the end of the 2s – 1d shell: ^{36}Ar, ^{40}Ca [40], the ratio $d\sigma/d\sigma_R$ decreases in the region of average angles, then again increases slightly, and at large angles it has an order of magnitude equal to one (second type of angular distributions) . The authors of [40, p.1016] called this type anomalous, implying that it can no longer be described within the framework of the standard optical model. Finally, in the scattering of alpha particles on the nuclei of 1p- [41-46] and the beginning of *2s–1d* - shells [47-49], especially on nuclei having an Nα-cluster structure: carbon and oxygen [44, p.951; 46, p.514], neon and magnesium [47, p.626], the envelope of the maxima of the $d\sigma/d\sigma_R$ ratio already rises in the region of average angles and reaches two to three orders of magnitude at the largest angles. Such angular distributions can be called abnormal in the wide range of angles and belong to the third type (figure 1.1).

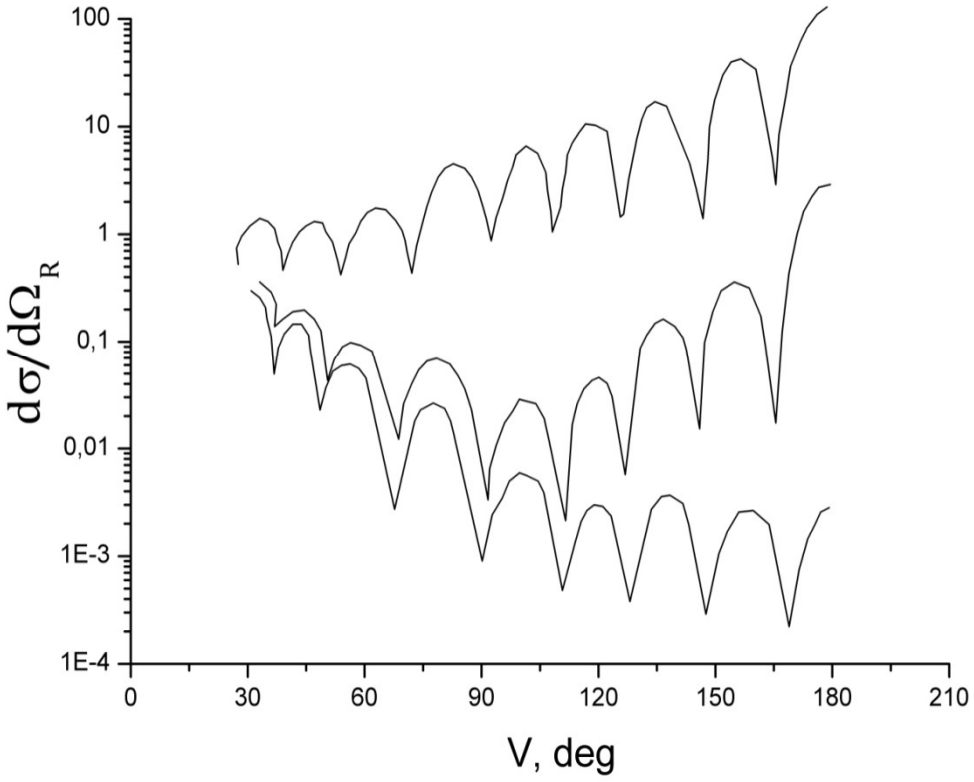

Figure 1.1–Abnormal angular distributions

The scattering of deuterons [37, p.832; 50-51], ^{3}He ions [45, p. 36; 52-53], and Li ions [54] on the nuclei of 1p and the beginning of 2s–1d shells occupies an intermediate place between the third and second types.

Let us stop briefly on the dependence of the ABS on the type of incident particle. It was experimentally established that the ABS manifests itself most clearly in the scattering of α particles, the most stable of all complex incident particles, and much less in the scattering of lithium ions, deuterons, etc. In work [55], the scattering cross sections for alpha particles (E_{α}=23–27 MeV), ^{3}He ions (E_h =23+29 MeV), and ^{6}Li ions (E_{Li} = 30 MeV) on ^{40}Ca and ^{48}Ca nuclei.

The ratios σ_{α}/σ_h are 50 and 10, and $\sigma_{\alpha}/\sigma_{Li}$ are 280 and 160 for ^{40}Ca and ^{48}Ca nuclei, respectively. In [56], where the angular distributions of ^{3}He and α particles elastically scattered by ^{27}Al were measured in a wide energy range of 13–40 MeV, the ratio σ_{α}/σ_h at an angle of 180° is approximately two orders of magnitude. ABS also depends on the structure of the target nucleus. Experimental data show that a strong peak is observed when scattering on nuclei with a filled shell (^{16}O, ^{40}Ca or filled with a filled shell (^{12}C), or with a hole in a filled shell (^{15}N, ^{39}K). As a rule, the ABS decreases slightly (by 1.5 ÷ 3 times) upon transition to other isotopes belonging to the same shell (^{12}C, ^{13}C, ^{14}C [53, p.1004;56, p.940]; ^{32}S, ^{34}S,^{36}Ar,^{38}Ar; ^{39}K,^{40}K [57]), and decreases sharply if two additional neutrons fall to the next shell (compare ^{16}O and ^{18}O [56, p.942], ^{38}Ar and ^{40}Ar, ^{39}K and ^{41}K; ^{40}Ca,^{42}Ca and ^{44}Ca [38, p.256].

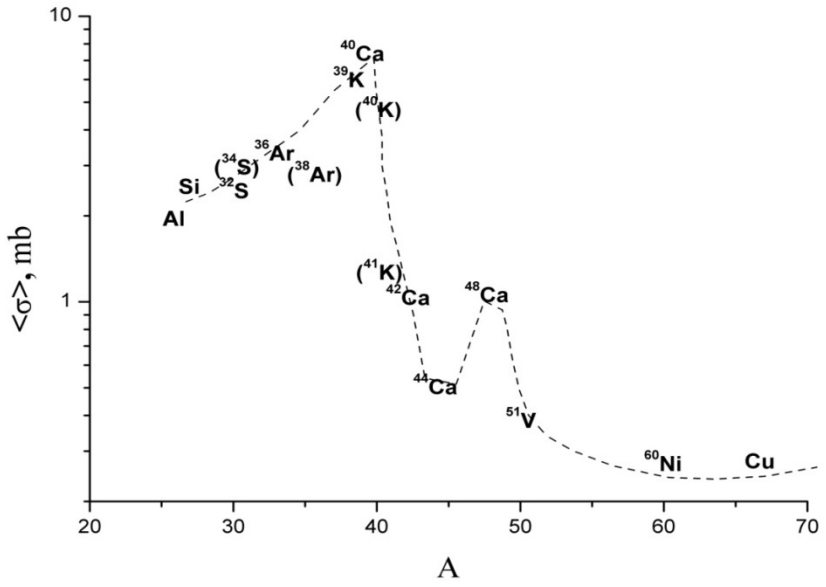

Figure 1.2– Cross sections for elastic scattering of α particles on nuclei of average atomic weight

In figure 1.2, taken from [57, p.559], shows the cross sections for elastic scattering of α particles on nuclei of average atomic weight, integrated over angles from 141° to 170° and averaged over energies from 23 to 27 MeV. It can be seen in the figure 1.2 that σα falls by an order of magnitude upon transition from ^{40}Ca to ^{42}Ca, from ^{39}K to ^{41}K, ^{38}Ar и ^{40}Ar, and also at least 2.5 times upon transition from ^{42}Ca to ^{44}Ca. Then, σ_α again increases for ^{48}Ca with a filled neutron $1_{f7/2}$ subshell. On the other hand, the averaged cross sections are close in magnitude for different nuclei with a similar structure (for example, for ^{40}Ag, ^{44}K, ^{42}Ca, each having two $1_{f7/2}$ neutrons over a partially unfilled subshell $1_{d3/2}$; for ^{13,14}C, ^{14,15}N with holes in 1p-shell). The described dependence of the ABS on the structure of the target nucleus (as well as on the type of the incident particle) suggests that the scattering of complex particles is not purely potential, and that nuclear processes that must be examined on a microscopic basis with accurate taking into account the structure involved in the scattering of particles.

Let us dwell separately on the dependence of the ABS on the energy of the bombarding particles. It is known that at some energy values the ABS can disappear (for example, during elastic scattering of alpha particles with E = 25 MeV on the ^{13}C nucleus [53, p.1004]) or move to the region of smaller angles (for example, during elastic scattering of ^{3}He ions with E = 24,5 MeV), on the ^{12}C nucleus a strong maximum is observed at $\theta \sim 165°$ [52, p.698], and during deuteron scattering from E = 13.8 MeV by ^{16}O it shifts even further to $\theta \sim 150°$ [51, p.672]). It should be noted that in this case, the behavior of the cross section in the rear hemisphere remains anomalous: $d\sigma/d\sigma_R >> 1$. In [5, p.669], the angular distributions of elastic scattering of alpha particles by ^{6}Li, measured at energies 18, 50 and 166 MeV are compared: ABS remains even for E = 166 MeV, although its absolute value decreases. A similar comparison was made in [58] for elastic scattering of alpha particles to the largest

angles on ^{40}Ca, ^{44}Ca nuclei in a wide energy range of 24–62 MeV, as well as at energies of 100 and 147 MeV. It turns out that ABS is present on both nuclei, at least up to 62 MeV, but the ratio $d\sigma/d\sigma_R$ at $\theta \sim 180$ ° decreases with increasing energy. For ^{40}Ca at $E \leq 36$ MeV, $d\sigma/d\sigma_R$ exceeds one, at $E \approx 60$ MeV, $d\sigma/d\sigma_R$ drops by an order of magnitude, at E = 100 MeV this ratio is $\sim 10^{-2}$, etc. A stable maximum, although shifted to $\theta \sim 165°$, is also observed in inelastic scattering of α particles by ^{40}Ca with the excitation of the 3^- state (3.73 MeV). Thus, the effect of the presence of ABS remains in a wide energy range, but the general behavior of the cross section in the rear hemisphere with an increase in energy ceases to be anomalous ($d\sigma/d\sigma_R << 1$). The anomaly boundary for the system $\alpha+^{40}Ca$ ~ up to 55 MeV, for other complex particles; deuterons, ^3He nuclei, Li ions - lower (~ 20 ÷ 30 MeV).

A similar situation occurs in the scattering of heavy ions on the nuclei of the 1p shell for nuclear systems having an Nα - cluster structure or structures with the addition of one or more nucleons.

This is especially important for studying the problems of nuclear astrophysics, the combustion of carbon, oxygen and silicon in stars associated with the period preceding a supernova explosion. A feature of elastic scattering on Nα nuclei is a pronounced rise in the cross section in the region of reciprocal angles [59–62]. Such a rise in the cross section most vividly decreases with decreasing energy of the incident ion in the region of the Coulomb barrier for systems: $^{12}C+^{16}O$, $^{16}O+^{20}Ne$.

For such systems, the optical model did not allow a sufficiently good description of the experimental data on the angular distributions in the region of large scattering angles, where an anomalous increase in the scattering cross section is observed. A modification of the model was required to solve this problem. Subsequently, an introduction was introduced into the expression of the interaction potential of an additional term, the repulsive core potential [63]. The study of the properties of a nuclear system with a repulsive core is reduced to determining the value of the compressibility coefficient of nuclear matter, which, as a rule, depends on the interacting nuclei and the energy of the projectile nucleus.

The specified modification did not always give the desired description of the experimental data. Later, it was suggested that in the region of large scattering angles, a different role is played by another reaction mechanism: the elastic transfer of the α-particle [64, 65]. In these studies, the combined method was used to take this process into account: in the region of small and medium scattering angles, the description is carried out in the framework of the optical model (OM), and in the region of large scattering angles, the method is distorted waves (DWM) with zero radius of nuclear forces.

Within the framework of the α-cluster model, the ^{12}C and ^{16}O nuclei can be considered as consisting of 3 and 4 α - particles, respectively. In this regard, the question arises of the distribution of α - particles in these nuclei. In describing the angular distributions in the framework of the α-cluster model, this work concludes that α particles are concentrated near the surface of the ^{16}O nucleus, which is confirmed by the results obtained in [66]. A similar distribution of α particles in the ^{12}C nucleus is assumed.

A characteristic feature of elastic scattering of neon by light clustered nuclei at energies above the Coulomb barrier is also an anomalous increase in cross sections at reverse scattering angles [67–69]. A description of the rise of the cross section at opposite angles at energy of 50 MeV in [67, p.1828] was achieved taking into account the contribution of the elastic transfer mechanism of the alpha cluster to the total cross section of the scattering process. When analyzing the refined data at this energy [69, p.235], we used a modified optical potential with a deep real part to describe the rise of the reaction cross section in the rear hemisphere.

A similar behavior of elastic scattering at reverse angles is observed for nuclear systems consisting of Nα + neutron nuclei. For example, a significant increase in the cross section for elastic scattering of ^{13}C ions on ^{9}Be nuclei is observed at energies above 2 MeV/nucleus in a number of works [70–72]. At a higher energy [72, p.2427] (E_{Be} = 50,46 MeV), it was shown that the increase in the elastic scattering cross section at reverse angles is related to the contribution of the α-particle exchange process between two identical ^{9}Be nuclei.

To detect these exchange mechanisms in interactions of non-Nα - nuclei with a mass difference greater than one or two nucleons, we also studied the elastic scattering of ^{14}N ions on ^{10}B nuclei. None of these nuclei has an Nα - structure, although it is known that the probability of spectral amplitude for the ^{14}N nucleus in its ground state, described as a ^{10}B nucleus associated with an α-particle, is quite high. Experiments with the exchange of alpha particles in elastic scattering [73, 74] and the results of theoretical calculations [18, p.1689; 75] showed that the spectral amplitude for the ground state of the ^{14}N nucleus is comparable to most Nα-nuclei of the lp shell, for example, -^{12}C + α. Earlier, for the ^{10}B + ^{14}N system, the Marquardt group investigated the excitation functions at the scattering angle $\theta_{m.m.}$ = 172°[76]. The results obtained by them show the presence of broad structures in comparison with other cases such as ^{16}O + ^{28}Si. In addition, resonance structures were observed in the excitation functions of the $^{10}B(^{14}N,^{12}C)^{12}C$ and $^{12}C(^{12}C,^{10}B)^{14}N$ reactions [77, 78]. These resonances were conventionally designated as molecular rotational states of ^{24}Mg formed in the intermediate reaction stage.

In [75, p.815], two orbitals with angular momenta *L =2* and *L =4* were found for the $^{14}N \rightarrow ^{10}B+\alpha$ system. It was shown that a configuration with a large angular momentum is more preferable, since the cluster in this case is in a peripheral orbit with a large average radius. The following theoretical spectroscopic factors were obtained for these configurations S_2 = 0.012 and S_4 = 0.69. The Wozniak group [73, p.815] in their studies of the $^{14}N \rightarrow ^{10}B+\alpha$ system obtained the value of the experimental spectroscopic factor equal to S_4 =0.41. Boyarkin in [79] gives the value of the spectrofactor – S =0.762.

The most complete experimental data on the angular range (θ_{ccm} = 14°-176°) are the data of the work of the Japanese group [80] measured at an energy interval of 38.1 - 50 MeV. In the calculations of alpha cluster transfer, the authors took into account only the configuration with the orbital momentum *L = 4*. The spectroscopic factor obtained by them is S_4 = 0,65, which is close to the theoretical value calculated in [80, p.741] – S_4 = 0.69 [75, p.815]. For all energies, a shallow optical potential was

used - V_R = 14 MeV. In general, they achieved a good description of the experimental data in the field of small and medium angles up to 160 degrees. At large angles (over 160 degrees), the calculated cross sections diverge from experiment. They explain this by the fact that there are probably multistage alpha-particle transfer mechanisms that must be taken into account in the calculations.

In a recent study of the elastic scattering of ^{15}N ions on ^{11}B nuclei at an energy of 84 MeV [81], a significant increase in cross sections at reverse angles was also reproduced by the contribution of the elastic transfer mechanism of the α cluster. Therefore, in the case of scattering of heavy ions on light nuclei, ABS occurs. Moreover, the ABS for such nuclear systems has the same dependence on the energy of incident ions and the structures of interacting nuclei, as in the case of scattering of alpha particles.

One can expect the most pronounced manifestation of the effects of cluster exchange in backscattering on light strongly clustered nuclei: for example, on the nuclei of lithium, beryllium, and boron isotopes. At present, scattering of helium ion isotopes on ^{6}Li and ^{7}Li nuclei having a pronounced cluster structure is quite systematically studied: ^{6}Li → "d+α", ^{7}Li →"^{3}He+t". The observed “anomalous” rise in the cross section at reverse angles can also be described taking into account the contribution of the exchange mechanism of cluster transfer, which is physically indistinguishable from potential scattering. Indeed, the study of elastic scattering of ^{3}He and α particles on the ^{6}Li nucleus [7, p.198; 82–83], the lower states of which are described by overlapping configurations (^{3}He+t) and (α+d) [84, 85], showed that taking into account the elastic The transfer of triton and deuteron, which is indistinguishable in experiment from potential scattering, allows one to describe the angular distributions in the full angular range. Note that intense exchange of clusters occurs between identical ^{3}He frames in the first case and α in the second.

The binding energy of the transferred cluster in the ^{6}Li nucleus strongly affects the nature of the manifestation of (α+d) and (^{3}He+t) - structures in various nuclear processes. So in the channel (α+d) it is only 1.47 MeV. This means that the deuteron and α-particle clusters are located quite far from each other for a considerable part of the time. Therefore, such a structure can be detected and investigated in surface collisions. On the contrary, the configuration amplitude (^{3}He + t) (ε_{bnd} = 15.79 MeV) in the surface region is small, while the destruction of a strongly coupled and almost free α -particle cluster is very difficult [86]. Therefore, the structure of (^{3}He+t) is best studied under conditions of greater sensitivity to the inner region of the nucleus. As shown in [7, p.198; 82, p. 405; 84, p. 361], both (α+d) and (^{3}He+t) structures are clearly manifested in the anomalous increase in the scattering cross sections of α particles and ^{3}He at large angles.

A similar situation also occurs in the scattering of частиц particles and ^{3}He on ^{7}Li and ^{9}Be nuclei. The binding energy of the частицы-particle in ^{7}Li and ^{9}Be is only 2.46 MeV, while the energies of separation of ^{3}He from the same nuclei are 25.94 and 21.18 MeV, respectively. Therefore, the structures (α+t) and (α+^{5}He), on the one hand, and (^{3}He+^{4}H) and (^{3}He+^{6}He), on the other hand, can manifest themselves in different ways in the angular distributions of scattered particles in the region of large

angles. Studies on these cores in the full angular range at ^{3}He energies above 10 MeV/n were not carried out until the mid-eighties. These studies are of great interest, since with increasing energy of the incident particles, the scattering sensitivity to the inner region of the nucleus will increase, and, as a result, there will be a real opportunity to study the structures (^{3}He+t), (^{3}He+^{4}H) and (^{3}He+^{6}He).

Thus, to date, the scattering of helium ion isotopes on ^{6}Li, ^{7}Li, and ^{9}Be nuclei having a pronounced cluster structure: ^{6}Li → (d+α) and (^{3}He+t), ^{7}Li → (α+t) and (^{3}He+^{4}H), and the ^{9}Be nucleus can be represented as α+α+n or α+^{5}He, ^{3}He+^{6}He. In this case, according to the general principles of quantum mechanics, a large contribution is expected from the exchange transmission ^{6}Li(α,^{6}Li)α, ^{7}Li(α,^{7}Li)α, ^{6}Li(^{3}He,^{6}Li)^{3}He, ^{7}Li(^{3}He,^{7}Li)^{3}He, ^{9}Be(α,^{9}Be)α and ^{9}Be(^{3}He,^{9}Be)^{3}He. The exchange mechanism is superimposed on a straight line if the angle θ is replaced by π-θ. In the calculations the DWUCK 5 program is used [87], to estimate the cluster exchange cross sections for the above nuclear reactions in the energy range 30–72 MeV, the Bor DWM approximation was used with exact allowance for the finiteness of the interaction radius [88]. In this case, the distorted waves for the input and output channels were calculated from the ODs established from the fit of the experimental data for the front angles with respect to OM [7, p.198; 10, p.20; 89]. Cluster (α+d), (α+t), (α+^{5}He), (^{3}He+t) and (^{3}He+^{4}H), (^{3}He+^{6}He) wave functions of ^{6}Li, ^{7}Li and ^{9}Be nuclei, respectively, were calculated using Woods-Saxon potential with a reduced radius of 1.25 fm and a diffusion of 0.65 fm. The depth of the well was found from fitting so that the desired binding energy of the clusters was obtained.

Moreover, the theoretical cross sections of the exchange mechanism in the elastic scattering of частиц particles for ^{6,7}Li nuclei in these studies, differing quite strongly in the front hemisphere, vary little in the region of large angles. Therefore, spectroscopic factors obtained from the normalization of the calculated cross sections to the experimental data in this particular range of angles remain stable. Thus, for the ground states of ^{6}Li, ^{7}Li, and ^{9}Be nuclei, the average values of cluster spectroscopic factors are equal to $S_{\alpha d}$ = 1.39±0.15, and $S_{\alpha t}$ = 1.03±0.1 and $S_{\alpha 5He}$=1.Theoretical calculations within the framework of the microscopic cluster model for the ^{6}Li nucleus predict the values $S_{\alpha d}$ = 0.93-1.07 [85, p.426; 89, p.455]. The experimental spectroscopic factors extracted from the reactions of quasielastic knocking out ^{6}Li (p,pd) and ^{6}Li (p,pα) are within the range $S_{\alpha d}$ = 0.53–1.34 [90–92]. For the ^{7}Li nucleus, the theory predicts $S_{\alpha t}$ = 1.12 [93], 1.19 [94]. Investigation of the ^{7}Li (p,pα) reaction at 100 MeV gives the value $S_{\alpha t}$ = 0.94±0.05 [92, p.69]. For ^{9}Be, the value $S_{\alpha 5He}$ = 0.81 is predicted [94, p. 300]. Thus, the results of a study of the isotopes of lithium and beryllium nuclei in the literature on spectroscopic factors for the ground states of nuclei are compatible within the existing uncertainties.

Therefore, in a number of works [4, p.393;7, p.198], taking this mechanism into account allowed us not only to obtain more reliable parameters of optical potentials, but also to extract cluster spectroscopic factors from the analysis of cross sections at large angles. In recent studies [8, p.540; 11, p.1853] on the scattering of ^{3}He and α particles, the values of spectroscopic factors were obtained for the configurations "d+α ", "^{3}He+t", and "t+α" not only for the ground but also for the excited states ^{6,7}Li

nuclei. In this case, the values of spectroscopic factors for the excited states were significantly less than their theoretical values. In addition, the spectroscopic factor for the "d+α" configuration, extracted from the binding to the experiment on scattering of α particles on ^{6}Li nuclei, was more than unity. Most likely, this was due to the fact that the transfer of the α -cluster in the elastic process can be realized in two ways: both through the "d+α" configurations and through the "np+α" configuration, which can take place in ^{6}Li nuclei. In the case of deuteron scattering on this nucleus, anomalous backscattering (ABS) can be formed only through the "d+α" configurations. A systematic analysis of deuteron scattering on ^{6}Li nuclei performed in [12, p.746; 13, p.840] for a wide energy range confirmed the possibility of describing the anomalous rise in the cross section at reciprocal angles due to the elastic exchange mechanism of the deuteron cluster taking into account the channel coupling with the spectroscopic factor for the configuration "d+α" of the nucleus ^{6}Li close to one. An additional criterion for the reliability of the obtained spectroscopic factors for the "^{3}He+t" cluster configuration of the ^{6}Li nucleus can be the extraction of these quantities from an alternative approach, namely, from the transfer of the t -cluster in nuclear reactions.

For example, the reaction (α, t) on ^{7}Li, ^{10,11}B, and ^{13}C nuclei was studied in the range of angles from 20 to 175^{0} at energies from 15 to 25 MeV [95]. It was shown that in the reaction (α, t) on the studied nuclei having different structures, maximum cross sections are observed in the region of large angles. A qualitative analysis carried out by the authors allowed us to conclude that, along with the simplest reactions associated with the collapse of the target nucleus, intermediate resonance processes may also contribute to the reaction cross section.

The reaction (d, t) on ^{7}Li nuclei was previously studied at energies of 12 MeV [14, p.273; 15, p. 978], 15 MeV [16, p.1249; 17, p.781], 18 MeV [18, p.1689], 20 MeV [19, p. 408], and 28 MeV [20, p.1059]. Only at E_d = 12 MeV [15, p. 978] were measurements performed in the full range of angles. The angular distributions for the ^{7}Li(d,t) ^{6}Li and ^{7}Li(τ,α) ^{6}Li reactions were measured and analyzed in the energy region shown to be relatively free from the resonance structure of the compound nucleus.

The cross section maxima of both the front and rear angles in the measured angular distributions were reproduced by ordinary DWBA without taking into account the exchange effects. The calculation of a DWBA with a zeroth approximation is 25 times smaller than the experimental section ^{7}Li(t,α)^{6}Li, and 2,5–4,5 times smaller than the section ^{7}Li(d, t)^{6}Li. At other energies (15, 20, 28 MeV), the measurements were performed in the region of the front hemisphere and only qualitative analysis was performed based on the plane wave approximation [16, p.1249; 19, p. 408; 20, p.1059]. The values of spectroscopic factors were not extracted.

Unlike other nuclei of the 1p-shell, a complete system analysis of the anomalous behavior of the scattering cross sections for light charged particles on nuclei ^{10}B and ^{11}B is absent from a limited set of experimental data on elastic and inelastic scattering [42, p.216;96-101]. This information, published before the end of the 90s, contains

very contradictory data mainly they were measured in the region of incident particle energies of not more than 5-10 MeV per nucleon, in a limited range of angles. To localize the discrete ambiguity of potentials, it is necessary to carry out measurements at sufficiently high energies of α particles and in the maximum angular range. This is due to the fact that the interaction of a complex particle with a nucleus at low energies is of a surface nature, the target nucleus is opaque to it, and the limited region of orbital moments makes the main contribution to the cross section of the process. In other words, elastic scattering at low energies is sensitive only to the peripheral part of the internuclear interaction and does not allow probing the nucleus-nucleus potential at small distances.

Inelastic scattering analysis is usually performed within the framework of the distorted wave method (DWM) [6, p.342; 86, p.300], which successfully describes the experimental data and contains additional information to refine the optical potentials and their localization. But in cases where the state of the nuclei is of a strong collective nature, it is necessary to take into account the coupling of channels and it is more reasonable to carry out calculations within the framework of the coupled channel method (CCM), which allows simultaneous analysis of elastic and inelastic scattering, and thereby determines the degree of their influence on each other. The coupled-channel analyzes of the experimental differential cross sections for elastic and inelastic scattering, carried out in the region of light nuclei [102–104], were, in general, more successful than the calculations without taking into account the strong coupling of the channels. At present, there is a lot of experimental data indicating that channel coupling is essential for describing inelastic scattering by nuclei. Among inelastic channels, the largest contribution is made by processes with the excitation of collective states of target nuclei. In this case, the channel coupling can be taken into account in the framework of the adiabatic approximation of the well-known formalism of the coupled channel method. Very few works have been devoted to the study of the structure of states of even the lowest rotational band of ^{10}B and ^{11}B nuclei, both experimentally and in relation to BCM analysis. There are studies on the quadrupole deformation of ^{11}B using the scattering processes of ^{3}He [105] and protons [106].

The data obtained on the states of the ^{11}B nucleus are far from ambiguous; moreover, there are no similar data on the study of inelastic scattering of α particles on this nucleus.

Therefore, the consistent study of quadrupole and hexadecapolar deformations of ^{10,11}B nuclei using elastic and inelastic scattering of частиц particles at energies above 10 MeV/nucleon at the lower states ($5/2^-$ and 7/2) of the main $3/2^-$ rotation band is one of the important urgent tasks of nuclear physics to study the properties of light nuclei and nuclear interactions. Therefore, a recent study [21, p.1303; 107] carried out a comprehensive study of the elastic and inelastic scattering of частиц-particle ions on isotopes of boron nuclei at energies of 40, 50.5, and 65 MeV.

An optimal description of the experiment on ^{11}B nuclei at 50.5 MeV was obtained at β_2 = 0.60 and β_4 = 0.1. A somewhat overestimated value β_2 = 0.65 is obtained experimentally at an energy of 40 MeV [21, p.1313]. Most likely, this is due

to the increasing role of the coupling of unaccounted channels at low incident particle energies. At lower energies, it seems necessary to take into account a large number of channel coupling. This statement is also confirmed by the fact that the quadrupole deformation parameter β_2 = 0.54 obtained from the description of the angular scattering distributions at E = 74 MeV of ^{3}He ions [105, p.118] on these nuclei is consistent with the results of [21, p.1313].

Summarizing the results of [21, p.1313], we can state that the theoretical angular distributions of elastic and inelastic scattering calculated in the framework of the OM of the nucleus and CCM are well described mainly in the region of the angles of the front hemisphere. It should be emphasized that with such a description of the data, the authors of [21, p.1313] obtained reasonable values of the parameters of the OP interaction. At the same time, only taking into account the mechanism of cluster exchange has led to a good description of the characteristic features of the behavior of differential cross sections in the full angular range [21, p.1313]. For a broader and more accurate interpretation of the results obtained from the experiment on elastic and inelastic scattering, it is extremely useful to consider other quasielastic processes on the same nuclei - the reactions of (α, ^{3}He) neutron disruption and (d, ^{3}He) pickup of the proton, or (α, ^{3}H) proton disruption and (d, ^{3}H) neutron pickup. With the help of such reactions, a more detailed test of the suitability of optical potentials can be carried out. In addition, in essence, the problem of a large scatter of the phenomenological values of spectroscopic factors (SF) extracted from the model analysis of direct nuclear reactions with nucleon transfer is to a large extent associated with the ambiguity in the choice of model parameters. The most significant scatter in the SF values is due to the strong dependence on the choice of the geometric parameters of the potentials of the bound state of the transmitted nucleon in these reactions — radius and diffuseness. Recently, interest in studying elastic and inelastic scattering of частиц particles and deuterons on ^{11}B nuclei has once again grown [21, p.1313]. This is due to the presence of "α-α-t" cluster structure of this nucleus. Studying the states of the ^{11}B nucleus, where both the cluster configuration (2α + t) and the structure of the shell model can coexist is useful for determining the characteristics of excited neutron halo states of a given nucleus. Indeed, it was suggested in a number of works that low-lying states of ^{11}B mainly have a shell structure, while cluster structures are well traced in states with negative parity above or near the threshold of collapse into clusters [22, p.034305;25 p.064315]. In addition, in recent experiments on resonance scattering on ^{7}Li nuclei [26, p.034306], a new band of negative parity was confirmed, which includes the following excited states: 8.56 MeV ($3/2^-$), 10.34 MeV ($5/2^-$), 11.59 ($7/2^-$) and 13.03 MeV ($9/2^-$). Since these states have large alpha decay widths, this band can be formed on the basis of cluster structures. In addition, the analogy of the cluster structure of the ^{11}B nucleus with the three ^{12}C cluster structure is a fascinating task to study. In particular, in [24, p.024302; 27, p.6], it was suggested that the $3/2^-_3$ state can have a structure consisting of three clusters in the form of the 2α + t configuration, and can be an analogue of the ^{12}C excited state with spin 0^+_2, which has a structure consisting of 3 alpha particles [28, p.57;30, p.177]. Nevertheless, in [25, p.064315], it was

suggested that the 8.56 MeV ($3/2^-$) state cannot correspond to the ^{12}C (0^+_2) state. The analogy between 8.56 MeV ($3/2^-$) and ^{12}C (0^+_2) is controversial and requires further study of this problem. Let us dwell on the results of recent studies evaluating the radius of the exotic state of $3/2^-$ (8.56 MeV) of the ^{11}B nucleus. Root mean square radii for the following ^{11}B states: $3/2^-$ (ground state), $1/2^-$ (2.125 MeV), $5/2^-$ (4.445 MeV), $7/2^-$ (6.743 MeV) and the "exotic" $3/2^-$ (8.56 MeV) were estimated within the framework of the modified diffraction model [21, p.1303; 107, p. 20; 108]. This method allows you to determine the root mean square radius <R*> of the excited state from the difference between the diffraction radii of the excited and ground states using the expression

$$R = R_0 + [R_{dif} \quad R_{dif}(0)] \qquad (1.1)$$

Here, R_0 is the root mean square value of the ground state of the nucleus under study, R^*_{dif} and $R_{dif}(0)$ are the diffraction radii determined from the positions of the maxima and minima of the experimental angular distributions of inelastic and elastic scattering, respectively. The mean square radii of the states $3/2^-$ (ground state), $1/2^-$ (2.125 MeV), $5/2^-$ (4.445 MeV), $7/2^-$ (6.743 MeV) are given in table 1.1 with Eα = 29, 40, 50.5 [21, p.1303; 107, p.20] and 65 [108, p.777] MeV. The obtained radii are in good agreement with the results obtained in other works within the framework of MDM and other approaches for determining the radii of excited states, such as antisymmetrized molecular dynamics (AMD) [109] and the orthogonality condition model (OCM) [25, p.064315] (table 1.1). The radius for the "exotic" $3/2^-$ state (8.56 MeV), equal to 2.88 ± 0.16 fm and 2.84 ± 0.12 fm at Eα = 29, 40 MeV, respectively, is ~ 1.25 times higher than the values for the ground state. In this case, the radii for other excited states - $1/2^-$ (2.125 MeV), $5/2^-$ (4.445 MeV), $7/2^-$ (6.743 MeV) are close to the radius for the ground state (table 1.2).

Table 1.1 – Root mean square radius of $3/2^-$ (8.56 MeV) state

	MDM (E_α=29 MeV)	MDM (E_α=40.5 MeV)	MDM [16] (E_α=65 MeV)	AMD	OCM
R_{rms}(fm)	2.88 ± 0.16	2.84 ± 0.12	2.87 ± 0.13	3.1	3.0

Table 1.2 – Root mean square radii of ground and excited states of ^{11}B, obtained within MDM

E_{lab}, MeV	R_{rms} (0.00), fm	R_{rms} (2.12), fm	R_{rms} (4.445), fm	R_{rms} (5.02), fm	R_{rms} (6.74), fm
29	2.29	2.33±0.10	2.25 ±0.12		2.25 ± 0.15
40.5	2.29		2.17±0.08		2.22 ± 0.10
50.5	2.29		2.30±0.15		2.31 ± 0.11
65		2.37 ±0.20	2.27±0.10	2.44±0.14	2.32 ± 0.14

Therefore, the study of the interaction of charged particles with lithium and boron nuclei is of great interest from the point of view of obtaining the structural characteristics of these nuclei. Namely, due to the structural features of lithium and boron, they are one of the most important elements of the fuel cycle in the most promising projects of thermonuclear reactors using deuterium-tritium plasma or alternative neutron-free fuel cycles. Another aspect is related to the issues of nucleosynthesis of light nuclei at an early stage of the evolution of the Universe and reactions proceeding with the formation of beryllium, lithium, and boron nuclei in a stellar medium.

2 BASES OF THE THEORETICAL DESCRIPTION OF NUCLEAR PROCESSES

2.1 Scattering Theory

The analysis of the scattering process between two nuclei is the task of many bodies (which always comes down to the two-body problem), a solution that is described in many textbooks. In this section, a brief summary of scattering theory is given, and attention is paid to the particular case of elastic scattering, which was given by Satchler [110]. The elastic scattering process between two nuclei A and B (represented as A (B, B) A can be described by finding a solution to the Schrödinger equation $H\Psi = E\Psi$, or equivalently:

$$\left[-\frac{\hbar^2}{2\mu}.\nabla^2 + V(\vec{r})\right]\Psi(\vec{r}) = E\Psi(\vec{r}) \tag{2.1}$$

where μ is the reduced mass of the system. The potential, as a rule, consists of two parts: the Coulomb and complex nuclear potential. The wave function $\Psi(\vec{r})$ is the sum of the incident plane and diverging spherical waves:

$$\Psi(\vec{r}) = A_0\left(\exp(i\vec{k}.\vec{r}) + f(\theta,\varphi)\frac{\exp(ikr)}{r}\right) \tag{2.2}$$

where $f(\theta,\varphi)$ is the scattering amplitude and k wave number of the incident wave.

Knowing this value allows us to calculate the differential scattering cross section, defined as the number of emitted particles in a solid angle $d\Omega$, divided by the flow of incident particles per unit time. Thus, we get the expression:

$$\frac{d\sigma}{d\Omega} = \left|f(\theta,\varphi)\right|^2 \tag{2.3}$$

In the following sections, we focus on the contribution of various central potentials $V(\vec{r}) = V(r)$ to the scattering cross section.

2.2 Elastic scattering

2.2.1 Nuclear potential elastic scattering

In the general case, when considering a spherically symmetric potential, the angular momentum of the system is a constant of motion. Thus, it is possible to

decompose the wave function with the angular momentum l (and its projection along the z axis, m) into a radial and angular component.

$$x_{lm}(\overrightarrow{r}) = u_l(r)Y_l^m(\theta,\varphi) \tag{2.4}$$

This means that each $l$moment of the particle takes part in the scattering process independently of each other. In this case, the Schrödinger equation can be divided into radial and angular parts.

The radial equation is written as $w_l(r) = ru_l(r)$

$$-\frac{\hbar^2}{2\mu}\frac{d^2}{dr^2}w_l + \left[V(r) + \frac{\hbar^2}{2\mu}.\frac{l(l+1)}{r^2}\right]w_l = Ew_l \tag{2.5}$$

where $\frac{\hbar^2}{2\mu}\frac{l(l+1)}{r^2}$ expression is a centrifugal barrier (or centrifugal potential) of a particle moving in orbit with $l\hbar$ angular momentum.

The entire scattering process can be represented as the interaction of several partial wave functions with l angular momentum with a central potential. Only those particles having $l\hbar$ angular momentum relative to the target less than the maximum value will effectively interact with the target nucleus (in the classical case, only those partial waves with $l \le kb$, where k is the wave number and $b$is the impact parameter of this reaction).

For the case of elastic scattering, the asymptotic limit leads to the approximation of equation (2.4)

$$x(r,\theta,\varphi) \to \exp(i\vec{k}\overrightarrow{r}) + f(\theta,\varphi)\exp(ikr)/r \tag{2.6}$$

If for simplicity we assume that the particles have no internal spins, the angular momentum l is conserved. Directing k along the z axis, one can express the scattering amplitude of the nuclear potential as follows:

$$f(\theta,\varphi) = \frac{1}{2ik}\sum_l (2l+1)\left[S_l - 1\right]P_l(\cos\ \theta) \tag{2.7}$$

where $P_l(\cos\theta)$are the Legendre polynomialsand S_l is a unitary scattering matrix, which is expressed as reflection coefficients A_l and scattering phases δ_l

$$S_l = A_l \exp(2i\delta_l) \tag{2.8}$$

The reflection coefficients are the attenuation of the amplitude of the l-th partial wave. When considering the real potential, attenuation is not expected if A_l=1. For complex potentials, the reflection coefficient is $A_l < 1$. Scattering phases $\delta_l$correspond to the angular shifts experienced by l-th partial wave compared to the undistorted wave in the absence of any potential. The potential of attraction (V<0) leads to a positive phase shift, while the repulsive potential (V>0) leads to a negative phase shift. In the absence of a nuclear potential, all phase shifts are equal to zero.

2.2.2 Elastic scattering at the Coulomb potential

The presence of electromagnetic interaction between two interacting nuclei requires the adoption of an additional condition for the wave function, which asymptotically takes the form

$$x_C(\vec{k}\vec{r}) \to \frac{1}{r}\exp\left[ikr - \eta\ln(2kr)\right] \tag{2.9}$$

with a phase shift with respect to the undistorted wave, which logarithmically depends on the distance r, as well as on the Sommerfeld parameter defined in equation (2.10).

$$\eta = \frac{Z_P Z_T e^2}{\hbar v} \approx 0.1575 Z_P Z_T \sqrt{\frac{\mu.MeV}{E}} \tag{2.10}$$

Given the correction from formula (2.9), the wave function in equation (2.6) will have the following form:

$$\begin{aligned} x(r,\theta,\varphi) &\to x_C(r,\theta) + x_N(r,\theta,\varphi) \\ &\to (f_C(\theta) + f_N(\theta,\varphi))\frac{1}{r}\exp[i(kr - \eta\ln(2kr))] \end{aligned} \tag{2.11}$$

The f_N amplitude takes into account all possible interactions. The Coulomb amplitude is written as

$$f_C(\theta) = -\frac{\eta}{2k\sin^2\left(\frac{\theta}{2}\right)}\exp\left[-i\left(\eta\ln\left(\sin^2\left(\frac{\theta}{2}\right)\right) + 2\sigma_0\right)\right] \tag{2.12}$$

while the scattering amplitude of the nuclear interaction is given in the following form

$$f_N(\theta,\varphi) = \frac{1}{2ik}\sum_l (2l+1)\exp(2i\sigma_l)[S_l - 1]P_l(\cos\theta) \tag{2.13}$$

the phase Coulomb shift σ_l, which expresses the effect of electromagnetic interaction on the scattering amplitude $f_N(\theta,\varphi)$, is determined by the following expression

$$\sigma_l = \left|\Gamma(l+1+i\eta)\right| \tag{2.14}$$

It should be noted that the sum over the angular momenta $l$in equation (1.13) has limitations in the limit from 0 to ∞, due to the infinite radius of action of the electromagnetic interaction. Given the influence of both electromagnetic and nuclear interactions, the total scattering amplitude is written as follows

$$f(\theta,\varphi) = f_C(\theta) + f_N(\theta,\varphi) \tag{2.15}$$

and therefore, the differential cross section for elastic scattering between two A and B nuclei is expressed as

$$\frac{d\sigma}{d\Omega}(\theta,\varphi) = \left|f_C(\theta) + f_N(\theta,\varphi)\right|^2 \tag{2.16}$$

2.2.3 Elastic scattering in comparison with diffraction phenomena

This section shows the similarities between the elastic scattering of nuclei and the optical phenomena of diffraction. For simplicity, details regarding optical approximations are omitted. We will consider the description given by Thompson and Nunes [111]. Taking into account the case when the incident particle "touches" the target nucleus (the incident particle scatters only when it reaches the surface of the target nucleus, with the interaction radius $R = R_1 + R_2$, that is, the sum of the radii of the incident particle and the target), we can derive the ratio between the scattering angle and Sommerfeld parameter:

$$\eta \approx \frac{1}{2} l_g \vartheta_g \tag{2.17}$$

The values l_g and ϑ_g are the angular momentum and the scattering angle of the incident particle in the tangent approximation (denoted by the subindex g), respectively. The trajectory for a particle approaching the target nucleus with the impact parameter b_g and scattered by the angle ϑ_g. The interaction radius for this process is considered as the sum of the radii of the target and the incident particle. In this approximation, the aiming parameter b_g can be characterized as the distance at which both nuclei collide on the surface. Based on this tangent approximation, we can consider two different cases in the scattering process:

- If the aiming parameter $b < b_g$, it can be assumed that the incident particle is absorbed by the target nucleus. If we approximate that an incident particle is described by a plane wave, then the interaction with the nucleus is described similarly by plane waves coming into contact with an opaque disk. In this case, a diffraction pattern arises, which corresponds to Fraunhofer diffraction. Such a result can be obtained when the Coulomb effects on the particle trajectory are small $E_{с.ц.м.} >> V_c$, or $\eta << 1$.

- In the case of a strong deflection of the incident particle by the Coulomb field ($\eta \geq 1$), a diffraction pattern known as Fresnel diffraction is obtained. This is the most typical case in applied optics, since the light source and the observer are at finite distances (in contrast to the Fraunhofer diffraction, in which it is assumed that the source is at an infinitely large distance from the observer).

2.3 Optical Model

To describe the nuclear reaction between two nuclei A_1 and A_2, the Schrödinger equation must be written for each nucleon of the system. Each nucleon is in a potential well created by other nucleons ($A_1 + A_2$-1). We get a system of equations N = $A_1 + A_2$, which are difficult to solve numerically if N is more than a few units. Thus, it is necessary to find other ways to solve the problem of N-body.

In the framework of OM [1, p.765], all interactions between the nucleons of the incident particle and the nucleons of the target are replaced by the average and central interaction potential *V(r)* between the incident particle and the target in the ground state. This simplifies the solution of the Schrödinger equation by replacing the N-body problem with the task of one body: a particle with mass μ (reduced mass of the system) is in the potential well *V(r)*, which replaces all interactions between different nucleons. Then the equation is written:

$$H\psi = \left(-\frac{\hbar^2}{2\mu}\Delta + V \right) \psi = E\psi \qquad (2.18)$$

with the reduced mass of the system $\mu = \frac{A_1 . A_2}{A_1 + A_2}$ and r is the distance between the center of mass of two nuclei.

The main idea of OM is that the case of a nucleon falling on a nucleus can be either elastic scattering or it can cause many different reactions. If the incident particle is represented as a wave, then in the classical language, it can be scattered, or it can be absorbed. In optics, this is similar to reflection and absorption of a light wave in a medium with a complex refractive index, and also, as the imaginary part of the refractive index takes into account the absorption of the light wave, so in the nuclear case the imaginary part of the complex potential describing the interaction takes into account all inelastic reactions. Then the averaged nuclear potential can be written as:

$$U(r) = V(r) + iW(r) \tag{2.19}$$

where *V(r)* is the real part of the potential and represents elastic scattering, i.e., reflection of the incident wave. *W(r)* simulates flow loss due to inelastic collisions. Historically, the basis of OM was developed by comparing the results of neutron scattering by nuclei with the data obtained in optics during light scattering on translucent spheres. The first optical potentials were built for the interaction of neutrons with nuclei, and then for the scattering of protons, α particles and heavy ions. In the first elastic scattering analysis, a rectangular well was used, which was then replaced with a more realistic shape:

$$U(r) = Vf(r) + iWg(r) \tag{2.20}$$

where *V* and *W* are the depths of the real and imaginary parts of the potential. The form factors *f(r)* and *g(r)* depend on the distance *r* between two nuclei. Since the nucleon – nucleon interaction appears at very short distances, the potential *Vf(r)*, which is an approximate sum of the nucleon – nucleus interactions, has the same behavior. Nucleons in the core cortex interact only with their nearest neighbors. Due to this saturation of nuclear forces, *Vf(r)* uniformly inside the nucleus and then decreases exponentially in the surface region. These variants of the real part of the interaction potential are reproduced with the Woods-Saxon form factor. The form factor of the imaginary part depends on the energy of the incident particle. At low energy (less than 10 MeV), absorption occurs on the surface of the nucleus. In this case, the form factor *g(r)* is the derivative of Woods-Saxon $g(r) = 4a\frac{\partial f(r)}{\partial r}$, located on the surface of the nucleus. At higher energy, the contribution to the imaginary part is due to two mechanisms: the surface term described above and the volume term also described by the Woods-Saxon potential. In addition, by analogy with the spin-orbit potential, included in the shell model for describing the nucleus, the spin-orbit potential $V_{so}(r)$ is introduced to take into account the interaction of the nucleus spin $\vec{s}$ with its orbital momentum $\vec{l}$:

$$V_{so}(r) \propto \frac{1}{r}\frac{df(r)}{dr}\vec{l}.\vec{s} \tag{2.21}$$

The Coulomb potential $V_c(r)$ is also added to the potential *U(r)*. Since scattering is not sensitive to the specific form of charge distribution and, therefore, there is no need to consider it blurred at the boundaries, it is assumed that the Coulomb potential is the uniform distribution between two charges with radii corresponding to electron scattering [112]. The complex potential *U(r)* used in OM will then look like this:

$$U(r) = V_C(r) + Vf(r) + iW_V f(r) + iW_S g(r) + V_{SO}(r) \tag{2.22}$$

Thus, the analysis of the experimental data on elastic scattering presented in this paper is carried out in the framework of the optical model, which consists of three different potentials:

- coulomb potential V_c;
- the real part of potential V_c with the Woods-Saxon parameterization;
- the imaginary part of the potential *Wc* with the Woods-Saxon parameterization.

$$U(r) = V_C(r) - V(r) - iW_V(r).$$

The first term is the Coulomb potential.

$$V_C(r) = \frac{Z_p Z_t e^2}{2R_C}\left(3 - r^2 / R_C^2\right) \text{for r} < \text{R}_\text{C}$$

$$V_C(r) = \frac{Z_p Z_t e^2}{r} \qquad \text{for } r > R_C, \tag{2.23}$$

The real part is as follows:

$$V(r)f(r,r_v,a_v) = V_0\left[1+\exp\left(\frac{r-r_V}{a_V}\right)\right]^{-1}, \tag{2.24}$$

Imaginary volumetric part:

$$W_V(r)f(r,r_w,a_w) = W_0\left[1+\exp\left(\frac{r-r_W}{a_W}\right)\right]^{-1}, \tag{2.25}$$

Thus, the interaction potential can be rewritten in the form

$$U(r) = V_c(r) - V_o\left[1+\exp\left(\frac{r-r_V.A^{1/3}}{a_V}\right)\right]^{-1} - iW_o\left[1+\exp\left(\frac{r-r_W.A^{1/3}}{a_W}\right)\right]^{-1}, \tag{2.26}$$

It is important to note that equation (2.27) represents the potential of an "ordinary" OM. But, in the dispersion analysis of the incident particle, the central real potential is the sum of three terms, namely, the Hartree Fock potential V_{HF}, volume, surface and dispersed component:

$$U_c(R) = V_{HF}(E)f(r,r_{HF},a_{HF}) + \Delta V_v(E)f(r,r_v,a_v) + iW_v(E)f(r,r_v,a_v) \tag{2.27}$$

The geometric shape of the imaginary part and the corresponding dispersion term are the same if the parameters of the imaginary potential r_w, a_w are independent of energy.

Thus, further progress requires a detailed theory of the optical potential from the point of view of the components of the nucleus-nucleus interactions. It is clear that this is a very difficult task for many bodies, but significant progress has been made in the works of Brueckner [113] and Bethe [114]. The formal theory of nuclear reactions, developed by Feshbach [115,116], allows one to determine their contribution to the OP, but they cannot be evaluated practically.

In practice, it is often found that many sets of parameters give equally good relevant data, and then the question arises if one of them has more physical significance than the others, and if so, which is preferable. These ambiguities of parameters, as they are called, are of two main types, discrete and continuous. We will talk about this in detail in the next section.

2.4 Optical potential ambiguities

The phenomenological approach has undoubted simplicity, visibility, ease of use. But it is well known that unambiguously choosing the parameters of the optical potential that successfully describe the experimental data in the wide energy region of various colliding nuclei is a rather difficult task. Therefore, uncertainties arise in the choice of parameters of the interaction potential [117].

Some of them are associated with measurement errors, with incomplete data, for example, with a limited range of scattering angle.

In the analysis of elastic scattering of α particles with an energy of E ≈ 40 MeV on ^{40}Ar, ^{64}Cu, ^{208}Pb nuclei, it was shown that there is a so-called continuous ambiguity [118], which for OP consists in the fact that the description of elastic scattering of α- particles in the front hemisphere can be obtained using potentials for which the value $V_0 \exp(\frac{R_V}{a_V})$ is approximately the same.

The authors of [119], when studying the elastic scattering of α particles on nuclei from hydrogen to uranium at an energy of E 25 MeV, discovered the existence of a number of discrete families of real potentials that equally well describe the experimental data of angular distributions. This is the so-called discrete ambiguity.

The criterion χ^2 does not allow making an unambiguous choice of a set of potential parameters. As a rule, to obtain additional information from the reaction and to describe the data more adequately, various integral characteristics of the potential are introduced: volume integrals of the nuclear potential, root mean square radius of the potential, the position of the Airy minima depending on the energy of the incident particle.

The volume integral of the nuclear potential J is a key quantity in the classification of various sets of potential parameters. Volume integrals assist in

choosing one or another potential from a discrete set. Volume integrals characterize the intensity of the potential.

As a rule, volume integrals are calculated by the formula:

$$J_{V,W} = -\frac{4\pi}{A_p A_t}\int_0^\infty U_{V,W}(r) r^2 dr \tag{2.28}$$

where A_p and A_t are the mass numbers of the incident particle and the target nucleus, respectively. $U_{V,W}(r)$ - the potential for nuclear interaction. The minus sign in expression (2.28) is introduced so that the volume integral is positive in the case of an attractive potential. The value of the integral is normalized by dividing by the product A_p and A_t and is the number of interacting nucleon pairs of the target nucleus and the incident particle.

Mohr in his work [120] proposed the energy parameterization of volume integrals:

$$J_{V,W}(E) = J_{0,V,W} \exp(-(E - E_0)^2 / \Delta^2) \tag{2.29}$$

The parameters $J_{0,V,W}, E_0, \Delta$ are determined by comparison with experiment or with theoretical values.

Brown and Rho [121] proposed the following parameterization of the volume integral of the imaginary part of the potential

$$J_w(E_{cm}) = \begin{cases} 0 & if\, E_{cm} \le E_0 \\ \dfrac{J_0 (E_{cm} \quad E_0)^2}{(E_{cm} \quad E_0)^2 + \quad ^2} & if\, E_{cm} > E_0 \end{cases} \tag{2.30}$$

where E_0 is the energy of the first excited state. J_0 - saturation parameter. is a parameter that is determined from a comparison with experimental data [121, p.397] demonstrated good agreement between the obtained dependences of volume integrals on the energy of relative motion by the optical model and by the parameterization proposed by the authors.

The root mean square radii of action of the real ($\langle r^2 \rangle_V$) and imaginary ($\langle r^2 \rangle_W$) parts of the nuclear potential are determined as follows:

$$\langle r^2 \rangle_{V,W} = \frac{\int_0^\infty U_{V,W}(r) r^4 dr}{\int_0^\infty U_{V,W}(r) r^2 dr} \tag{2.31}$$

where $U_{V,W}$ is the real and imaginary parts of the nuclear potential. The root mean square radius characterizes the radius of action of the potential.

Volume integrals and root mean square radii are convenient quantities in the study of the energy dependence of the potential.

2.5 Double folding model (folding potential)

The potential nucleus-nucleus interaction can be determined microscopically, for example, by folding (by folding). The double-folding (DF) model is widely used with success to calculate the nucleus-nucleus interaction potential or nucleon-nucleus interaction potential [122]. Here, the real part *V(r)* of the microscopic potential is calculated by adding the nuclear densities of the частицы incident particle and the target nuclei with an effective force that represents the interaction between one nucleon of the incident particle and one nucleon of the target nucleus:

$$V(r) = \iint \rho_p(r_p)\rho_t(r_t)\upsilon(r_{tp})d^3r_p d^3r_t \qquad (2.32)$$

where *r* is the distance between the centers of mass of the nuclei and is the effective nucleon-nucleon force. Figure 2.1 shows the coordinate system for the double-folding model.

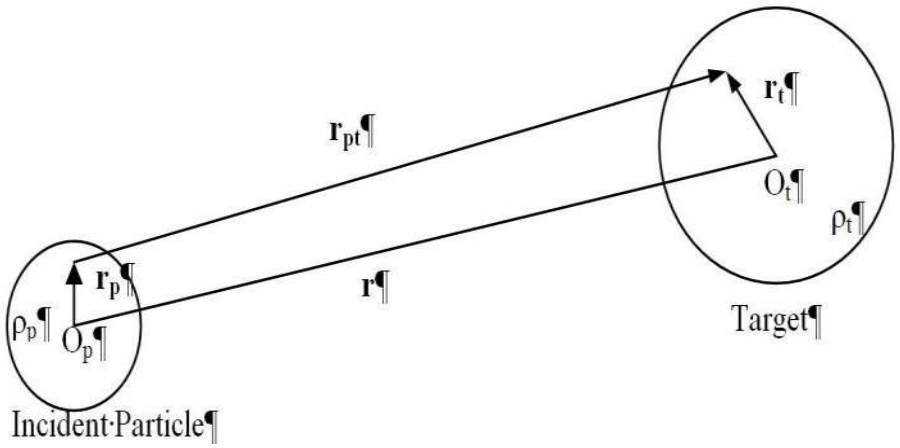

Figure 2.1 – The coordinate system of the double-folding model

Different nuclear densities, semi-microscopic or microscopic, can be introduced into the folding calculations. Nuclear densities can be obtained, for example, by solving the Hartree – Fock – Bogolyubov equation [123, 124] or by using the approximation of quasiparticle random phases with Skyrme forces [125]. The effective nucleon-nucleon forces that are used for folding are real. Usually, Yukawa interactions [126] in the form of M3Y [127] are used. Initially, these M3Y interactions were developed for the distorted wave method (DWM) from the analysis of reactions (p, p '), but they were also additionally used for the interaction of heavy nuclei at low and intermediate energies [128]. Later, new studies of nucleus-nucleus

reactions raised the question of the validity of M3Y interactions. In order to take into account the decrease in internucleon interaction with increasing nuclear density [129], the dependence of the densities was presented in [15, p.978]. The imaginary part of the potential *W(r)*, which is the absorption, is constructed using the phenomenological model, since the folding model is not adapted to this [128, p.183]. In general, parameterization with the Woods-Saxon form is used.

2.6 Coupled Channel Method

To analyze data on the scattering of α-particles on deformed nuclei, in which the first excited levels are collective in nature, it is advisable to use coupled channels method (CCM) [2, p. 42] of nuclear processes.

The task of describing nuclear processes is an essential multichannel task. The solution of the scattering problem is reduced to the solution of the many-particle Schrödinger equation with the corresponding boundary conditions, and the determination of differential and integral cross sections on the basis of this solution. In this method, the problem of solving the many-particle equation reduces to solving the system of Schrödinger equations:

$$\left[H_0\left(\vec{r}\right)+V_{nn}\left(\vec{r}\right)-E_n\right]f_n\left(\vec{r}\right)=-\sum_{n\neq n'}^{N}V_{nn'}\left(\vec{r}\right)f_{n'}\left(\vec{r}\right),\qquad n=1,2,\ldots,N \tag{2.33}$$

Where

$$V_{nn'}\left(\vec{r}\right)=\int\Phi_n^*\left(\vec{r_1}\ldots\vec{r_A}\right)V\left(\vec{r},\vec{r_1}\ldots\vec{r_A}\right)\Phi_{n'}\left(\vec{r_1}\ldots\vec{r_A}\right)d\vec{r_1}\ldots d\vec{r_A} \tag{2.34}$$

- matrix elements of the channel coupling, with the help of which the “meshing” of N single-particle equations occurs (2.33). The joint solution of this system of equations corresponds to the problem of the simultaneous description of the elastic and all inelastic interactions with the excitation of N states of the target nucleus in the presence of strong channel coupling. The channel coupling matrix elements (2.34) include the wave functions Φ_n of the excited states of the target nucleus; therefore, the analysis of experimental data in this method makes it possible to extract information on the properties of the nuclear structure on a unified basis. To apply this formalism to the description of inelastic scattering of particles by nuclei, we select from the full interaction of the incident particle with the target nucleus the potential of the mean field and the potential of residual interaction. Here we will follow the approximate procedure adopted in the collective model that the full interaction $V\left(\vec{r},\vec{r_1},\ldots,\vec{r_A}\right)$ is replaced by a nucleon potential $V\left(r,\theta,\vartheta;\alpha_{\lambda\mu}\right)$, which depends not only on the coordinates of the incident particle, but also on the collective variables of the target nucleus $\alpha_{\lambda\mu}$. This parameter determines the radius of the potential acting on the particle through the radius of the half-fall of the potential R_0 in the form:

$$R(\theta,\vartheta)=R_0\left[1+\sum\alpha_{\lambda\mu}\mathrm{Y}_{\lambda\mu}(\theta,\vartheta)\right] \tag{2.35}$$

Here, the deviation of the radius from spherical symmetry is decomposed in a complete orthonormal system of spherical harmonics $\mathrm{Y}_{\lambda\mu}$. Then,

$$V\left(r,\theta,\vartheta;\alpha_{\lambda\mu}\right)=\frac{V_0}{1+\exp\dfrac{r-R_0\left[1+\sum\alpha_{\lambda\mu}\mathrm{Y}_{\lambda\mu}(\theta,\vartheta)\right]}{a}} \tag{2.36}$$

Having expanded this expression in a Taylor series near the point (r-R_0) we have:

$$V\left(r,\theta,\vartheta;\alpha_{\lambda\mu}\right)=V\left(r-R_0\right)-R_0\sum_{\lambda\mu}\alpha_{\lambda\mu}\mathrm{Y}_{\lambda\mu}(\theta,\vartheta)\frac{\partial V\left(r-R_0\right)}{\partial r}+\ldots \tag{2.37}$$

The spherically symmetric part of the interaction of the incident nucleon with the nucleus $U_{cp}=V(r-R_0)$ is taken as the potential of the middle field, and the deviation of the form of the potential from the spherically symmetric is considered the residual interaction.

$$V_{\text{îñò}}=-R_0\sum_{\lambda\mu}\alpha_{\lambda\mu}\mathrm{Y}_{\lambda\mu}(\theta,\vartheta)\frac{\partial V(r-R_0)}{\partial R}+\frac{1}{2}R_0^2\left[\sum_{\lambda\mu}\alpha_{\lambda\mu}\mathrm{Y}_{\lambda\mu}(\theta,\vartheta)\right]^2\frac{\partial^2 V(r-R_0)}{\partial r^2}+\ldots \tag{2.38}$$

Here we will consider the rotational version of the collective model of inelastic interaction, therefore, passing from the laboratory coordinate system to our own system, we write:

$$\sum_{\lambda\mu}\alpha_{\lambda\mu}\mathrm{Y}_{\lambda\mu}(\theta,\vartheta)\to\sum_{\lambda}\beta_{\lambda}\mathrm{Y}_{\lambda 0}(\theta',\vartheta') \tag{2.39}$$

In this case, the distribution of matter in the core is considered axially symmetric, - the parameters of static deformation.

In the framework of this approach, the elements of the T or S matrix are calculated and summed over all final states and averaged over the initial states i, we obtain the expression for the differential cross section:

$$\frac{d\sigma}{d\Omega}=\frac{\mu}{2\pi\hbar}\frac{K_f}{k_i}\sum_{LM}\frac{2I_f+1}{(2I_i+1)(2L+1)}\left|T_{LM}\right|^2 \tag{2.40}$$

In formula (2.37), the spherically symmetric part of the potential describes elastic scattering, and the subsequent terms corresponding to the deviation of the potential from the spherically symmetric describe inelastic processes.

2.7 Distorted Wave Method

To describe direct mechanisms, the method of distorted waves (DWM) or the distorted waves Born approximation (DWBA) was developed in the middle of the last century. This is the most common, although not the only model for describing direct nuclear reactions [6, p.342].

DWM can be considered as a generalization of OM to inelastic channels. Studying nuclear reactions, it is no longer possible, as in the case of elastic scattering, to neglect the internal structure of interacting particles. The wave function in each reaction channel is represented as (for example, for the input channel)

$$\Psi_i = \tilde{\Psi}_a \tilde{\Psi}_A \chi_i \tag{2.41}$$

where $\tilde{\Psi}_a$ and $\tilde{\Psi}_A$ are the wave functions describing the incident particle and the target nucleus, χ_i is the wave function that describes the relative motion of particles in the channel.

The fact that the incident particle transfers its energy and momentum to a small number of degrees of freedom of the nucleus is used in the DWM. This allows us to obtain an approximate solution of the many-particle Schrödinger equation using the perturbation theory. The complete Hamiltonian of the system is written as

$$\mathrm{H} = \mathrm{H}^0 + \mathrm{H}^{\mathrm{res}} \tag{2.42}$$

where H^0 is the Hamiltonian of a system consisting of two particles, the interaction between which is described by the optical potential V^{opt}, H^{res} is the Hamiltonian-residual interaction, which is considered as a small perturbation that transfers the system to a final state.

The interaction process is thus divided into 3 stages:

- the movement of the incident particle in the "distorting" optical potential of the target nucleus;
- transfer of nucleons under the influence of residual interaction;
- the movement of the emitted particles in the field of the final nucleus.

The amplitude of the scattered wave has the form

$$f(\vec{k}_a, \vec{k}_b) = \frac{\mu_b}{2\pi\hbar^2} \left\langle \Phi_f(\vec{k}_b) \middle| H^{res} \middle| \Psi_i(\vec{k}_a) \right\rangle \tag{2.43}$$

where μ_b is the reduced mass, $\vec{k}_a$ and $\vec{k}_b$ are the wave vectors of the input and output channels, $\Psi_i(\vec{k}_a)$ and $\Phi_f(\vec{k}_b)$ are the wave functions in the input and output

channel, $\Phi_f(\vec{k}_b)$ and is the optical wave function. In the Born approximation, the exact wave function $\Psi_i(\vec{k}_a)$ is replaced by the optical wave function. The expression for the section is:

$$\frac{d\sigma}{d\Omega}^{DWM} = \frac{\mu_a k_b}{\mu_b k_a}\left|f(\overline{k_a},\overline{k_b})\right|^2 \tag{2.44}$$

All of the above formulas of the distorted wave method are embedded in the FRESCO program [130] with the help of which theoretical cross sections were calculated.

2.8 Nuclear rainbow formalism

Based on the analogy between the scattering of light and particles, we can conclude that in rainbow scattering there is an angle near which classical trajectories condense, which leads to an increase in the intensity of scattered particles near the angle of the rainbow. Rainbow scattering is observed at $\frac{d\Theta}{dl} = 0$. If we neglect absorption, the cross section near the rainbow angle is determined as follows [131]:

$$\frac{d\sigma}{d\Omega}(\theta \approx \theta_r) \approx k^{1/3}\frac{2^{5/3}\pi b_r}{\sin\theta}\left|\frac{d^2\Theta}{db^2}\right|^{-2/3}[Ai(z)]^2 \tag{2.45}$$

$$z = \pm\frac{\mathrm{sgn}(C)2^{1/3}(\theta_r-\theta)k^{2/3}}{\left|\frac{d^2\Theta}{db^2}\right|^{1/3}} \tag{2.46}$$

where θ_r is the rainbow angle, $C = \frac{1}{2k^2}\frac{d^2\Theta}{db^2}$, b_r is the collision parameter at which the rainbow angle is observed, Ai (z) is the Airy function. For scattering angles smaller than the rainbow angle, the Airy function has the form of oscillations. At the scattering angle closest to the rainbow angle, an extremum is observed, which is interpreted as the primary rainbow. The following observed extrema correspond to higher order rainbows. If the argument of the Airy function is positive, an exponential decay is visible.

To observe the phenomenon of a nuclear rainbow, several conditions are required:

A) The particle energy should be large enough.

In the classical approximation, the deviation function is determined by the expression [131, p.607]:

$$\Theta(b) = \pi - 2b\int_{r_0}^{\infty} drr^{-2}[r^2(1-\frac{U(r)}{E}) - b^2]^{-1/2} \quad (2.47)$$

We introduce the notation:

$$u(r) = r\sqrt{1-\frac{U(r)}{E}} \quad (2.48)$$

It can be shown that [132]:

$$\frac{du}{dr} > 0,$$

then for energy we get the following expression:
E_{crit}=[U(r) +r/2d/drU(r)]$_{max}$

$$E_{crit} = \left[U(r) + \frac{r}{2}\frac{d}{dr}U(r)\right]_{max} \quad (2.49)$$

where $U(r)$ is the nuclear potential.

Rainbow scattering is observed at $E > E_{крит.}$. When $E < E_{крит.}$ orbiting is observed, that is, twisting near the power center.

B) For the appearance of rainbow effects, a slight transparency of the core in the region of small angular momenta is required.

In the 19th century, astronomer George Airy first mathematically described a rainbow phenomenon in optics using the so-called Airy function (figure 2.2). There are primary extremes corresponding to the maximum deviation angle, and extrema of higher orders. Subsequently, this function was successfully used in nuclear physics to describe scattering processes.

The full spectrum of Airy minimums can be observed in systems without absorption. But in real nuclear processes there is absorption, and single Airy minima are observed in angular distributions. For example, in elastic scattering of nuclei such as ^{12,13}C and ^{16}O in angular distributions, more than one broad maximum can manifest in the region of angles behind the Fraunhofer diffraction. Often such extremes are interpreted as primary, secondary, and higher order rainbows. Only by experimental data it is often impossible to accurately determine the serial number of the rainbow maximum. This is due to the fact that the primary rainbow can be in the region of angles above 180° in the center of mass system. The quality of the experimental data does not always clearly identify the Airy extremum. In the analysis of identical particles, due to the symmetry properties, the region up to 90° remains informative. This leads to airy ambiguities. Different potentials corresponding to different Airy

functions (shifted relative to each other) show different serial numbers of the Airy structures observed and at the same time give a similar description of the data [133].

This problem was first considered in [134,135]. To solve this difficulty, it was proposed to construct the energy dependence of the Airy positions of the minima. During the analysis, it was found that the minima are clearly grouped and lie practically on straight lines. Each group has a rainbow maximum number.

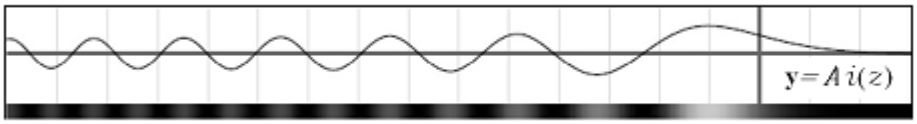

Figure 2.2 – Airy function

In [136] it was shown that the position of the primary Airy minimum is determined as follows:

$$\Theta_r \cong \Theta_r^C - 0.56(\frac{R_V}{a_V})^{1/2}\frac{V}{E} \tag{2.50}$$

$$\Theta_r^C = 2arctg(\frac{V_C}{2E}) \tag{2.51}$$

$$\Theta_r^N = -0.56(\frac{R_V}{a_V})^{1/2}\frac{V}{E} \tag{2.52}$$

where Θ_r^C is the angle of the Coulomb rainbow. The Θ_r^N value is the angle of the nuclear rainbow. R_V , a_V , V - radius, diffuseness, depth of the real part of the nuclear potential of the Woods-Saxon type, E - energy of the incident particle. The authors of [136, p.307] indicate an inverse relationship between the position of the angle of the nuclear rainbow and the energy of the incident particle.

3 METHODOLOGY AND CHARACTERISTICS OF OF EXPERIMENTAL SETUPS

The simultaneous measurement of cross sections, angular and energy distributions of scattering and reaction products occurring under the action of deuterons and α particles with an energy of ≤ 10 MeV/nucleon at the nuclei, in our case ^{7}Li, ^{11}B, imposes certain requirements on the quality of the experimental setup and equipment. High energy and angular resolution, selectivity for the type of detected particles, their wide dynamic energy range, the possibility of measurements in a wide range of angles, including the region of extremely large angles — these are the main criteria that determine the effectiveness of the experimental complex for studying the structure of nuclei and the mechanism of nuclear reactions.

The experimental results, which form the basis of the work, were obtained on the extracted beams of the U150M cyclotron INP (Kazakhstan). Further, in the following sections, we give the characteristics of this cyclotron.

3.1 Characteristics of experimental setup

3.1.1 Cyclotron U-150M

The U-150M isochronous cyclotron of the Institute of Nuclear Physics of the Republic of Kazakhstan (INP RK) allows accelerating protons up to 30 MeV, deuterons up to 25 MeV, ^{3}He up to 60 MeV and α particles up to 50.5 MeV [137].

Charged particles in a cyclotron are formed in a source located in the central part of the chamber in an arc discharge when a corresponding gas (hydrogen, deuterium, helium-3, helium-4) is supplied. Their acceleration occurs in the interpolar space of a one and a half meter magnet at the time of the passage of particles between the dees.

When setting the operating parameters for particle acceleration, special attention is paid to the mode of operation of the ion source, its duty cycle, the microstructure of the current pulse, as well as the quality of the beam to the target. Such optimization of the spatial and temporal characteristics of the beam made it possible to significantly reduce the level of various noise and the uneven loading of electronic equipment.

The energy and energy spread in the beam are determined by measuring the energy spectrum of particles elastically scattered from a thin gold target mounted in the scattering chamber of the laboratory of nuclear processes of the INP RK [138]. In this case, when measuring at small angles (about 10 °), errors associated with inaccuracies in the knowledge of the target thickness and the angular dispersion of particles in the beam can be avoided. For the absolute calibration of the energy scale, a “triple” alpha source consisting of ^{241,243}Am + ^{244}Cm was used [139].

The error in the absolute value of the energy was no more than 1%, the error in measuring the energy spread of the beam was determined mainly by the energy width of the channel and did not exceed 30 keV. According to measurements, the energy spread in the beam was about 1%, so it made the main contribution to the total energy resolution, which was about 150 keV for deuterons with an energy of 14.5 MeV.

In the measurements, a beam duty cycle of 2 was used, which ensures the minimum load of the equipment at currents on the target of 0.1 - 0.3 μA.

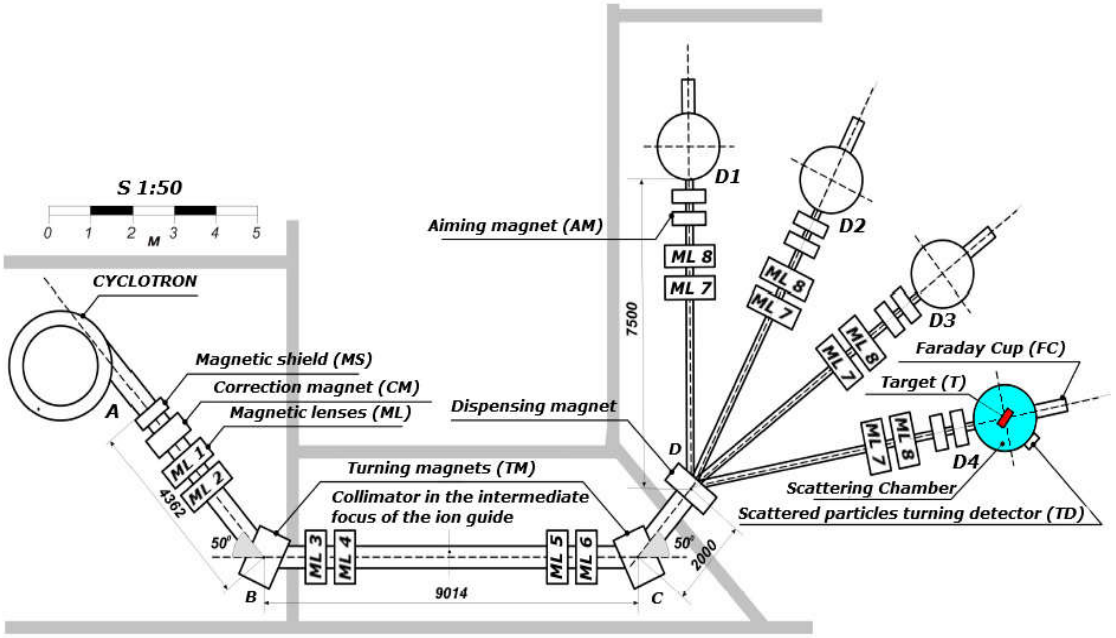

A, B, C, D - characteristic points of rotation of the beam of accelerated ions

Figure 3.1 – Scheme of transportation of a cyclotron ion beam to a scattering chamber

The scheme for transporting the accelerated ion beam from the cyclotron chamber to the scattering chamber [140], located 24 m from the beam exit is shown in figure 3.1. It includes a system of quadrupole lenses, two rotating lenses, a diverging lens, two targeting magnets, and a collimator system. All these installations, together with targeting and correction elements, provide a beam of charged particles with an angular solution of no more than 0.4° and a diameter of 3 mm on the target. The alignment of the collimator and the center of the scattering chamber relative to the axis of the ion guide was carried out by the optical method and was controlled using twelve quartz screens and television cameras transmitting the image to the cyclotron control panel. Experiments on beams of accelerated ^{3}He ions and α particles were carried out on the fourth channel of the U150M (D-4) accelerator shown in figure 3.1.

3.1.2 Scattering chamber at the U-150M cyclotron

In solving experimental problems in the physics of nuclear reactions, it is necessary to measure the angular distributions of elastic and inelastic scattering and nuclear reactions in a wide range of scattering angles, including angles less than 10° [141].

The prototype of the scattering chamber on the U-150M cyclotron was the experimental setup described in Ref. [142]. A diagram of the installed camera on the U150M cyclotron is shown in figure 3.2.

The chamber made of stainless steel consists of a hollow cylinder B with an inner diameter of 715 mm, a height of 370 mm and the so-called “pocket” A, which is an additional volume elongated along the beam. In the main volume, three (E-E) silicon telescopes of silicon semiconductor detectors are installed on the camera in two independent remotely controlled angular displacement drives, which cover scattering angles of 10–70 ° with an accuracy of ~ 20′

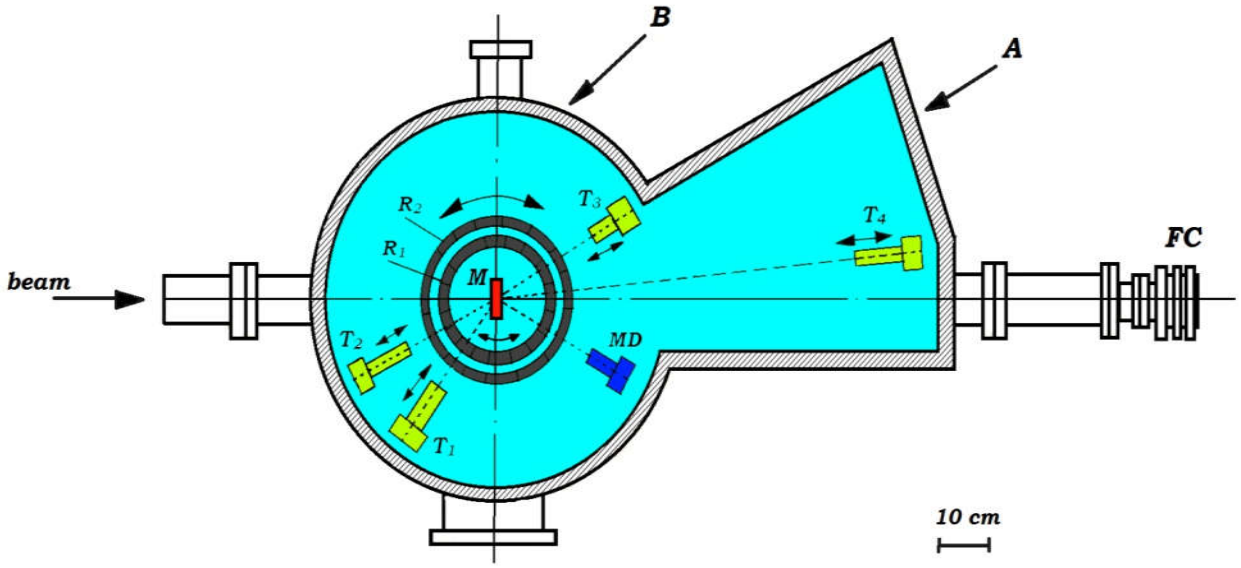

R1, R2 - independently rotating rings driven by stepper motors; M is the target; E – ΔE detectors attached in pairs to the rings R1 and R2; T1, T2, T3, T4 - telescopes of FC - Faraday Cylinder; MD– detector for scattered beam monitoring

Figure 3.2– Scattering chamber diagram

If necessary, the distances of telescopes from targets can be remotely varied within 100 ÷ 350 mm. In volume A, a fourth telescope with an independent drive is installed, designed for measurements in the range of departure angles 2 ÷ 20°. A significant distance from the target (1000 mm) allows 10-15 times to reduce the loading of the recording equipment, due to the processes of elastic scattering during measurements at extremely small angles. There are flanges on the cylindrical part of the chamber for technological purposes and for connecting a gas target. On the top cover of the camera there is a viewing window with a diameter of 290 mm, which allows you to visually control the experimental situation (installation angles of telescopes, the state of targets, etc.).

A flange with high vacuum electrical connectors is mounted on the bottom of part B; inside this part, a mounting plate with a diameter of 685 mm is installed on three adjustment screws. A device is mounted on the mounting plate for simultaneous rotation of the detectors 4 and 5 relative to the target and, independently of them, the movement of the detectors 7 and 8, which is carried out by rotating the rings 3 and 1, are mounted on the mounting plate. Detectors 4 and 5 are mounted on brackets to ring 3, and 7 and 8 to ring 1. Two stepper motors are used to rotate rings 1 and 3.

In order to reduce the influence of background radiation from the Faraday cup on the detectors, the system was reconstructed. A unit containing a Faraday cylinder was manufactured and tested. For this, the diameter (up to 190 mm) of the ion duct, where the Faraday cylinder was placed, was significantly increased, which avoided the penetration of accelerated beam ions on the walls of the ion duct both during extraction and tuning of the beam, and directly during the measurement of cross sections. The Faraday Cylinder is located at a considerable distance from the target node and the recording detectors. A new version of the Faraday cup is 1 m away from the reaction chamber. Inside the ion duct where the Faraday cup was mounted, a beam current control system was designed and created that is independent of the Faraday cup for constant monitoring and correction of the current on the target during measurement.

For optimal focusing of the beam of accelerated ions on the target, the input collimator is selected with a diameter of 3 mm at a base distance of 440 mm. To quickly change targets, change its orientation with respect to the beam, measure the thickness and periodically monitor its thickness during the experiment, the target unit device — was manufactured and mounted on a special holder (crosspiece).

The camera was aligned using a laser beam and consisted of bringing an extended collimator, telescopes, a target assembly, and a Faraday cup to the geometrical axis of the ion guide, as well as installing them using the level in the horizontal plane of the mounting plate and the base plate of the far telescope.

3.1.3 Particle registration and identification system

The system of registration and identification of reaction products is based on ($\Delta E \div E$) - a method based on the simultaneous measurement of the specific energy loss of a charged particle in a substance dE/dx and its total kinetic energy E. This method is based on the famous Bethe-Bloch equation connecting the energy of the charged particle with its specific ionization in matter:

$$\frac{dE}{dx} = \frac{kMz^2}{E}, \tag{3.1}$$

where k is a constant value that weakly depends on the types of particles, M and z are the mass and charge of the emitted particles.

It can be seen from this relationship that while measuring E and dE/dx, each sort of particles occupies its own hyperbola in the coordinate space $(E, \Delta E)$, which allows us to select the desired sort of particles in the experiment. A typical view of the projection onto the E-ΔE plane is shown in figure 3.3. As can be seen from this figure 3.3, for the lightest nuclei ^{1}H-^{4}He, the product Mz^2 varies discretely from 1 to 16 and is a fairly favorable identification parameter.

In the telescope of the detectors, ORTEC surface-barrier silicon detectors were used as “shot” ΔE counters with a working layer thickness of 15, 50, 100 μm with thin input (~ 40 μg/cm^2 Au) and output (~ 40 μg/cm^2 Al) windows, energy resolution in the telescope of the detectors which is 25-50 KeV for α particles.

ORTEC detectors made of high-purity silicon of 1 and 2 mm thickness were also used as a stop counter.

All measurements were carried out at the measuring and computing complex of the laboratory, the basis of which is a multi-dimensional process analysis system based on ORTEC and PC/AT electronic units [143].

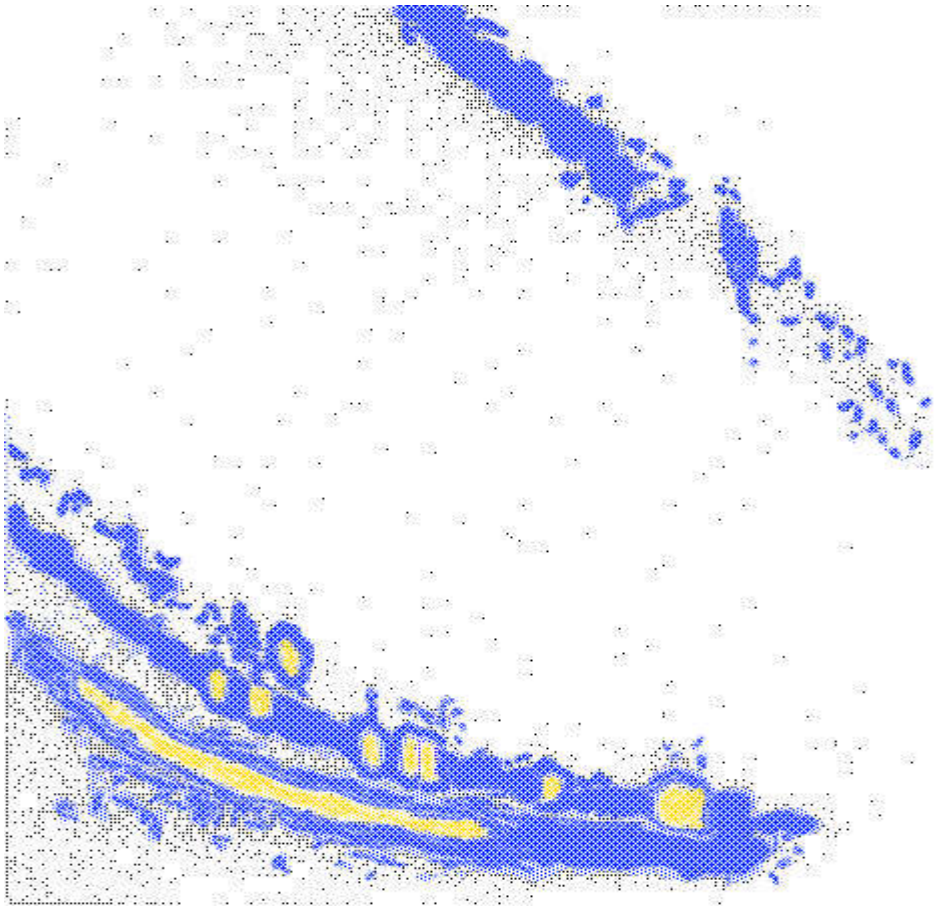

The lower locuses are singly charged particles, the upper ones are doubly charged

Figure 3.3 – Typical ΔE-E distribution of charged particles

Figure 3.4 shows the block diagram used in the experiments of an electronic installation structurally consisting of three measuring lines and a multivariate programmable analysis system.

In the first spectrometric line, the signals from the ΔE and E detectors passing through charge-sensitive preamplifiers (PA) are fed to spectrometric amplifiers (SA) with an active filter and pole compensation by zero, which allow avoiding distortion of the spectra arising from overlapping emissions of one of the opposite sign of the signals and reduce dead time during overload [144]. The spectrometric signals in the amplifiers are formed by differentiation schemes and 4-fold integration, and this form of signals turned out to be the most optimal with respect to the noise of the spectroscopic setup and its temporal resolution.

Amplifiers have two spectrometric outputs - direct, for time reference and delayed by 2 μs. From the direct output, bipolar spectrometric signals are sent to

single-channel analyzers (SCA), which produce standard logic signals with adjustable delay, which then pass to the coincidence circuit (CC) with a time resolution of 1 μs. The logical signals generated by the coincidence circuit were then fed to the control inputs of two analog-to-digital converters (ADC-E and ADC-*ΔE*). The presence of a low level signal at the ADC control input served as a sign of the beginning of conversion of the amplitude of the spectrometric signal to the ADC analog input into a code.

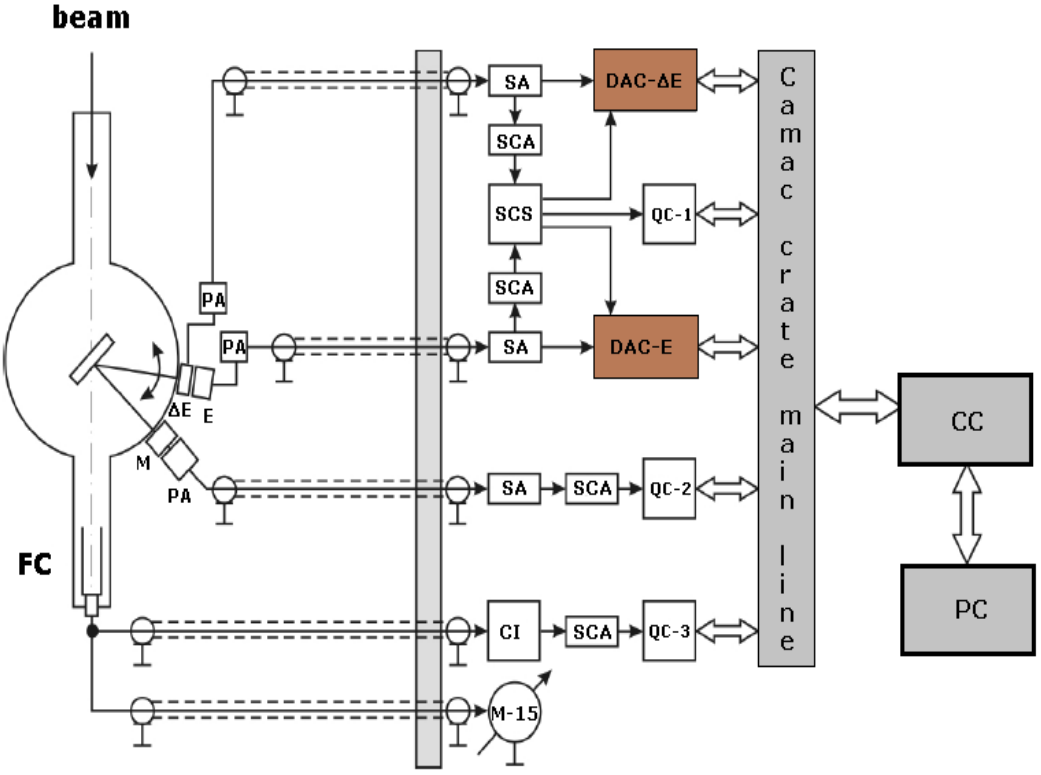

PA-pre amplifiers; SA– spectroscopic amplifiers; SCA – single channel analyzer, SCC- Slow coincidence circuit; DAC-Digit amplitude converter; QC –quadruple pair counters with 32 bits capacity; CC– crate controller; FC – Faraday cup, CI – current integrator, PC – personal computer

Figure 3.4 – Block diagram of electronics for the DE-E technique

At the end of the conversion, the ADC puts the received code into its data register and issues a request for interruption along the CAMAC crate. Single-channel analyzers, in addition to timing, perform another function - they were used as amplitude differential discriminators to select the dynamic range of amplitudes. The efficiency of the registration system was determined by dynamically comparing the number of resolution pulses from the coincidence circuit (QC-1, which is quadruple pair counters) to the number of events recorded by the interrupt processing program.

The second line is designed to monitor the quality of the measurement system, which was carried out by a spectrometer located at an angle of 300 relative to the incident beam, according to the counting intensity of particles elastically scattered by the target under study. Particles were recorded with a surface-barrier silicon detector. Such a monitoring method allows one to correctly take into account both the change

in the particle beam current and the change in the effective thickness of the target with a possible migration of the maximum beam intensity over its area. Pre-amplified signals from the detector through amplifiers and integrated discriminators were applied to the conversion circuits (QC-2). During the measurement, the relationship between the account number of the monitor channel and the current integrator was carried out automatically, the value of which was kept constant within 1%.

The third line is used to measure the total number of particles passing through the target during the exposure time, consists of a Faraday cup (FC), taken from the scattering chamber at a distance of 1 m and recording the total charge of particles that got into it. A Faraday cylinder mounted at an angle of 0° relative to the axis of the beam was connected through a M-95 type nanoammeter with a current integrator, converting this charge into a number of pulses recorded by a counter (QC-3) with an operating current measurement range of 0.5 nA-10 μA and a constant component value (1.58 ± 0.02) × 10^3μC/count [145]. In the latest series of measurements, an ORTEC current integrator was used, the counting characteristic of which depends on the number of charges in a linear manner.

The error in determining the integrator constant, which determines the number of particles passing through the target, is ± 1% [146].

3.2 Processing of experimental data

The processing of experimental data conventionally consists of three stages: energy calibration of the spectra and identification of peaks corresponding to the excited levels of the nucleus, calculation of peak areas taking into account the background, and calculation of reaction cross sections and errors in their determination in the laboratory system (l.s.) and the center of mass system (c.m.s.)

The energy spectra were calibrated (figure 3.5) by the position of the elastic peak at different angles using the LISE ++ [147] and Origin programs.

The absolute values of the differential cross sections for the interaction (mb/sr) of particles with nuclei are usually calculated by the formula:

$$\frac{d\sigma_{LS}}{d\Omega}(\Theta_{LS}) = \frac{NAk_1k_2}{N_{\text{int}}\Omega\eta C d_{eff}} \tag{3.2}$$

where N is the number of particles detected at a given angle θ_{ls}, A is the mass number of the target nucleus, k_1 is the miscalculation coefficient of the equipment, k_2 = 0.531*10^{-6} is the normalization constant, N_{int} is the number of readings of the current integrator during the exposure time,Ω is the solid angle (sr), C is the relative content of the studied isotope in the target, ηis the integrator constant (μC/count), and d_{eff} is the effective thickness of the target (mg/cm^2) located at an angle φ to the incident beam.

The error of the absolute values of the differential cross sections was determined as the error of indirect measurements. The absolute error in the laboratory coordinate system is calculated from the relation

$$\Delta \frac{d\sigma(\Theta_{LS})}{d\Omega} = \frac{d\sigma(\Theta_{LS})}{d\Omega} \delta_{LS} \tag{3.3}$$

where $\delta_{LS}$is the relative mean square error, having the form:

$$\delta_{LC} = \left[(\delta N)^2 + (\delta N_{\text{int}})^2 + (\delta\Omega)^2 + (\delta d_{eff})^2 + (\delta C)^2\right]^{1/2} \tag{3.4}$$

where $\delta N, \delta N_{\text{int}}, \delta\Omega, \delta d_{eff}, \delta\tilde{N}$ are the relative errors of the quantities from (3.2).

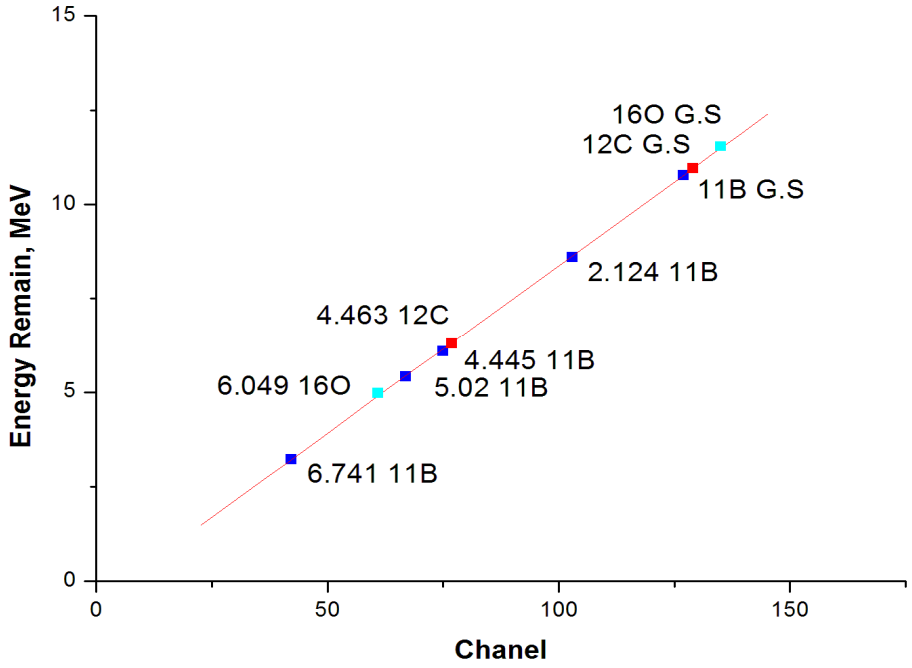

Figure 3.5 – Calibration of the energy spectrum by elastic scattering of deuterons by ^{11}B

The largest contribution is made by: a) statistical errors $\delta N = (1/N)^{1/2}$, which are 1-5% for elastic scattering and 1-10% for inelastic and reaction; b) the error in determining the thickness of the target (5-7%); c) calibration error of the current integrator (~ 1%). Errors in the determination of the remaining components (3) amounted to ~ 1%.

The conversion of the cross section values from the laboratory to the center of mass system is performed on the basis of the known kinematic relations:

$$\frac{d\sigma_{CM}}{d\Omega}(\Theta_{CM}) = G(x, \Theta_{LS}) \frac{d\sigma_{\ddot{e}\tilde{n}}}{d\Omega}(\Theta_{LS}) \tag{3.5}$$

$$G(x, \Theta_{LS}) = \frac{(1 - x^2 \sin^2 \Theta_{LS})^{1/2}}{(x \cos\Theta_{LS} + (1 - x^2 \sin^2 \Theta_{LS})^{1/2})^2} \tag{3.6}$$

$$\delta^2 = \frac{ab}{AB}\left[1+(1+\frac{a}{A})\frac{Q}{E_{LS}}\right]^{-1} \tag{3.7}$$

$$\Theta_{CM} = \arcsin(x\sin\Theta_{LS}) + \Theta_{LS} \tag{3.8}$$

here a, b, A, B are the masses of particles from the reaction $A(a,b)B$, Q is the reaction energy, E_a is the energy of the incident helions. The relative mean square error δ_{CM} of the absolute value of the cross sections (3.5) in c.m.s. defined as:

$$\delta_{CM} = (\delta_G^2 + \delta_{LS}^2)^{1/2} \tag{3.9}$$

where

$$\delta_G = \frac{1}{G}\left[(\frac{dG}{d\Theta})^2(\Delta\Theta_{LS})^2 + (\frac{dG}{dE_a})^2(\Delta E_a)^2 + (\frac{dG}{dQ})^2(\Delta Q)^2\right] \tag{3.10}$$

Here are absolute errors in determining the angle of registration of the emitted particle, beam energy, and reaction energy, respectively.

Comparisons of the accuracy of determining the cross sections with the well-known ones, as well as their multiple evaluations in different series of measurements, make it possible to attribute the obtained differential cross sections for scattering to an accuracy of no worse than (7-10)%. The relative errors of the measured cross sections are determined by the statistical accuracy of 1–3%, with the exception of the inelastic cross sections at minima at large angles, where it reached 7%.

A program was developed and created for converting the one-dimensional spectrum of Win EdE into a digital format or an analogue of the Origin graphics editor. Conversion is necessary for accurate calculation and separation of states for various reactions of double peaks, in cases where a direct analysis of these states is not possible. The sum of the peaks for such states was extracted using the Gaussian function, and always had a fixed peak width, since the energy resolution for the peak remains fixed and practically does not change from angle to angle and is tied to the resolution of the detector. This method showed that for a fixed peak width, the output differential cross sections are less prone to fluctuations than an analysis with different widths. This program was created to simplify the translation of analog data into a digital equivalent. The purpose of creating this program was to reduce the mechanical work of translating data, as well as the accelerated receipt of ready-made data for calculating cross sections.

The main stages of the program to convert the spectrum from screen to digital:

1) capture screen information of the spectrum;

2) convert to table;

3) saving it in the form of a graph or a numerical array.

Key features of the program:

a) converting the spectrum from analog to a numerical array;

b) the ability to capture images of both one-dimensional and two-dimensional spectrum with its subsequent transformation into a moving spectrum;

c) continuous operation, with automatic switching.

The result of writing this program was a reduction in spectrum translation time. The comparative manual translation time for a spectrum of 256 channels is 10 minutes per file. With the use of this program, automation allowed to reduce the time of spectrum enumeration to 30 seconds, and also to make the process pipelined, switching from file to file occurs automatically requiring minimal user participation.

3.3 Test of the surface barrier VPE GaAs detector

3.3.1 Characterization of the surface-barrier VPE GaAs sensors on α-sources

Schematic design of the sensor and electrical specifications.

The experimental samples of the detectors were fabricated on GaAs epitaxial layers with a carrier concentration of 3 10^{11} cm^{-3} at the Moscow Institute of Steel and Alloy [148,149]. The films were grown by the method of chloride gas-phase epitaxy (Ga-$AsCl_3$-H_2 system) on two-inch n^{++} - GaAs substrates with an orientation of <100>. The Schottky barrier based on the Pt/TiN/Au system with a thickness of 0.1 μm was used as a rectifying contact. The electrophysical properties of such a contact were considered earlier in [150, 151]. Contact pads were formed by dusting the TiN/Au metallization system followed by galvanic deposition of thick Au (3-4 μm). The Ni/AuGe/Au system was used as an ohmic contact to the n ++ substrate. Isolation of the active region was carried out by mesa technology using reactive ion beam etching in CF_4 plasma. As a passivating coating, polyimide was used.

The basic design and photograph of the surface-barrier GaAs sensor are shown in figures 3.6 and 3.7.

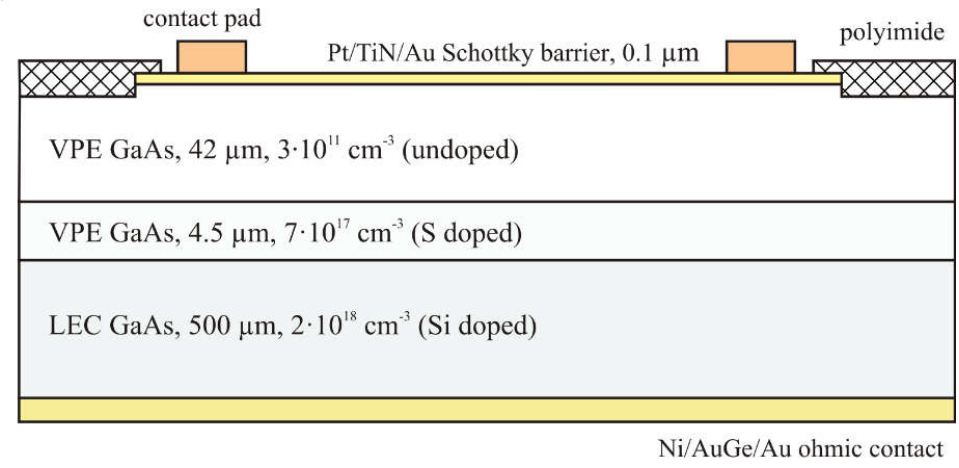

Figure 3.6 – Schematic design of the surface-barrier GaAs sensor

The manufactured detectors demonstrated very low dark currents for GaAs: at a reverse bias of 100 V, the dark leakage currents were 1.8 nA, respectively. The specific capacity of the fabricated structures at zero bias was 280 pF/cm^2, which corresponds to the complete depletion of the working layer.

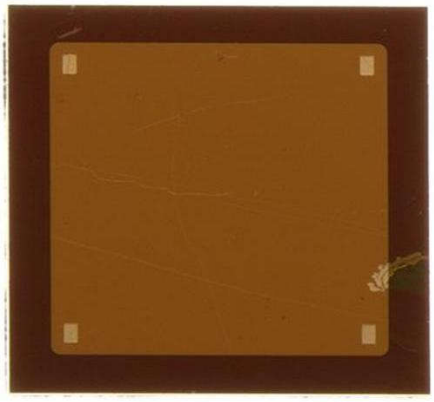

Figure 3.7 – Photo of the surface-barrier GaAs sensor
(active region size 5 mm × 5 mm)

To assess the spectrometric characteristics of the fabricated surface-barrier detectors, the spectra froam the ^{238}Pu α source were measured. The measurements were carried out at room temperature. The detectors were located at a distance of 70 mm from the α source in a special vacuum chamber at a residual pressure of 1.33 Pa to reduce the contribution of oblique ranges in the "dead" layer of the detector and to reduce the energy loss of α particles in air. Measurements of the efficiency of charge collection depending on the α-particle energy were carried out using a ^{226}Ra source based on the E-E methodology of the Institute of Nuclear Physics ME RK. The detector was connected to a 512-channel analyzer through a low-noise charge-sensitive preamplifier and an amplifier-former.

Irradiation was carried out in a special vacuum chamber with a residual pressure of 10^{-2} mm. Hg. column and room temperature, the beam of α particles collimated. Figure 3.8 shows a typical spectrum of the ^{238}Pu α-source obtained using GaAs detectors with a reverse bias of 40 V (spectrum acquisition time 30 min). As can be seen, peaks from α particles with energies of 5.456 and 5.499 MeV are clearly resolved in the spectrum. The energy resolution of the detectors (FWHM - full width at half maximum) was estimated on the 5.499 MeV line, and its average value was 22.3 keV with a generator peak width of 6.0 keV.

For all the studied detectors, the measured dependence of the charge collection efficiency, depending on the bias voltage applied to the detectors, shown in figure 3.9, behaved in a similar way. It can be seen from the figure 3.9 that the efficiency of charge collection from the longest running particles reaches a maximum at a supplied voltage of 60 V, which leads to a choice of the magnitude of the working bias of at least 65 V. It is obviousaa that for the developed detectors, despite the complete depletion of the working layer, a strong dependence is observed the efficiency of charge collection from the energy of alpha particles. This behavior of the detector

characteristics is explained by the asymmetry of drift lengths in GaAs. According to the Ramo-Shockley theorem, for the case when the range of α particles is comparable with the thickness of the working layer, the charge collection efficiency is determined by both types of carriers. Thus, due to the small drift length of the holes, the efficiency of charge collection will largely depend on the collection of the hole component of the signal, which is determined by the range of α particles. In our case, the estimate of the ranges using the GEANT4 program for alpha particles with energies of 4.784, 5.489, 6.002, and 7.687 MeV in GaAs, respectively, gives values of 18, 21.5, 24, and 34 μm (figure 3.10).

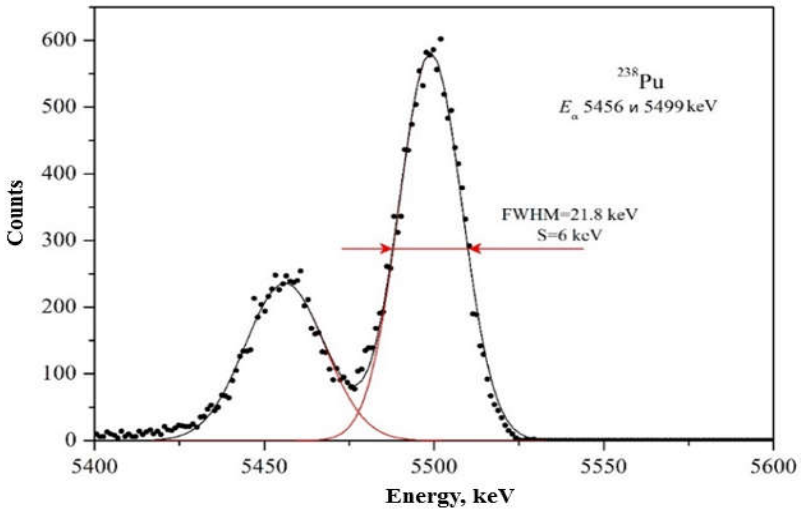

Figure 3.8 – Energy spectrum from a ^{238}Pu source, measured using developed surface-barrier GaAs detectors

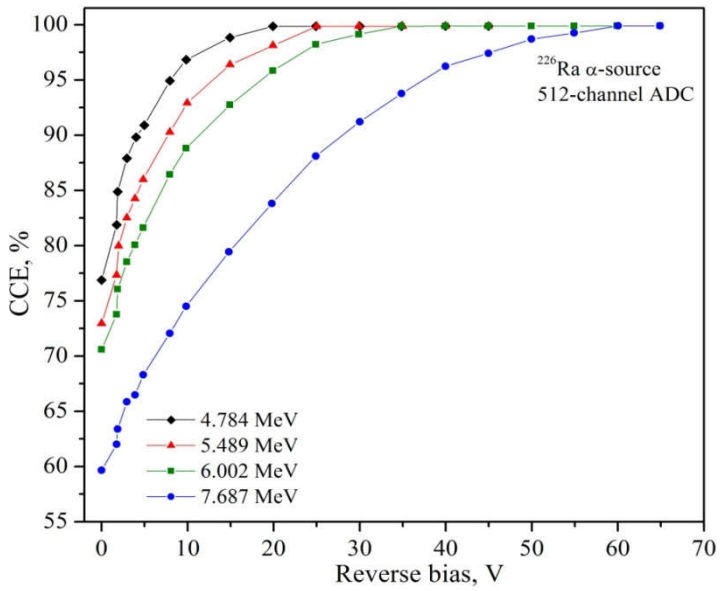

Figure 3.9 – The efficiency of charge collection of manufactured samples of detectors, measured for various source lines ^{226}Ra

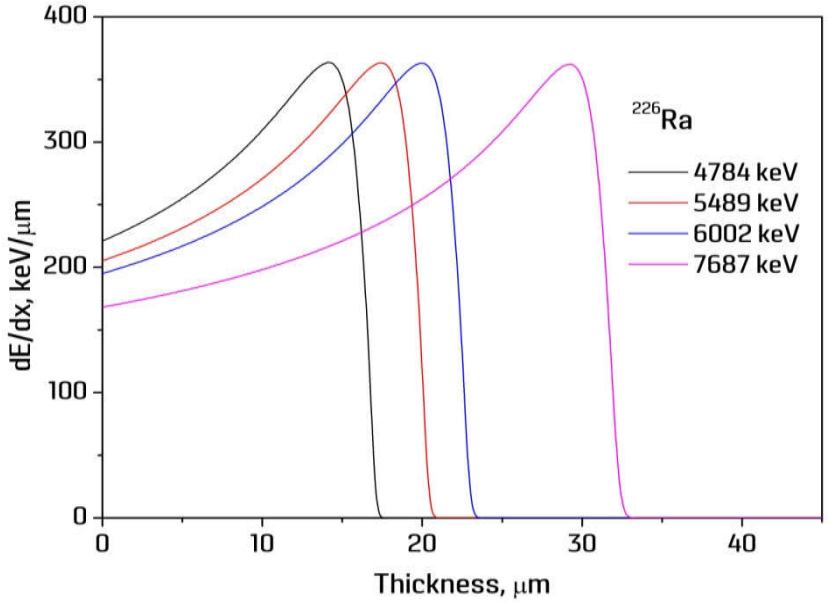

Figure 3.10 – Distribution of ionization losses of alpha particles emitted by a ^{226}Ra source in the working layer of the GaAs detector
(losses in the dead layer were not taken into account)

3.3.2 Analysis of the components of energy resolution

To assess the possibility of improving the characteristics of the manufactured detectors, an analysis was made of the various components of the energy resolution of the detector. As is known, the total energy resolution of the detector can be defined as

$$FWHM_{total} = \sqrt{FWHM_i}\ , \tag{3.11}$$

where $FWHM_i$ are various components due to processes in the detector and external causes. The main components were considered: intrinsic width of the α-line of the source - $FWHM_{source}$; the contribution due to fluctuations in the number of generated electron-hole pairs is $FWHM_{ion}$; detector noise and pick-up electronics - $FWHM_{noise}$; contributions related to the spread of α-particle energy loss in the dead layer of the detector - FWHMDL and fluctuation of the number of collected electron-hole pairs $FWHM_{CCE}$. The contribution of fluctuations in the energy loss of α particles in nuclear scattering events was not taken into account.

We briefly consider the methods for determining the various components. The intrinsic width of the α-line of the source was determined by the manufacturer and was no more than 7 keV. The contribution due to fluctuations in the number of generated electron – hole pairs was calculated as

$$FWHM_{ion} = 2.35\sqrt{FEw}, \tag{3.12}$$

where F is the Fano factor (0.1 for GaAs), E is the particle energy, w is the ionization energy (4.7 eV for GaAs).

The ionization energy was calculated as follows,

$$w=3E_g+h\omega_o \tag{3.13}$$

where E_g is the GaAs band gap, and $h_{\omega o}$ is the energy of the optical phonon.

The corresponding $FWHM_{DL}$ contributions were calculated using a package for simulating the interaction of radiation with GEANT4. To evaluate the noise of the detector and the measuring path, a signal was measured from the pulse generator of the exact amplitude. $FWHM_{CCE}$ was calculated from full resolution, taking into account other components. The corresponding values are presented in table 3.1. As you can see, the main contribution to the resolution of the detector is the dispersion of α-particle energy loss in the dead layer of the detector, which means that it is possible to significantly improve the characteristics of the detector by reducing the thickness of the Schottky barrier.

Table 3.1 – Components of the energy resolution of manufactured detectors

Component	Value, keV
$FWHM_{total}$	22.3
$FWHM_{source}$	7
$FWHM_{ion}$	3.6
$FWHM_{noise}$	~6.0
$FWHM_{DL}$	18.8
$FWHM_{CCE}$	8.2 at -40 B

3.3.3 Temperature test

To carry out temperature measurements, a stand was developed that allows measurements in vacuum in the temperature range from 25 to 150 ° C. The results are shown in figure 3.11. At room temperature, the measured resolution of the FWHM detector was 52 keV with an energy equivalent of noise of 27 keV. It is worth noting that the main contributions to the energy resolution in this case were the energy loss of α particles in the protective coating of the source and the noise of the electron path. As can be seen, at a working bias of -60 V, the detector can withstand temperature increases up to 80 °C, with a further increase to 100°C, a 214 keV amplitude deficit is observed for the 7.687 MeV line and the energy resolution decreases significantly - up to 282 keV. Such a behavior of the spectrum should be associated with a decrease in the transfer parameters due to a decrease in carrier mobility and lifetime due to an increase in the concentration of ionized recombination trapping centers (primarily E_{L2} centers). An increase in the working bias to -90 V allows you to level out the effect of temperature as shown in figure 3.11 b, and the detector characteristics are fully restored and correspond to those at room temperature. As shown by the experiment, the detector retains spectrometric qualities to a temperature of the order of 110°C,

however, it is necessary to increase the working bias to 110–130 V. A further increase in temperature to 130 °C leads to a catastrophic deterioration in the characteristics of the detector — the detector does not "distinguish" individual source lines at operating displacements of less than 150 V. In the future, the behavior of the spectral characteristics of the detectors from temperature will be presented and discussed in detail. However, it can already be argued that the temperature range of the studied detectors is limited by the temperature 110–120 °C and is determined by the presence of deep EL2 centers in the material [152]. The result obtained significantly exceeds the characteristics of silicon detectors, which lose their spectrometric qualities even at a temperature of 50 °C [153].

Thus, testing the characteristics of the developed detectors showed that they can be operated in a wide range of temperatures. Taking into account their high radiation resistance, these detectors were used in our experiments to measure the differential cross sections of the investigated nuclear reactions in the region of extremely large angles, where there is a high temperature and radiation load for the detectors.

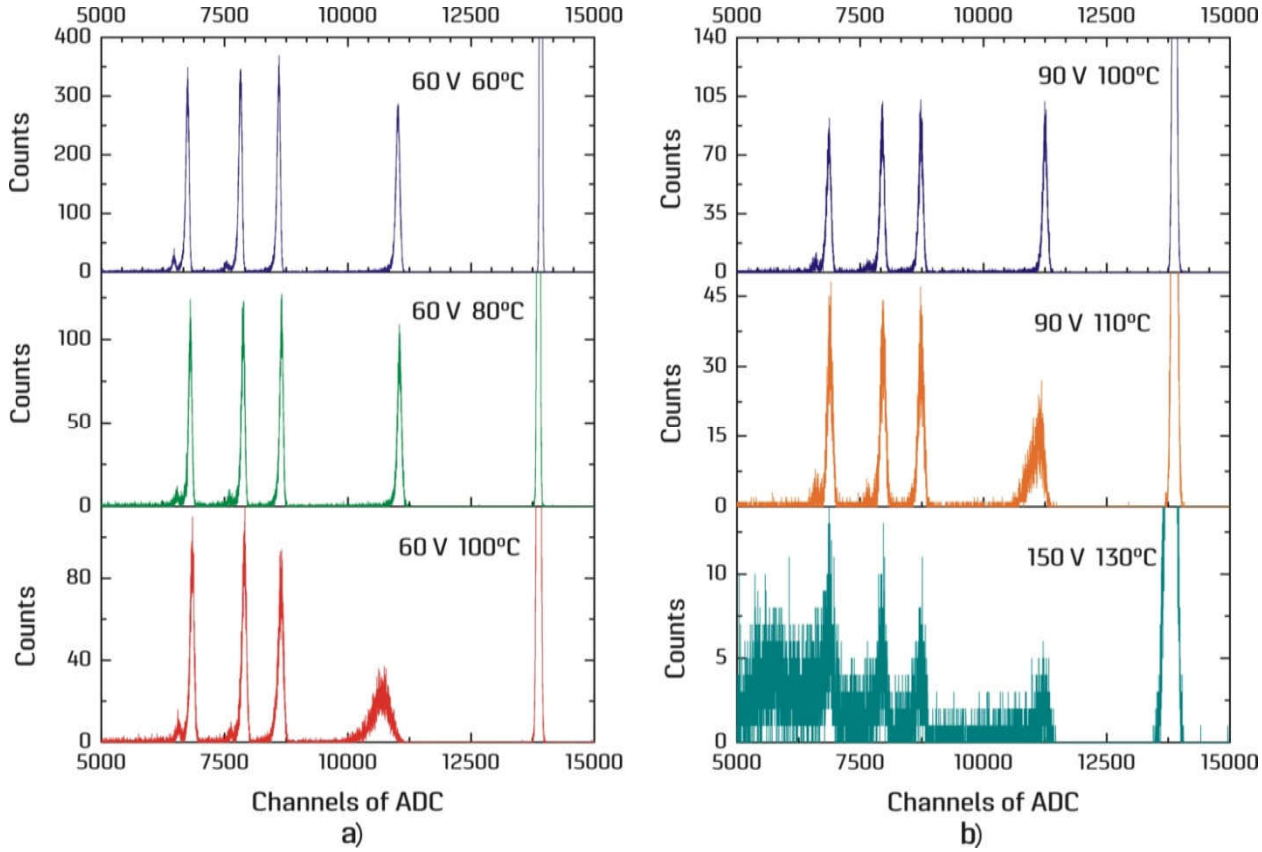

Figure 3.11 – Spectra of α-particles from ^{226}Ra, measured using developed detectors at different temperatures

3.4 Production of targets and determination of their characteristics

In experiments of light charged particles with ^{11}B nuclei, self-sustaining boron isotope 11 targets were used. For the ^{11}B target manufacturing, the VUP-4 universal vacuum station was used (figure 3.12). The VUP-4M is an installation designed to

carry out a wide range of work at a residual air pressure in the working volume 10^{-2} - 10^{-6} mm Hg.

Due to the fact that ^{11}B is a refractory material, the ion-plasma method [154] of sputtering at the VUP-4M installation was used to manufacture such targets. An electron gun with a tungsten spiral was used. The filament current was gradually applied to the electron gun and the formed electrons were pulled onto the sample (boron) by applying a high positive voltage to it. Under the influence of electrons, the sample was strongly heated and evaporated, precipitating on glass, on which a thin layer of sodium chloride was previously applied. The next step after spraying is the process of separating the film from the glass surface, the installation diagram is shown in figure 3.13. After the spraying is finished, the glass is slowly lowered into distilled water. Salt dissolved in water, and a thin carbon film floated on the surface of the water. With the help of target holders, the film was removed from the water and dried.

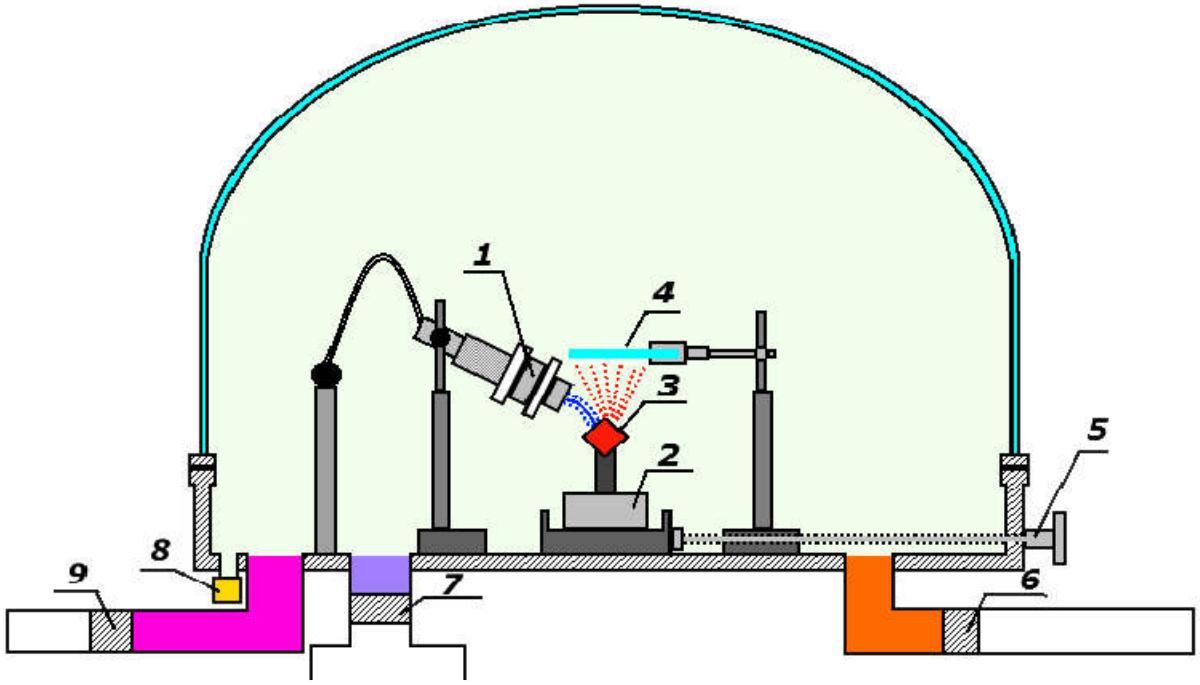

1 - Gun anode (100 V potential), 2 - Cathode (10 kV potential), 3 - Target, 4 - Glass, 5 - Geometry operating handle, 6 - Low vacuum valve, 7 - High vacuum valve , 8 - High vacuum lamp, 9 - Air intake

Figure 3.12 – Block diagram of the VUP-4M vacuum chamber device used for the manufacture of targets ^{11}B

The following basic requirements are imposed on a boron film: a film diameter with a thickness of 240 μg/cm^2 of at least 15 mm; sufficient resistance of the film to various influences, in particular, to mechanical microvibrations during its transportation and installation in the scattering chamber.

The most suitable in our case is the method of producing a thin film from boron by evaporation of boron in vacuum on a smooth surface covered with a soluble

intermediate layer, followed by removal, washing and fixing of the film from boron on an appropriate frame.

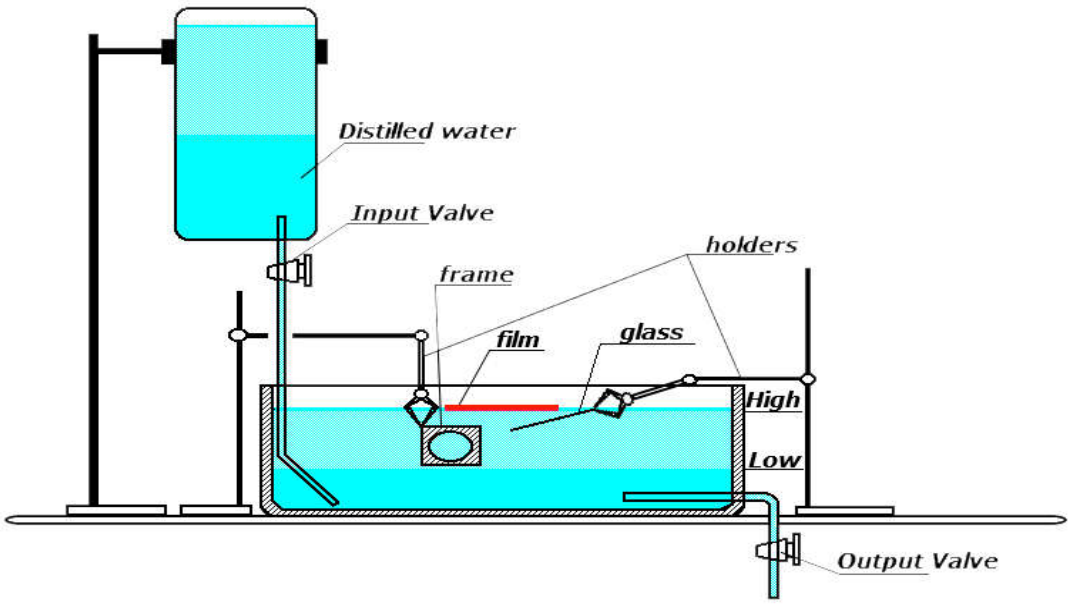

Figure 3.13 – Diagram of a device for removing thin films from glass used for the manufacture of targets ^{11}B

For the evaporation of boron, the VUP-4M universal vacuum post was used, providing a vacuum of no worse than 5×10^{-6} mm Hg. Since the temperature of effective sublimation of boron exceeds 3000 °C, its evaporation was carried out by an electron beam emitted by an electron gun. As a substrate, an emulsion-free glass photographic plate was used for scientific work with an extremely smooth surface, providing a thin film without defects. After thoroughly washing the working surface of the glass, on it in a vacuum of 5×10^{-6} mm Hg. by evaporation from a tantalum boat at (900 ÷ 1000) ºC from a distance of (9 ÷ 10) cm, a well-soluble intermediate layer of a chemically pure compound NaCl with a thickness of (10 ÷ 20) μg/cm^2 was applied. Then, after no more than one minute under the same vacuum from a distance of (7–8) cm, boron was evaporated by an electron beam to obtain a layer with a thickness of ~ 240 μg/cm^2.

To impart deformation stability to the boron film, samples on glass were annealed in a muffle furnace at temperatures from 170 to 240 ºC, the annealing time of each sample varied depending on the layer thickness and ranged from one to several hours. This made it possible to strengthen the crystal structure of boron by quenching. In practice, this led to more successful film stripping, the reject rate was less than 40%, whereas in similar cases without this process it was 80%.The resulting glass with a film of boron from above was very slowly immersed in distilled water at an angle of several degrees, while the intermediate layer of NaCl was dissolved and the film of boron remained floating on the surface of the water to wash out NaCl residues for several hours. The speed and angle of immersion of the glass were selected empirically, based on the need to prevent the bending of the film leading to

defects. Then the film was lifted "on a ring and rectangular frame and dried. For reliable extraction, the rate of water inlet and outlet was selected individually. Levels “High” and “Low” were used to control the spontaneous tension of the film on the target frame (figure 3.13).

The thicknesses of the produced targets were measured at the UKP-2-1 accelerator complex of the INP RK according to the procedure [155] and were performed in two stages: calibration of the proton energy of the accelerator and direct measurement of the target thicknesses.

The accelerator was calibrated according to the energy of charged particles using the so-called “resonance chamber” (figure 3.14), which is mounted on the axis of the beam and is adjacent to the output flange of the central chamber [156]. The principle of operation of the resonance chamber is that a regulatory potential from 0 to 60 kV with different voltage is applied to the target placed in the resonant chamber.

By smoothly changing the energy of protons incident on the target, with the help of the regulatory potential, one can observe very narrow resonances in energy. In this way, the beam energy is determined with high accuracy.

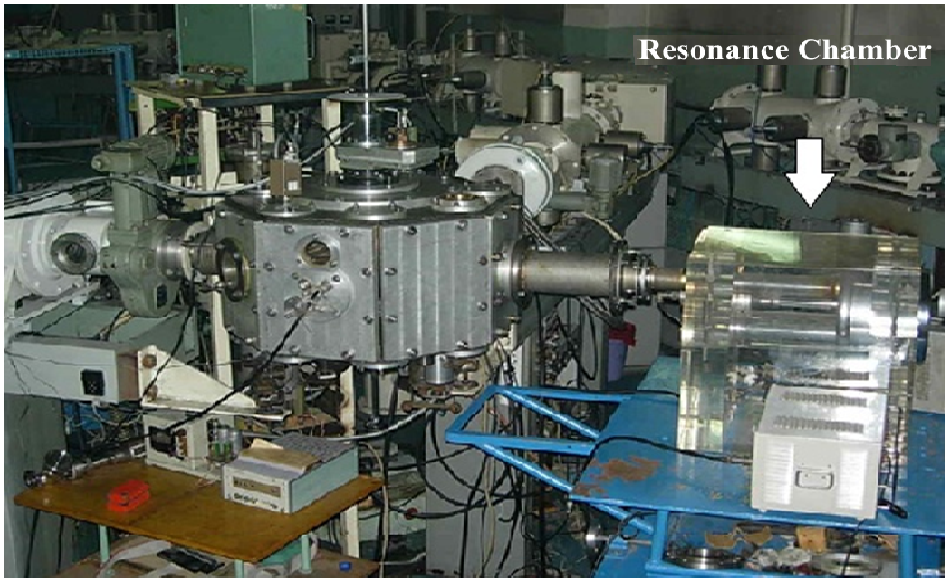

Figure 3.14 – Experimental equipment in the hall of the accelerator UKP-2-1, designed to calibrate the energy of protons

The energy of the proton beam was calibrated using reactions with narrow, well-defined resonances. For this purpose, we used the reactions ^{27}Al (p,γ) ^{28}Si at $E_{p,\ lab.}$ = 632, 773, 992, 1089 keV [157] and ^{19}F (p, γα) ^{16}O at $E_{p,\ lab.}$ = 340 keV [158]. The calibration accuracy in this case is ±1 keV.Figure 3.15 shows the yield curve in the region of 992 keV resonance.The dependence of the true energy of accelerated protons on the energy produced by the UKP-2-1 control accelerator by a computer is shown in figure 3.16.

To register the formed gamma rays, a germanium detector with a high energy resolution (1-2 keV) is used.The method for determining the film thicknesses is based

on the well-known reaction ^{27}Al (p,) ^{28}Si at $E_{p,\,lab.}$ = 992 keV, which has a narrow and strong resonance, i.e. the output of gamma quanta is much larger than at other proton energies. This principle is the basis for determining the thickness of the films.

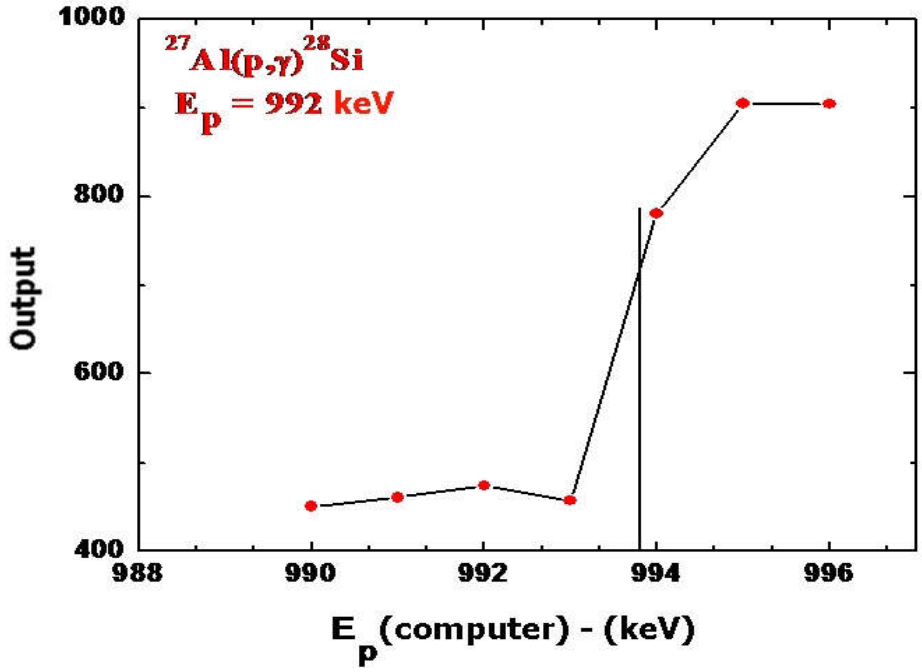

Figure 3.15 – The yield curve in the region of 992 keV of the resonance of the ^{27}Al (p, γ) ^{28}Si reaction, obtained for the purpose of energy calibration of the accelerator

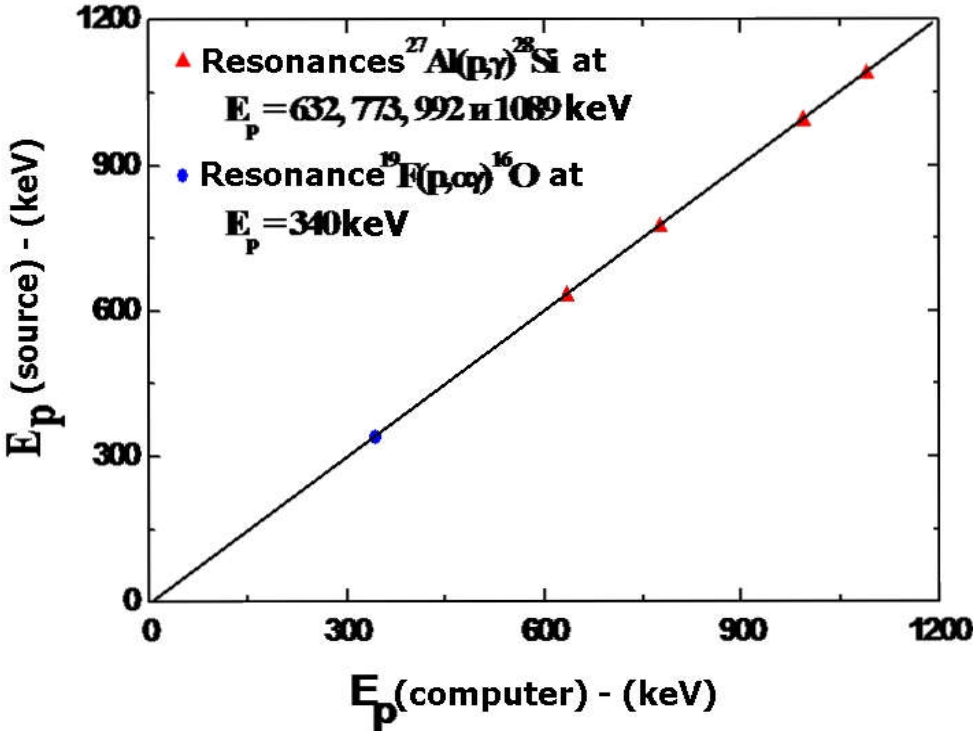

Figure 3.16 – The calibration curve of the accelerator UKP-2-1

When passing through the target layer, the protons partially lose energy, and the resonance of this reaction, which occurs on the alundum film (Al_2O_3) or on a thin aluminum foil (which is placed behind the target under study), is shifted. Then, using the tabulated values of the breaking values $S(E_p)$ [MeV cm^2/g], the thickness of the studied film is determined [159]. This method allows one to determine target thicknesses in the range of 10 - 1000 μg/cm^2 with an error of about 5%. As an example, figure 3.17 shows the result of measuring the thickness of carbon-13 isotope films. The shift of this resonance in the ^{27}Al (p, γ) ^{28}Si reaction was 65.0 keV, which corresponds to a target thickness of 350 μg/cm^2

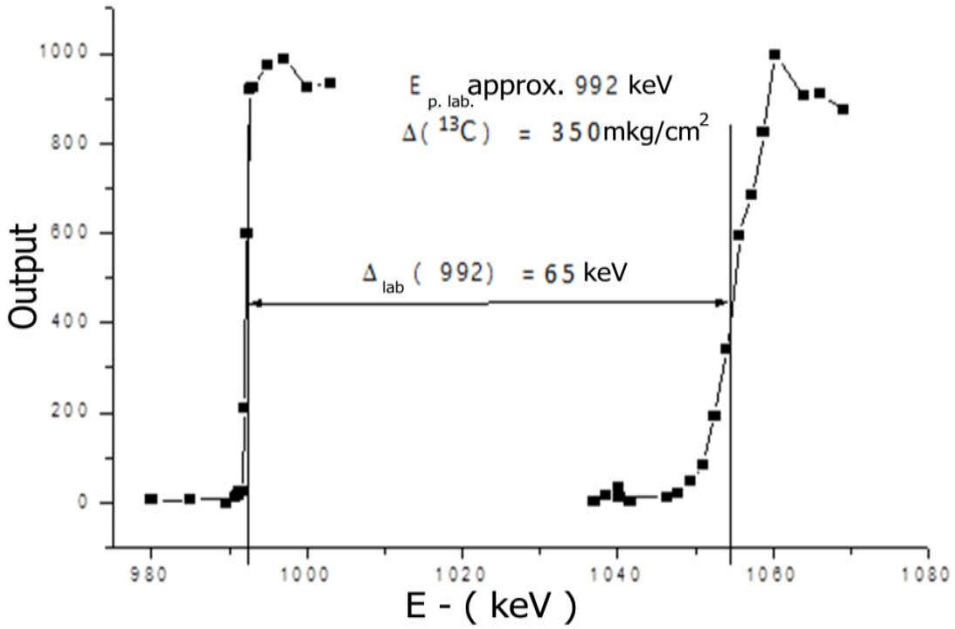

Figure 3.17– The resonance shift of the ^{27}Al (p, γ) ^{28}Si reaction (at E_p = 992 keV), due to the loss of energy by protons during the passage of the carbon layer

4 STUDY OF THE INTERACTION OF DEUTRONS WITH ^{7}LI NUCLEI AT LOW ENERGIES

4.1 Investigation of the scattering of deuteron nucleus ^{7}Li at an energy of 14.5 MeV

The pronounced cluster structure of lithium isotopes is an excellent test for testing various theoretical nuclear models. The systematics of the processes of scattering of hydrogen and helium nuclides on light nuclei in the energy region of >10 MeV/nucleon showed an anomalous increase in scattering in the region of large angles. In the reviews [7, p. 198; 82, p. 405; 84, p.361; 160-162] it was shown that other mechanisms, such as metabolic processes, make a significant contribution to the formation of the scattering cross section in the region of large angles.

A systematic analysis of deuteron scattering on ^{6}Li nuclei performed in Ref. [160, p.2047] for a wide energy range confirmed the possibility of describing the anomalous rise of the cross section at reciprocal angles due to the elastic exchange mechanism of the deuteron cluster taking into account the channel coupling with the spectroscopic factor for the ^{6}Li nucleus close to "d+α" configuration to one.

The differential transmission cross section of the deuteron cluster was obtained taking into account the channel coupling with the spectral value of the coefficient for the configuration of the ^{6}Li nucleus as “d+s” close to one.

In this work, in order to refine the parameters of the optical potential of the ^{7}Li nucleus and to assess the presence of a deuteron cluster, we studied the deuteron scattering process at an energy of 14.5 MeV using literature data in a wide energy range.

4.1.1 Experiment Results

The experimental angular distributions of elastic scattering ^{7}Li(d,d)^{7}Li were measured on the extracted beam of the U150-M Institute of Nuclear Physics isochronous cyclotron at an energy of E_d = 14.5 MeV.

As a target, a film from the ^{7}Li isotope sprayed on an alundum (Al_2O_3) substrate was enriched with 90% enrichment. The thickness of the target was determined by weighing, as well as by the energy loss of the α-particles of the radioactive source ^{241}Am-^{243}Am-^{244}Cm and ^{239}Pu. The ^{7}Li target thickness thus determined was 0.393±0.030 mg/cm^2.

For registration and identification of nuclear reaction products, the (ΔE-E) technique was used [142, p.45]. Thin surface-barrier silicon detectors with thicknesses of 100 or 50 μm (for forward angles) and 30 μm (for backward angles) were used as a ΔE counter. A surface-barrier silicon detector with a thickness of 2 mm was used as an E counter.

The angular distributions of elastic and inelastic deuteron scattering on ^{7}Li nuclei were measured in the angle range 18^0–128^0 with a step of 2^0. The systematic error in the cross sections is related to the uncertainty in the target thickness (6–9)%, solid angle of the spectrometer (1)%, and current integrator calibration (<10)%.

The statistical error of the analyzed data is (1-5)% and only at the section minimums reached (6-15)%.

The energy resolution of the registration system (~ 150 keV) made it possible to reliably identify all low-lying levels of the ^{7}Li core. Typical deuteron spectra are shown in figure 4.1a. In the deuteron spectra, transitions to states with an excitation energy E_x = 0.478 MeV (1/2$^-$) and 4.65 MeV (7/2$^-$) were observed in addition to the elastic peak (3/2$^-$). The peaks from the excited states of ^{12}C (4.43 MeV) and ^{16}O (6.09 MeV) nuclei (due to the presence of carbon and oxygen impurities in the target) did not allow reliable identification of the 4.65 MeV state of the ^{7}Li nucleus in the energy spectra. Thus, this condition was excluded from further analysis. The peaks located, higher in energy from the ground state of ^{7}Li belong to the nuclei of oxygen, aluminum (from the substrate) and carbon. The latter is associated with the burning of the carbon film on the target during the experiment.

When processing the peak of elastic scattering of deuterons on ^{7}Li nuclei in the region of the leading angles, the contribution of impurities was taken into account using literature data on elastic scattering of deuterons on ^{12}C, ^{16}O nuclei at an energy of E = 13.6 MeV [163]. Figure 4.1b shows the measured differential cross sections for deuteron scattering by ^{7}Li at energy of 14.5 MeV.

As can be seen from figure 4.1b, the manifestation of the diffraction structure is characteristic of the measured angular distributions. In contrast to deuteron scattering by ^{6}Li nuclei [160, p.2048], for which a significant rise in the cross section in the rear hemisphere is observed, in the case of a ^{7}Li nucleus the scattering cross section gradually decreases with increasing scattering angle.

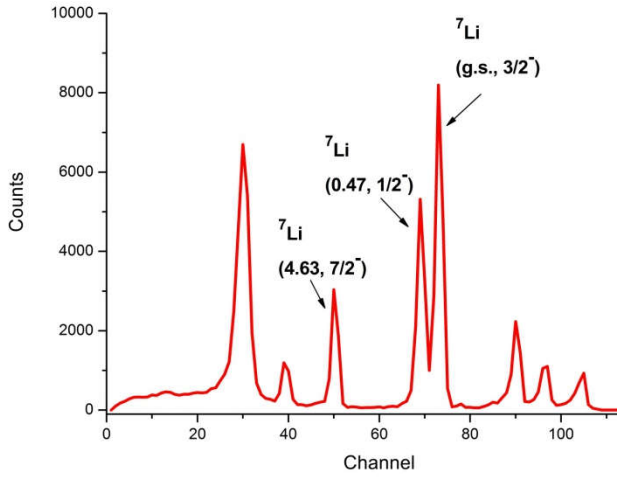

Figure 4.1a – Energy spectrum of deuterons for the reaction ^{7}Li(d,d)^{7}Li (θ_{lab} = 70^{o}) at an energy of 14.5 MeV

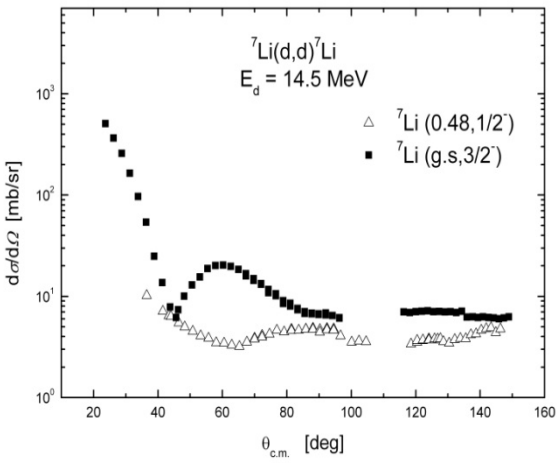

Figure 4.1b – Differential scattering cross section at an energy of E = 14.5 MeV. Black squares are sections of elastic scattering; white triangles - sections of inelastic scattering

This fact confirms the absence of a deuteron cluster in the ^{7}Li nucleus. Note that the experimental data measured at energy of 14.5 MeV are consistent within the experimental errors with the published data at nergy of 14.7 MeV [164].

4.1.2 Analysis of elastic scattering d + ^{7}Li by the optical model and discussion of the results

Systematization of optical potentials for elastic scattering of deuterons on ^{7}Li nuclei.For the theoretical calculation of differential cross sections for elastic scattering, an optical model of the nucleus (OM) is used [1, p.765]. The parameters of the phenomenological optical potential (OP) are found from a comparison of the calculation results with experimental data. The potential with the Woods-Saxon parameterization is usually used.

Taking into account the specific features of the interaction between the deuteron and the nuclei, the surface absorption type W_D was used as the imaginary potential, and the contribution of the spinorbit potential V_{SO} to the scattering process was also taken into account.

The potential parameters corresponding to the optimal ratio of experimental and theoretical values of the cross sections were found by minimizing χ^2.

It should be noted that choosing the potential parameters as optimal, we follow the physically justified value of the volume integral of the real and imaginary parts of the OP - J_V and J_W. The value of J_V should be close to the corresponding value of the nucleon – nucleon interaction potential, which is approximately 400 MeV MeV fm^3 [3, p.419].

It is well known that the parameters of optical potentials have discrete and continuous ambiguities [165]. Therefore, to eliminate the discrete ambiguity of the real part of the potential, its dependence on energy is often used.

For this purpose a global systematics of the OP parameters was carried out for the d + ^{7}Li system in a wide energy range using published data. For this, we used experimental data on the elastic scattering of deuterons on ^{7}Li nuclei measured at energies of 7–12 MeV [14,p.266;166], 14.7 MeV [164,p.1345], 25 MeV [167], and 27.7 [20,p.1059].

It was found that with increasing energy of the incident particle, the discrete ambiguity is eliminated, for example, at energies above 12 MeV per nucleon. Based on this, first of all, the experimental data were analyzed at energies of 28 and 25 MeV. As starting parameters, we used their values established in [168] on the global systematics of optical potentials for elastic deuteron scattering in the energy range 20–90 MeV for the atomic mass range from A = 12 to A = 238.

The search for the parameters of the optical potential was carried out by fitting the calculated angular distributions to the experimental data using the FRESCO computer code [130, p.177]. To eliminate the discrete ambiguity in determining the optical parameters, the radii of the real (r_v) and imaginary (r_w) parts of the potentials were fixed. The experimental data were adjusted to theoretical calculations by varying the 4 remaining OP parameters (V, W are the depths of the real and imaginary parts of the potential; a_R and a_w are the diffuseness of the real and

imaginary parts of the potential, respectively). The fitting of the calculated cross sections to the experimental data was carried out in the most complete angular range. The diffusivity parameters established in this approach strongly depend on energy at low energies (figure 4.2, the left graph), which possibly reflect the effects of resonances in the d + ^{7}Li system (set A in table 4.1). As can be seen from the figure 4.2 the right graph, these sharp changes in the parameters with an increase in energy turn into a constant.

Table 4.1 – Parameters of optical potentials for elastic scattering d + ^{7}Li

$E_{d,}$ MeV	Ser.	V_R (MeV)	r_R (fm)	a_R (fm)	W_D (MeV)	r_D (fm)	a_D (fm)	V_{SO} (MeV)	r_{SO} (fm)	a_{SO} (fm)	r_C (fm)
1	2	3	4	5	6	7	8	9	10	11	12
7	A	62.96	1.17	1.22	9.08	1.325	0.4	6.76	1.07	0.66	1.3
	B	89.7	1.17	0.9	3.99	1.325	0.75	6.76	1.07	0.66	1.3
	C	66.0	1.35	0.9	4.5	2.37	0.3	8.0	0.86	0.25	1.3
	D	77.78	1.173	0.809	14.21	1.327	0.551	3.703	1.23	0.813	1.69
8	A	67.53	1.17	1.105	12.47	1.325	0.304	6.76	1.07	0.66	1.3
	B	91.62	1.17	0.9	4.36	1.325	0.75	6.76	1.07	0.66	1.3
	C	65.0	1.35	0.88	4.9	2.3	0.3	8.0	0.86	0.25	1.3
	D	77.62	1.173	0.809	14.13	1.327	0.551	3.702	1.23	0.813	1.69
9	A	72.65	1.17	1.02	19.22	1.325	0.217	6.76	1.07	0.66	1.3
	B	94.31	1.17	0.9	4.87	1.325	0.75	6.76	1.07	0.66	1.3
	C	62.0	1.35	0.86	6.0	2.15	0.3	8.0	0.86	0.25	1.3
	D	77.46	1.173	0.809	14.05	1.327	0.551	3.702	1.23	0.813	1.69
10	A	73.41	1.17	0.988	23.29	1.325	0.195	6.76	1.07	0.66	1.3
	B	95.85	1.17	0.9	4.65	1.325	0.75	6.76	1.07	0.66	1.3
	C	61.5	1.35	0.83	7.2	2.18	0.3	8.0	0.86	0.25	1.3
	D	77.29	1.173	0.809	13.974	1.327	0.551	3.702	1.23	0.813	1.69
12	A	68.84	1.17	1.0	11.08	1.325	0.64	6.76	1.07	0.66	1.3
	B	72.35	1.17	0.9	6.21	1.325	0.75	6.76	1.07	0.66	1.3
	C	64.0	1.35	0.79	10.5	2.1	0.3	8.0	0.86	0.25	1.3
	D	76.96	1.173	0.809	13.815	1.327	0.551	3.702	1.23	0.813	1.69
	A	73.97	1.17	0.986	9.57	1.325	0.74	6.76	1.07	0.66	1.3
7	B	73.08	1.17	0.9	7.95	1.325	0.75	6.76	1.07	0.66	1.3
	C	62.0	1.35	0.73	12.0	2.0	0.3	8.0	0.86	0.25	1.3
	D	76.49	1.173	0.809	13.60	1.327	0.551	3.702	1.23	0.813	1.69
	A	81.14	1.17	0.91	14.37	1.325	0.75	6.76	1.07	0.66	1.3
25	B	75.94	1.17	0.9	10.7	1.325	0.75	6.76	1.07	0.66	1.3
	C	57.0	1.35	0.72	12.9	1.94	0.3	8.0	0.86	0.25	1.3
	D	74.60	1.173	0.809	12.78	1.327	0.551	3.70	1.23	0.813	1.69
	A	75.32	1.17	0.9	10.28	1.325	0.75	6.76	1.07	0.66	1.3
28	B	75.32	1.17	0.9	10.28	1.325	0.75	6.76	1.07	0.66	1.3
	C	55.62	1.35	0.72	12.9	1.94	0.3	8.0	0.86	0.25	1.3
	D	74.02	1.173	0.809	12.54	1.327	0.551	3.70	1.235	0.813	1.69

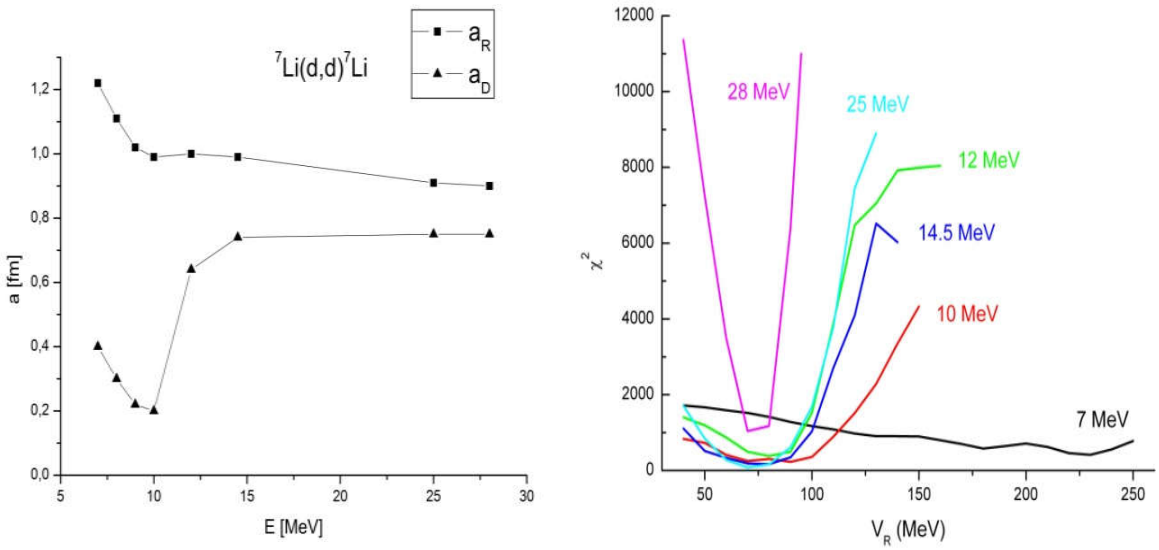

Figure 4.2 – The upper graph – the dependence of the OD diffusivity on energy for the reaction ^{7}Li (d, d) ^{7}Li. The bottom graph is the dependence of χ^2 on the depth of the real part of the potential

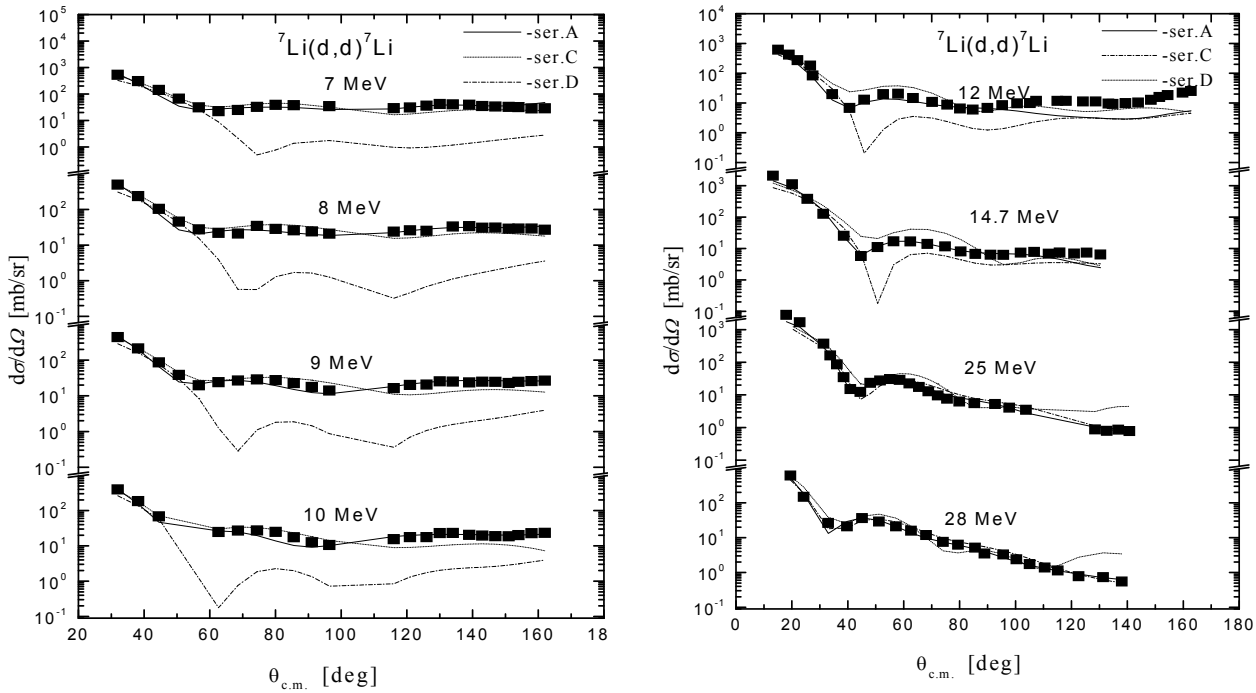

Symbols - experimental data; solid lines — OM calculations with set A; dashed lines - calculations with set C; dashed-dotted lines - calculations with set D.

Figure 4.3 – Differential cross sections for elastic scattering of deuterons on ^{7}Li nuclei

As expected, with increasing energy of the incident particles, the discrete uncertainty of the depth of the real part of the potential was eliminated. The results of the description of the experimental angular distributions of elastic scattering of deuterons on the studied nucleus are presented in figure 4.3. Since the experimental data on elastic scattering at energies of 14.7 and 14.5 MeV are practically indistinguishable within the error range, the graphs show data at energy of 14.7 MeV (these data cover extremely large angles).

The optimal OP parameters established in this work will be used later in the analysis of data on inelastic deuteron scattering and ^{7}Li (d, t) reactions at an energy of 14.5 MeV to refine the structural characteristics of lithium isotopes.

4.2 Study of the ^{7}Li(*d*,*t*)^{6}Li reaction at the energies of 14.5 MeVand 25 MeV

As it is well known, attempts to describe the scattering and nucleon transfer reactions between the light nuclei are often failed in the frameworks of the simple optical model and conventional DWBA [167 , p.1037]. The reason is small amount of target nucleons and cluster effects, which become apparent as an anomalous large-angle scattering. The nature of this phenomenon for the lithium nuclei can be stipulated for their pronounced (α + *d*) and (α + *t*) cluster structure [169]. At the same time, the reactions with lithium nuclei are of great significance as lithium is one of the most important elements of the fuel cycle in the promising projects of the fusion reactors, and in connection with the problem of nucleosynthesis of light nuclei. Such reactions were studied extensively in 70-ies, but consecutive analysis of their mechanisms and obtaining the correct spectroscopic information has been carried out in last decade [13,p.840;167, p.1037;170].

The ^{7}Li(*d*,*t*)^{6}Li reaction with the production of tritium is of particular interest for applications [171]. The (*d*,*t*) reaction on ^{7}Li nuclei were previously studied at 12 MeV [14, p.265; 15, p.978], 15 MeV [16, p.1249;17, p.781], 18 MeV [18, p.1689], 20 MeV [19, p.408], 25 MeV [167,p.1037] and 28 MeV [20, p.1059] energies. The measurements in the full angular range were done at E_d= 12 MeV and 25 MeV [14, p.265; 167, p.1037] only. In other cases, they were performed in the forward hemisphere. The standard DWBA with zero and finite-range interaction, used in the calculation of the angular distributions in [14, p.265; 15, p.978], does not describe the experimental cross sections at large angles.

This work is intended to trace the energy dependence of pick-up of one neutron in the reaction ^{7}Li(*d*,*t*)^{6}Li in totality with [167,p.1037], where the calculations were made taking into account the α-cluster exchange mechanism in the framework of the coupled reaction channels (CRC) method.

4.2.1 Experimental technique and measurement results

The experiment was performed using the deuteron beam with energies of 14.5 MeV and 25 MeV, extracted from the U-150M isochronous Cyclotron of Institute of Nuclear Physics (Almaty, Kazakhstan).

Differential cross sections for elastic and inelastic scattering of deuterons and for tritons from the (d,t) reaction on ^{7}Li nuclei were measured in the angular range from 18º to 128º (lab). Experimental errors not exceeded 8%.

Deuterons and tritons were detected and identified using the E–E telescope of two silicon counters with thicknesses of 30-100 microns (E detector) and 2 mm (E detector). The total energy resolution was around 150 keV. It was determined mainly by energy spread of the beam and target thickness. The typical deuterons and tritons spectra are shown in figure 4.4.

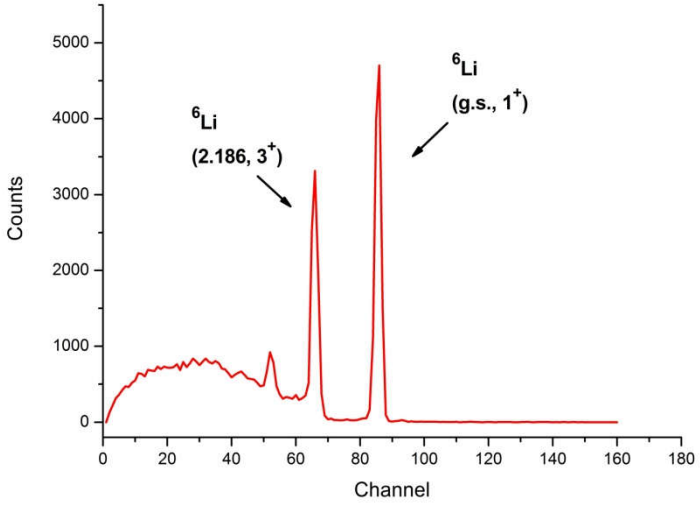

Figure 4.4 – Typical energy spectra of tritons from ^{7}Li(d,t)^{6}Li reaction, measured at $\theta_{lab} = 36^{o.}$

4.2.2 Analysis and discussion

The ^{7}Li nucleus has a weakly bound structure ^{7}Li = α+t, and, in this case, the exchange mechanism with α-particle transfer ^{7}Li(d,^{6}Li)t can give a significant contribution to the cross section of the ^{7}Li(d,t)^{6}Li reaction in the rear hemisphere.This effect for the ^{7}Li(d,t)^{6}Li reaction was investigated very carefully in [167,p.1037] at the energy of 25 MeV. Therefore, the calculation of the cross sections for the deuteron scattering and the ^{7}Li(d,t)^{6}Li reaction was carried out in the framework to the coupled reaction channels which presented in a similar manner as in the article [167,p.1037] via the FRESCO [130, p.177] code using potentials found from the analysis of the elastic scattering.

Only the one step processes with neutron pick-up and the α-particle cluster transfer ^{7}Li(d, ^{6}Li)$t$were taken into account. The coupling scheme is shown in figure 4.5.

The system of nine nucleons presented in the entrance channel as ^{7}Li + d was replaced by three subsystems:

I. d + ^{7}Li;
II. t + ^{6}Li;
III. ^{6}Li + t.

All states of subsystems II and III are coupled with subsystem I by the reactions with neutrons and α-particles transfers. Couplings between ground and excited states of nuclei ^{7}Li and ^{6}Li were calculated using the rotational model with the form factor for quadrupole transitions (λ = 2).

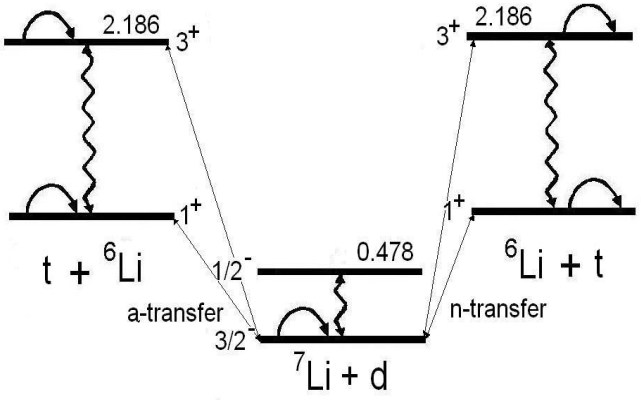

Figure 4.5 – The coupling scheme used in the CRC calculations for the ^{7}Li(d,t)^{6}Li reaction. The arcs show the spin reorientations of ^{7}Li and ^{6}Li nuclei in ground and excited states

The prior representation of DWBA with a finite range interaction, incorporated in the FRESCO code, was used in the calculations of neutron and α-particle transfer reactions. The wave functions of the bound states of ^{7}Li →^{6}Li + n, ^{7}Li →α + t, ^{6}Li →α + d and t →d + n were calculated in a standard way by fitting a depth of the real part of the Woods–Saxon potentials, giving the known binding energy ("well-depth"-procedure). Geometric parameters of the potentials (radii and diffuseness) used the same as given in [167, p.1039] and were fixed. The sets of the optical potentials (OP) [167,p.1039] for the input d + ^{7}Li and output t + ^{6}Li channels obtained from analysis of the elastic scattering of deuterons and ^{3}He on ^{7}Li and ^{6}Li nuclei respectively, at the incident particle energies in the range of 25–35 MeV [2, p. 100; 170, p. 20;172] were used.

The best description of the experimental data for the elastic scattering ^{7}Li(d, d)^{7}Li gives the set 4 from[167,p.1039] (table in article [167, p.1039]). The calculated cross sections for the elastic and inelastic scattering with excitation of the E_x = 0.478 MeV (1/2$^-$) level of the ^{7}Li nucleus are presented in figure 4.6. It can be seen that the CRC calculations well describe the experimental cross sections in full angular range for the elastic scattering ^{7}Li(d, d)^{7}Li.

It should be noted that the initial parameters of the potentials of set 4 [167,p.1039] used in this calculations were slightly changed because thecurrent energy of the incident deuterons is significantly less comparing with 25 MeV given in [167,p.1039]. With decreasing energy, the depth of the real part of the potential is increasing. So two parameters were subjected to change –the depths of real parts for the ^{7}Li + d channel (V_o = 89.5 MeV) and the ^{6}Li + t channel (V_o = 191 MeV) to fit the elastic scattering ^{7}Li(d,d)^{7}Li. Also, in order to achieve agreement between the cross sections calculated at large angles with the measured cross sections, the depth of the

imaginary potential was reduced to the value W_d= 6.7 MeV for ^{7}Li(d,d)^{7}Li reaction. The potentials used in the calculations are shown in table 4.2.

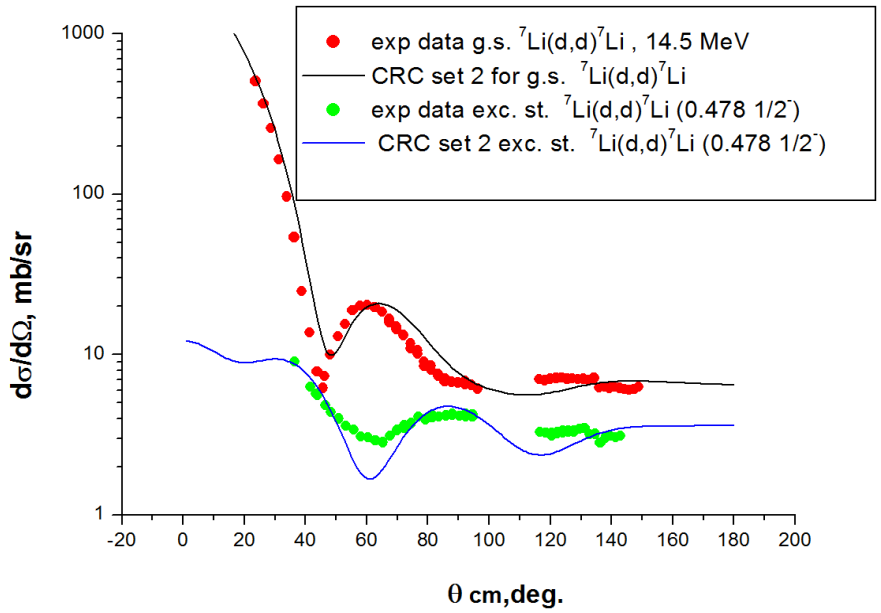

The solid points are experimental data. The curves represent results of the CRC calculations with the potentials of Set2 (black line for ground state and blue line for 1/2$^-$ state) from table 4.2

Figure 4.6 – The angular distributions for elastic and inelastic (E_x= 0.478 MeV, 1/2$^-$) scattering of deuterons on ^{7}Li nuclei at the beam energy of 14.5 MeV

Table 4.2–Optical potentials used in the coupled reaction channels calculations of the scattering and ^{7}Li(d,t)^{6}Li reaction cross sections at the deuteron beam with the 14.5 MeV energy

Set 1	V_0, MeV	r_V, fm	a_V, fm	W_V MeV	r_W fm	a_W fm	W^* MeV	r_D fm	a_D fm	V_{so} MeV	r_{so} fm	a_{so} fm
^{7}Li + d	89.5	1.24	0.74				12.7	1.24	0.74	10.44	0.82	1.05
^{6}Li + t	191.0	1.11	0.69	17.0	1.39	0.59				1.72	1.36	1.18
Set 2												
^{7}Li + d	89.5	1.24	0.74				6.70	1.24	0.74	10.44	0.82	1.05
^{6}Li + t	191.0	1.11	0.69	17.0	1.39	0.59				1.72	1.36	1.18

As for the ^{7}Li(d,t)^{6}Li reaction, the calculations were carried out using the potential (set 1) given in table 4.2. A comparison of the calculated cross sections with the experimental data is shown in figure 4.7. The calculations give fairly good description of the measured differential cross sections at large angles with taking into account the contribution of α-transfer mechanisms to the scattering process.

To sum up, the potential of set 1 from table 4.2 (the green line in figure 4.7) describes quite well the experimental data on ^{7}Li(d,t)^{6}Li, but does not fit the elastic

scattering ^{7}Li(d,d)^{7}Li. At the same time, set 2 (the blue line in figure 4.4) describes very well the elastic scattering ^{7}Li(d,d)^{7}Li, but does not the ^{7}Li(d,t)^{6}Li reaction.

The deformation lengths (δ_2) and spectroscopic factors (*SF*) extracted from the analysis with set 2 of the OP are shown in table 4.2. The spectroscopic factor of ^{6}Li=α+d was taken from [94,p.103]. As a result, the *SFs* for α+t and n+^{6}Li configurations of ^{7}Li have been obtained (table 4.3) from the analysis. Also, the analysis of the data at the forward hemisphere was carried out using the modified DWBA method as it was made in [170,p.20] for obtaining the asymptotical normalization coefficient for the ^{7}Li$_{g.s.}$= ^{6}Li+n configuration. The contribution of one-step neutron pick-up was evaluated by matching the *SFs* for this configuration extracted from the ordinary DWBA analysis and the CRC method.

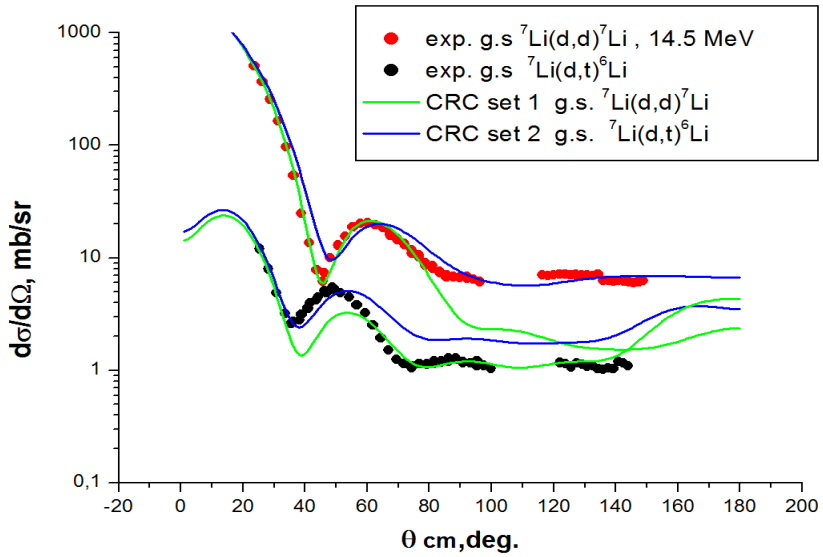

The solid points are experimental data. The curves represent results of the CRC calculations with the potential parameters of Set 1 (green line), Set 2 (blue line) from table 4.2

Figure 4.7 – The angular distributions for the deuterons elastically scattered on ^{7}Li and for tritons from the ^{7}Li(d,t)^{6}Li reaction at the beam energy 14.5 MeV

The values of the deformation parameters (δ_2) and spectroscopic factors (*SF*) extracted in this analysis are in good agreement with the results obtained in [167,p.1039] and with theoretical calculations within the framework of the translational invariant shell model [94,p.103].

Table 4.3 – Deformation lengths (δ_2) and spectroscopic factors (*SF*) extracted from present analysis

δ_2, fm		*SF*					
Li	Li	t→d+n	^{7}Li→^{6}Li+n	^{7}Li→^{6}Li*+n	^{6}Li→α+d	^{6}Li*→α+d	^{7}Li→α + t
4.0	3.0	1.5	0.77	0.49	1.35	0.44	1.19

Cross sections calculated in the framework of the optical model agree well with the experimental data in the forward hemisphere but the simple model fails to describe the rise of the cross section at large angles.Therefore, the CRC calculations were applied in order to reproduce this behavior at backward hemisphere.

The contribution of the α-transfer mechanism does not affect the behavior of the cross sections in the main maximum of the angular distributions (up to 40 ^{o} – 60 ^{o} angles) and the neutron pick-up dominates for angles up to 40^{o}–50^{o}.

The cross section at angles of 120^{o} – 150^{o} is fully reproduced by direct exchange mechanism with the transfer of α-particles in the ^{7}Li(*d*, ^{6}Li)t reaction (figure 4.7) with reasonable values of the ^{7}Li→ α+*t* and ^{6}Li→ α+*d* spectroscopic factors.

4.3 Analysis ofthe ^{7}Li(*d*,*t*)^{6}Li reaction at energy of 25 MeV using modified distorted waves method

Calculations of the cross sections for the deuteron scattering and reaction ^{7}Li(*d*,*t*)^{6}Li at energy of 25 MeVwere done in the framework of the coupled reaction channels method using the FRESCO [130, p.177] program. Only the one step processes with neutron pick-up and exchange mechanism with the α-particle cluster transfer ^{7}Li(*d*,^{6}Li)*t*were taken into account.

The wave functionsof the bound states of ^{7}Li → ^{6}Li+*n* (1*P*), ^{7}Li → α+*t* (2*P*), ^{6}Li→ α+*d* (2*S* for the ground and 1*D* for excited state) and *t* → *d*+*n* (1*S*) were calculatedin a standard way by fitting a depth of the real part of the Woods-Saxon potentials, giving the known binding energy («well-depth» - procedure). Geometric parameters of the potentials (radii and diffuseness) were fixed (table 4.4).

Table 4.4 – Geometric parameters for the Woods-Saxon potentials for the calculation of the bound state wave functions

System	*R*, fm	*a*, fm
^{6}Li + *n*	2.31	0.65
d + *n*	1.85	0.65
d + α	2.33	0.65
t + α	2.48	0.65

Spectroscopic amplitudes for *d*+*n* and α+*t* configurations were taken from the theoretical calculations in the framework of the translationary invariant shell model [94, p.103]. The remaining spectroscopic amplitudes were determined by fitting the calculated angular distributions to the experimental data.

Ground state (3/2^{-}) of ^{7}Li nucleus was described as an interaction of the ^{6}Li (1^{+}) core with a neutron in the state s*j* =1/2 and 3/2, according to the shell model. It is well known that the shape ofthe calculated angular distributions is determined by transferred orbital angular momentum (*l* =1) only and practically independent on *j*. Therefore, at absence of the experimental information about polarization, only summed value ofthe spectroscopic factors $S = S_{1/2}+S_{3/2}$ can be extracted in our analysis. Nevertheless, the calculations were performed with spectroscopic

amplitudes for j =1/2 and j =3/2, using as starting their theoretical values [94, p.103]. Calculations were performed with the optical potentials listed in table 4.5.

Four sets of the optical potentials (OP) for the input d+^{7}Li and output t+^{6}Li channels obtained from analysis of the elastic scattering of deuterons and ^{3}He on ^{7}Li and ^{6}Li nucleires pectively, at the incident particle energiesin the range 25-35 MeV [2,p.30;169, p.203;172, p. 74;] were used. Some of the potentialsin the table 4.5 have been successfully tested before in the coupled reaction channels analysis of the reaction ^{6}Li(^{3}He,d)^{7}Be at the energy 34 MeV [170, p.20]. In the present calculations only the depths of the imaginary potential (W_V, W_D) were varied to fit theoretical cross sections to experimental data. The deformation length (δ_2) and SF (S) obtained from the analysis with different sets of the OP are shown in table 4.6. Averaged values of the SF obtained in the present studies are in reasonable agreement with the theoretical values calculated in the framework of the shell model [94,p.103;173, 174].

Table 4.5 – Optical potentials used in the coupled reaction channels calculation of the scattering and ^{7}Li(d,t)^{6}Li reaction cross sections at the deuteron beam energy 25 MeV

Set	System	V_R (MeV)	r_V (fm)	a_V (fm)	$W_{V/D}$* (MeV)	r_w (fm)	a_w (fm)	V_{SO} (MeV)	r_{SO} (fm)	a_{SO} (fm)	r_C (fm)
1	^{7}Li+d	81.14	1.17	0.91	11.09D	1.325	0.75	6.76	1.07	0.66	1.3
	^{6}Li+t	113.00	1.15	0.74	20.80D	1.220	0.80	4.00	1.15	0.80	1.3
2	^{7}Li+d	81.14	1.17	0.91	10.09D	1.325	0.75	6.76	1.07	0.66	1.3
	^{6}Li+t	120.00	1.15	0.65	30.00V	1.460	0.85	4.00	1.15	0.80	1.3
3	^{7}Li+d	90.00	1.15	081	9.60D	1.340	0.87	6.00	1.15	0.81	1.3
	^{6}Li+t	120.00	1.15	0.65	25.00V	1.46	0.85	4.00	1.15	0.80	1.3
4	^{7}Li+d	74.00	1.24	0.74	12.70D	1.240	0.74	10.44	0.82	1.05	1.3
	^{6}Li+t	171.0	1.11	0.69	17.00V	1.39	0.59	1.72	1.36	1.18	1.3

Table 4.6 – Deformation parameters (δ_2) and spectroscopic factors (S) from nalyze at energy 25 MeV

Set	δ_2		S(j)			
	^{7}Li	^{6}Li	^{7}Li→^{6}Li+n	^{7}Li→^{6}Li*+n	^{6}Li→α+d	^{6}Li*→α+d
1	3.0	3.0	0.72 0.32 (1/2)+0.40 (3/2)	0.57 (3/2)	1.13	0.67
2	2.5	3.0	0.60 0.27 (1/2)+0.33 (3/2)	0.46 (3/2)	1.12	0.52
3	3.5	3.0	0.60 0.27 (1/2)+0.33 (3/2)	0.46 (3/2)	1.12	0.74
4	4.0	3.0	0.58 0.26 (1/2)+0.32 (3/2)	0.37 (3/2)	1.35	0.44
Averaged over all sets			0.63 0.28 (1/2)+0.35 (3/2)	0.47 (3/2)	1.18	0.59
Theory[94, p.103]			0.97 0.43 (1/2)+0.54 (3/2)	0.54 (3/2)	1.13	1.12
Theory[173, p.10]			0.72 0.29 (1/2)+0.43 (3/2)	0.55 (3/2)		

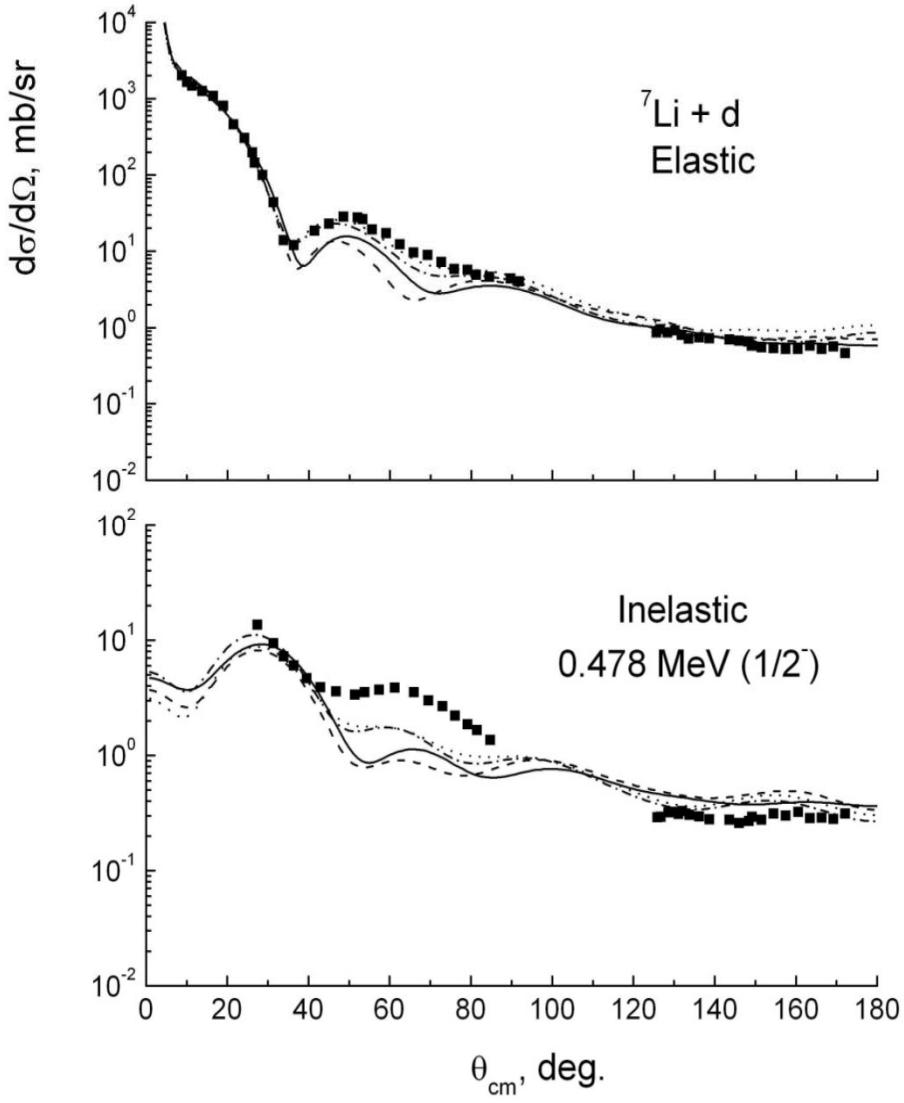

Squares – experimental points. Curves – CRC calculations with all couplings shown in figure 4.8. The OP sets used in the calculations are in table 4.5: Set 1 – dashed-dotted, 2 – dotted, 3 - dashed and 4 - solid curves

Figure 4.8 – Angular distributions of deuterons elastically and inelastically scattered on the ^{7}Li nuclei at the beam energy 25 MeV with excitation of E_x = 0.478 MeV (1/2$^-$) state

The comparison of calculated cross sections for elastic and inelastic scattering with excitation of the E_x = 0.478 MeV (1/2$^-$) level of the ^{7}Li nucleus and the ^{7}Li(d,t)^{6}Li reaction with the transitions to the ground (1$^+$) and excited (3$^+$) states of ^{6}Li nucleus with experimental data is shown in figure 4.8 and 4.9 for different sets of the optical potentials from table 4.5. The securves were calculated taking into account all couplings shown in figure 4.5. One can see that the calculations reproduce rather well the characteristic features of the experimental angular distributions at small (up

to 40°-50°) and large angles, and only at the medium angles (50^{o} - 80°) the calculated cross sectionsare lower than the experimental ones.

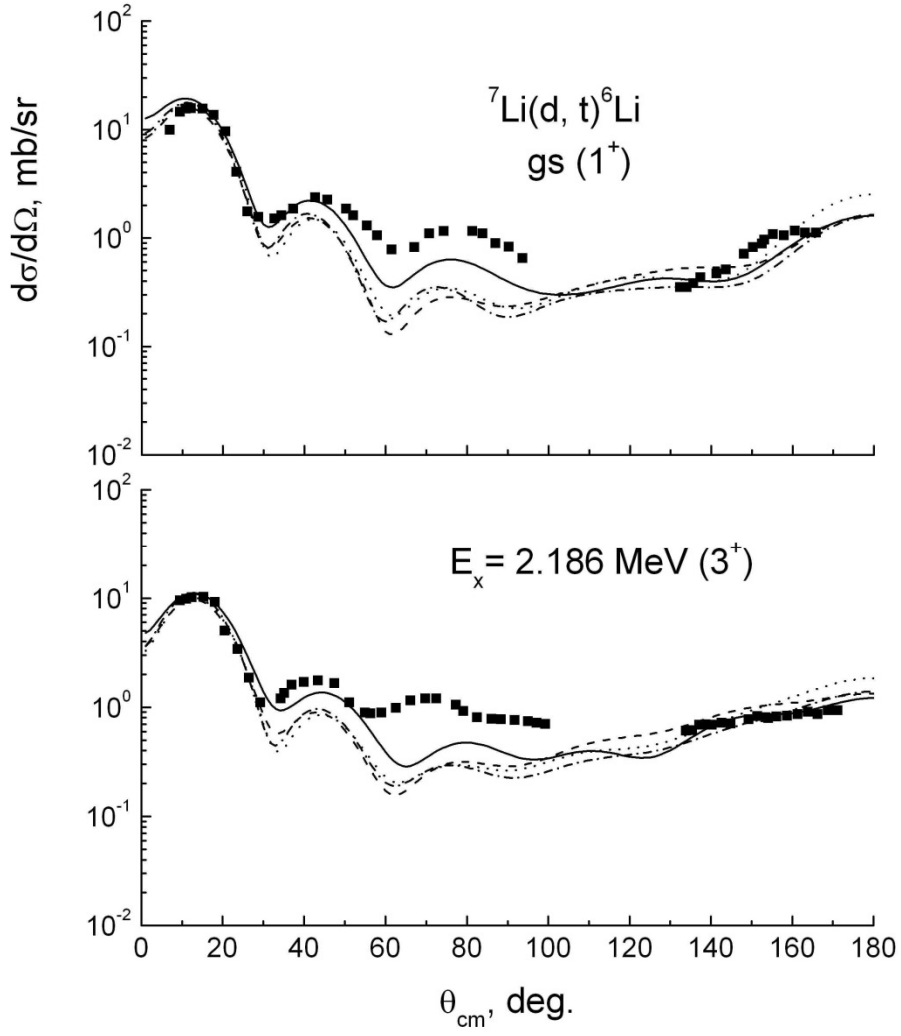

Squares – experimental points. The OP sets used in the calculations are in table 4.5: Set 1 – dashed-dotted, 2 – dotted, 3 – dashed and 4 – solid curves

Figure 4.9– Angular distributions of tritons from thereaction ^{7}Li(d,t)^{6}Li, corresponding to transitions to the ground (1^{+}) and the first excited state (E_x = 2.186 MeV (3^{+})) states of ^{6}Li

The results of more detailed calculations are shown in figure 4.10 for a set 4 of potentials (table 4.5). Dashed-dotted curves in this figure 4.10 correspond to the direct neutron pick-up in the reaction ^{7}Li(d,t)^{6}Li and exchange mechanism of α-particles transfer in the ^{7}Li(d,^{6}Li)t reaction, calculated taking into account all couplings, shown in figure 4.5. Solid curves are their coherent sum. In whole, the analysis with using all sets of potential parameters, shows that only contribution of the exchange mechanism allows to describe the behavior of the cross sections at large angles. Dashed-dotted curvesin figure 4.10 shows the angular distribution of the

tritons from direct neutron pickup mechanism in the reaction ^{7}Li(*d, t*)^{6}Li,calculated using the method of finite range distorted waves method (FRDWBA) with non-contributed couplings.

Another important conclusion is appeared from our analysis (it is well illustrated in figure 4.10), notably: contribution of coupled channels and exchange mechanism does not affect the behavior of the cross in the main maximum of the angular distributions (up to 40 °-50 ° angles), andthe mechanism of the pick-updominates for angles up to 40 °-50 °. This case as well as the peripheral character of the process allows us touse a modified distorted waves method to extraction the values of the asymptotic normalization coefficients for the ^{7}Li → ^{6}Li + *n* system.

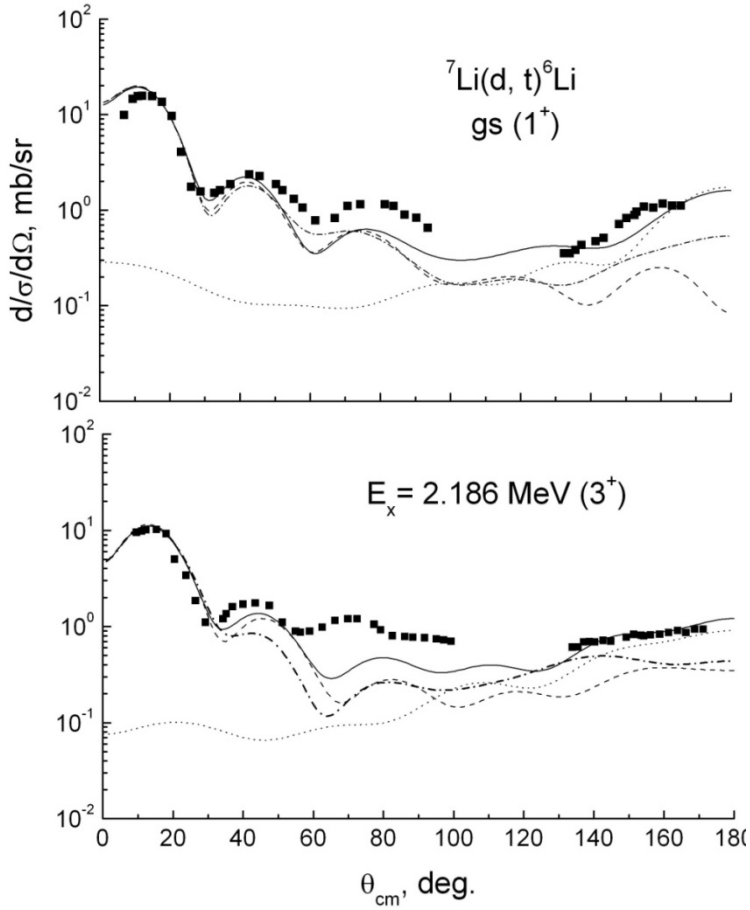

Squares–experimental points. Curves–calculations with OP set4 from table 4.5: Solid curve –all couplings are taken into account, dashed curves –all couplings in the^{7}Li(*d, t*)^{6}Li process but without the contribution of α-particle transfer, dotted curves –transfer mechanism with α-particles exchange in the ^{7}Li(*d,*^{6}Li)*t* reaction.Dashed-dotted curve– calculation of the reaction^{7}Li(*d, t*)^{6}Li without coupled channels processes (distorted waves with a finite radius of interaction)

Figure 4.10–Angular distributions of tritonsfrom the reaction ^{7}Li(*d, t*)^{6}Li, corresponding to transitions to the ground(1^{+}) andfirst excited(E$_x$ = 2.186MeV(3^{+})) states of ^{6}Li nucleus

Below we present the main features of the modified distorted-wave method (MDWBA) in application to the ^{7}Li(d, t)^{6}Li reaction to extract the value of the coefficient of asymptotic normalization (ANC) for the ^{7}Li$\rightarrow^6$Li + n system. According to [175, 176] for the pure peripheral neutron transferring (what is expected to be dominant within the main maximum of the tritons angular distribution) we can write the differential cross section in the form:

$$\frac{d\sigma}{d\Omega} = \left(\frac{C_{0,1/2}}{b_{0,1/2}} \right)^2 C_{l,j}^2 R(E,\theta;b_{l,j}), \qquad (4.1)$$

where

$$R(E,\theta;b_{l,j}) = \frac{\sigma^{DW}(E,\theta;b_{l,j})}{b_{l,j}^2}. \qquad (4.2)$$

Here $C_{0,1/2} = C_t$ and $C_{l,j}$are the ANCs, which determine the amplitudes of tails of the overlap functions for $t\rightarrow d + n$ and $^7\text{Li}_{\text{g.s.}}\rightarrow^6\text{Li} + n$ configurations; $b_{0,1/2}= b_t$ and $b_{l,j} = b$are the asymptotical coefficients of the shell model wave functions for the bound $t\rightarrow d + n$, $C_t$and $^7\text{Li}_{\text{g.s.}}\rightarrow^6\text{Li} + n$ states, respectively. There is assumed in MDWBA formalism, that the asymptotic behavior of the overlap integral of the radial wave functions and model wave functions is the same and corresponds to the Hankel function of the first order [18, p. 1689]. $\sigma^{DW}(E,\theta;b_{l,j})$ is the single particle cross section of neutron transferring calculated in the DWBA.

E and θare the relative kinetic energy of the interacting nuclei in the entrance channel and the emission angle of the triton in the CM-system. The values of the total angular momentumof the transferred neutron are j =1/2 or 3/2 for ground and j =3/2 for E_x = 2.186 MeV excited states of the final nucleus ^{6}Li at the transferred orbital momentum l = 1 for the considered reaction. As shown in [176, p. 485], the square of the ANC(C^2) is explicitly related tothe square of the modulus of nuclear vertex constants ($|G|^2$) and spectroscopic factor (S) for any vertex $B \rightarrow A + d$ by the following expression (indexes are omitted):

$$C^2=[(\mu c/\hbar)^2/\pi]\,|G|^2=Sb^2, \qquad (4.3)$$

whereμ is the reduced mass of the particles A and$d$.

So, seemingly, one could obtain the ANC directly through the spectroscopic factor ($S_{l,j}$), extracted from theanalysis of the experimental differential cross sectionsusing the FRESCO program and the value $b_{l,j}$ determined from the asymptotic behaviorof the Schrödinger equation for the bound state of ^{6}Li + n with the Woods-Saxon binding potential. However, at that one mustbe assured that the transfer of the neutronis a peripheralone-step process.Only at this case, the spread of extracted ANC values conditioned by ambiguities of the geometric parameters of the bound state potential will besmall enough (unlike SF values). The MDWBA provides the possibility to certain that the reaction proceeds through the tail of the appropriate

overlap function and to evaluate the model uncertainties of the obtained ANC value. In MDWBA formalism, function $R(E,\theta;b_{l,j}) = R(b)$ should not substantially depend on the $b_{l,j}$ (for example [177]) and consequently on varying the potential geometric parameters of the bound state, if the transfer occurs at the periphery of interacting nuclei. It should be stressed that both b_j and $\sigma_j^{DW}(E,\theta;b_j)$, and hence, SF depend strongly on the geometry parameters.

To confirm the peripheral character of the neutron transferring in thea rea of main peak of tritons angular distribution from the ^{7}Li(d,t)^{6}Li reaction the behavior ofthe function *R(b)* (2) was analyzed. In the figure 4.11 the value areas of the $R(b)$ is shown at varying the values r_0 and a within physically reasonable ranges of these parameters 1.0 ÷ 1.5 fm and 0.45 ÷0.85 fm correspondingly.The calculations were carried out with OP's of set 4 from table 4.5 for the triton emission angle corresponding to the main maximum of the angular distribution, θ_{CM}= 12°.One can see that the function *R(b)* weakly depends (within± 5%) on the geometrical parameters in theranges shown above for both ground and excited states of ^{6}Li. A similar result was obtained with other sets of OP's from table 4.5, indicating that the neutronpick-up is peripheralat least for tritons emitted to small angles. On the other hand, as it follows from the analysis performed in above, the neutronpick-up process dominates in this angular region. Thus, using the (4.1) and (4.2) equations, it is correct to evaluate the square ANC value for ^{7}Li → ^{6}Li + n by means of SF values and the corresponding values b_{lj} from table 4.7. But the more correct way is using the relation (4.3) with the values of SF, obtained in above accounting the contribution of other possible mechanisms.

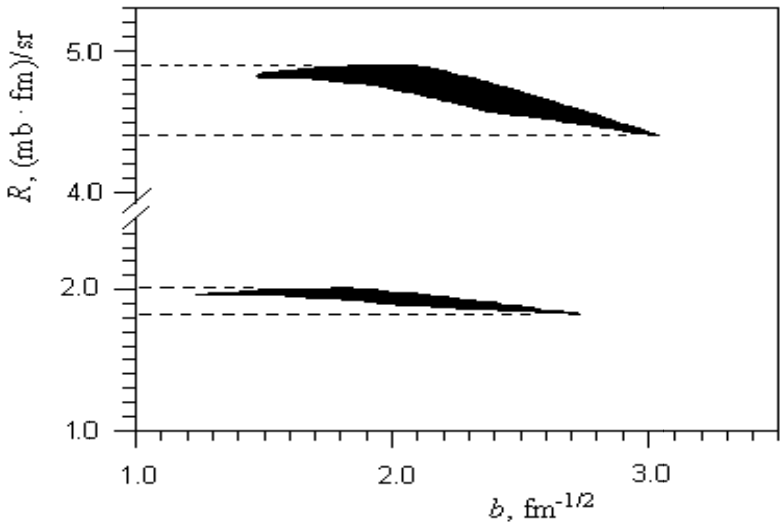

Excitations of ^{6}Li: E_x =0.0 MeV (1^+) - top, E_x =2.186 MeV (3^+) - bottom

Figure 4.11– Range of $R(b)$ values for the ^{7}Li (d, t)^{6}Li reaction for varying values of geometrical parameters r_0, a within the intervals 1.0 fm ÷ 1.5 fm and 0.45 fm ÷ 0.85 fm, respectively

Table 4.7–Spectroscopic factors S_{lj}, averaged over the sets of OP, ANC for ^{7}Li→^{6}Li+n states and nuclear vertex constants fort he corresponding vertex

State	l, j	S_{1j}	b_{1j}, fm$^{-1/2}$	C_{1j}^2, fm^{-1}	$\left\|G\right\|^2$, fm
^{7}Li→^{6}Li$_{g.s.}$+n	1, 1/2	0.28±0.02	2.087	1.22±0.17	
	1, 3/2	0.35±0.03	2.176	1.66±0.23	
	1, 1/2+3/2	0.63±0.05	2.133	2.88±0.40	0.55±0.08
^{7}Li→^{6}Li$_{2.186}$+n	1, 3/2	0.47±0.06	2.841	3.79±0.59	0.73±0.11

It should be emphasized that, as mentioned above, the extracted value of SF S_{lj} for (^{6}Li + n) configuration strongly depends on the geometrical parameters of the bound state potential. As is shown in figure 4.12, the value of SF is changed to five times along their variation in the mentioned above range, whereas the square of the ANC in thiscase varies in arange of 5% only. At the same time strong variations of the value S_{lj} is compensated by opposite phase variations of the value of single-particle ANC b_{lj}.

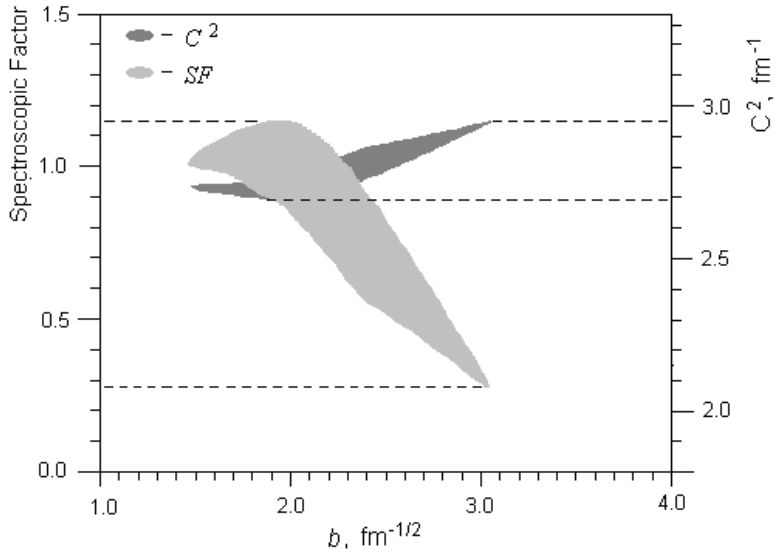

Figure 4.12– Ranges of SF and square values of ANC, correspondingto variation of r_0, a parameters (and, hence, value b), derived from MDWBA analysis of the ^{7}Li(d, t)^{6}Li$_{g.s.}$ reaction

The values of the squares ANC calculated by (3) for the ground state of ^{7}Li with ^{6}Li core at the ground and excited (E_x = 2.186 MeV) states are shown in table 4.7, column 5. In the column 4 the corresponding calculated values of the asymptotic coefficients b_{lj} are presented. The squared modul of the vertex constants $\left|G\right|^2$ for ^{7}Li → ^{6}Li$_{g.s.}$ + n and ^{7}Li → ^{6}Li$_{2.186}$ + n vertexes (the polar diagram in figure 4.5, left) are shown in sixth column. They were calculated by formula (3) with the obtained values S_{lj} and b_{lj}. The $\left|G\right|^2$ values are in good agreement with the results of [18, p. 1689] for the deuteron energy 18 MeV ($\left|G\right|^2$ = 0.60 ± 0.10 fm and 0.80 ± 0.09 fm for the vertexes ^{7}Li → ^{6}Li$_{g.s.}$ + n and ^{7}Li → ^{6}Li$_{2.186}$ + n, respectively). This evidence

indicates a lack of the energy dependence of the "experimental" $|G|^2$ at least in the energy range 18 ÷ 25 MeV, which was mentioned in the introduction. Underestimation of the value $|G|^2$ (= 0.3 fm) obtained in [18, p. 1689] from the analysis of the data [20, p. 1059] at E_d = 28 MeV, is apparently due to the fact that the experimental data include only the second and third diffraction maxima (θ> 40 °) where the contribution of the exchange mechanism, as shown in above, is not small.

The errors for SF, which are listed in table 4.7, include the standard deviations at averaging over sets of the OP. Absolute errors for the ANC squares include by statistically independent way the experimental errorsin the differential cross sectionsof the main maximum angular region, the model uncertainties due to the ambiguity of the parameters of the neutron binding potential (figure 4.11) and spread of values conditioned by ambiguity of the OP parameters in the entrance and exit channels.

The valuesof neutron SF for a number of nuclei were extracted in [178] from analysis of the angular distributions of the *(p, d)* and *(d, p)* reactions. In particular, for $^7\text{Li}_{\text{g.s.}} \rightarrow ^6\text{Li}+n$ the value $S = S_{1,\ 1/2+3/2} = 1.85 \pm 0.37$ was obtained from the $^7\text{Li}(p, d)^6\text{Li}$ reaction.This is in contradiction not only with theoretical predictions (table 4.6), but also with results of analysis ofthe inverse reaction (*d, p*), performed by the authors of this paper [178, p. 485] ($S = 1.12 \pm 0.32$) and with our result ($S = 0.63 \pm 0.05$). The discrepancy can be explained by the factthat the reaction $^7\text{Li}(p, d)^6\text{Li}$ is not peripheral (as it has been shown in [18, p. 1689]), since the value R is strongly dependenton the value of b (formula (4.2)). Consequently, it can't be used to obtain the reliable spectroscopic information within the distorted-wave method. Whereas the peripheral character of the $^7\text{Li}(d, t)^6\text{Li}$ reaction,as it was shown byour analysisand by the data of [18, p. 1689], is not in doubt.

It is also interesting to compare the values of ANC for the neutron and proton binding at ground states of the mirror nuclei ^{7}Li and ^{7}Be. There is an active discussion in recent years concerning the accuracy of a strong correlation between them ([179] and references therein). Indeed, if the SFs of these states are equal, the relation (4.3) implies: $C_p^2/C_n^2 = b_p^2/b_n^2$. This implies that the parameters of the nuclear potentials of bound states of the proton and neutron are equal. Equality of the nuclear parts of the binding potentials at the observed separation energies of nucleons (well-depth-procedure) is achieved for the Coulomb radius parameter values r_C = 1.575 fm for j_p = 1/2 and r_C = 1.515 fm for j_p = 3/2. There with, the value b_p^2 and so, the ratio b_p^2/b_n^2 for the mirror states practically does not depend onthe parameter r_C, as was shown in [180]. Moreover, our estimates show that the values S, C_p^2, b_p vary only within 0.2% when the r_C changes from 1.3 fm to 1.52 fm.The empirical square value of the ANC, $C^2_{^7\text{Be} \rightarrow ^6\text{Li}+p}$, obtained from analysis of the reaction $^6\text{Li}(^3\text{He},d)^7\text{Be}$ in MDWBA formalism is 3.13 ± 0.27 fm^{-1} [170, p. 10]. The single-particle asymptotic coefficients b_{lj} for $^7\text{Be}_{\text{g.s.}} \rightarrow ^6\text{Li} + p$ configuration are 2.145 fm$^{-1/2}$ (j_p =1/2) and 2.234 fm$^{-1/2}$ (j_p =3/2), and the average value b_p= 2.190 fm$^{-1/2}$ for the mentioned above nuclear -equivalent potential of a bound state. At the same time, taking into account the values b_{lj} and C_{lj}^2 from table 4.7 for the neutron bound state, the b_p^2/b_n^2 and

C_p^2/C_n^2 ratios are 1.05 ± 0.10 and 1.09 ± 0.10, i.e. well satisfy the $C_p^2/C_n^2 = b_p^2/b_n^2$ relation within the error limit.

Summuryto capter 4

The differential cross sections for elastic and inelastic scattering of ^{7}Li (d, d) ^{7}Li were measured at an energy of E_d = 14.5 MeV in the range of angles from 18° to 128° with a step of 2°.

From the analysis of experimental data on elastic scattering in the framework of OM, optimal parameters of optical potentials are found that satisfactorily describe the angular distributions in the full angular range.

Differential cross sections of deuterons scattered on ^{7}Li nuclei with excitation of the 0.478 MeV ($1/2^-$) state and tritons from the ^{7}Li(d, t)^{6}Li reaction with transition to the ground (1^+) state of the ^{6}Li nucleus have been measured at the deuteron beam with the energy 14.5 MeV. The differential cross sections for elastic and inelastic scattering with excitation of the 0.478 MeV ($1/2^-$) of ^{7}Li nuclei have been measured in the angular range 8°-169° (lab) at the deuteron beam energy of 25 MeV as well as the cross sections of the reaction ^{7}Li(d, t)^{6}Li with transitions to the ground (1^+) and excited (E_x = 2.186 MeV, 3^+) state of the ^{6}Li.

The experimental angular distributions were analyzed in the framework of the coupled reaction channels (CRC) method, with taking into account the exchange mechanism in the process ^{7}Li(d,^{6}Li)t with α-particle transfer. It was shown, that the channel coupling affects the triton emission cross sections only at the angles greater than 40°. In the main maximum region of the angular distributions for the ^{7}Li(d, t) ^{6}Li reaction, the CRC and the DWBA give an equivalent description ofthe experimental data. It was established that the mechanism of the one-step neutronpick-up dominates at the angles up to 40°, and that the reaction occurs on the surface of a nucleus.

The values of SF for ^{7}Li → ^{6}Li + n and ^{7}Li → ^{6}Li* + n systems were obtained by comparison of the calculated angular distributions with experimental data. The results are close to the theoretical predictions. The domination of the pick-up mechanism at the forward angles of triton emission and peripheral character of the ^{7}Li(d, t)^{6}Li reaction gives a possibility to obtain the reliable values of the ANC for ground state of ^{7}Li nucleus in ^{7}Li → ^{6}Li$_{g.s.}$ + n (C_{lj}^2 = 2.88 ± 0.40 fm^{-1}) and ^{7}Li → ^{6}Li$_{2.186}$ + n (C_{lj}^2 = 3.79 ± 0.59 fm^{-1}) configurations. It was shown that the square of the ANC for ^{7}Li → ^{6}Li$_{g.s.}$ + n configuration satisfy theoretically predicted ratio $C_p^2/C_n^2 = b_p^2/b_n^2$ for mirror nuclei ^{7}Li and ^{7}Be and is consistent with the value obtained in [170, p. 10].

5 Study of the interaction of deuterons and alpha particles with ^{11}B nucleus at low energies

5.1 Scattering and reaction (d, t) on ^{11}B nuclei at an energy of deuteron of 14.5 MeV

Nuclear reactions with the capture of one nucleon and, in particular, the reaction (d, t), are a convenient means of studying the hole states of nuclei resulting from the nucleon being pulled out of the shells of the target nucleus. However, you can use this tool only when the direct mechanism dominates.

In the analysis of such reactions, the method of distorted waves with potentials is usually used, the optimal parameters of which are found by comparing the theoretical elastic scattering cross sections calculated by the optical model with experimental data. However, in the field of light nuclei, such a procedure meets certain difficulties that do not allow one to obtain a satisfactory description of the experimental cross sections in the full range of angles.

The reaction ^{11}B (d, t) was previously studied only in one work [181]. In this work, at a deuteron energy of 11.8 MeV, the elastic scattering of deuterons and the angular distributions of tritons from the reaction (d, t) were measured for the four lower states of the ^{10}B nucleus. In the analysis of the measured angular distributions of tritons, an optical model and the method of distorted waves were used, suggesting a direct neutron capture mechanism.The calculated differential cross sections are in good agreement with the experiment in the region of small angles (up to 60°), but in the region of medium and large angles, the theoretical sections are much higher than the experimental ones. In addition, the spectroscopic factors extracted from the analysis for the states of the ^{10}B nucleus are two to three times higher than the theoretical values calculated in the framework of the shell model. The authors of [181, p. 449] see the reason for the poor description in the absence of suitable optical potentials for the interaction of tritons in the output channel and the too low energy of the emitted tritons from the reaction (d, t) at a reaction energy of Q = -5.197 MeV. To this we can add that the indicated work did not take into account the possible contribution to the reaction (d, t) of the exchange mechanism with the transfer of the heavy ^{8}Be cluster in the reaction ^{11}B (d, ^{10}B) t, which is physically indistinguishable from the pickup reaction ^{11}B (d, t) ^{10}B. It should also be noted that boron nuclei belonging to the nuclei of the middle of the p shell have an extremely high quadrupole deformation [3], therefore, when describing the angular distributions in the reaction (d, t), the collective nature of the states of these nuclei must be taken into account. So in [182], in which the reaction ^{11}B (α, t) ^{12}C was analyzed, it was shown that the quadrupole bonds of the ground (0^+) excited 4.44 (2^+) states of the ^{12}C nucleus quite strongly affect the cross sections of the reaction (α, t) during the transition into these states. It can be expected that the effects of channel coupling will also affect the reaction (d, t) and will be one of the reasons for the failure of the distorted wave method.

In the present work, in more detail than previously done at an energy of 11.8 MeV, we study the reaction mechanism of ^{11}B (d, t) ^{10}B at a deuteron energy of 14.5

MeV with transition to the ground state (3^+) and excited 0.72 MeV (1^+), 1.74 MeV (0^+, T = 1) and 2.15 MeV (1^+) states of the ^{10}B nucleus. The main objective of the study was to obtain information on the role of the direct neutron capture mechanism and the exchange mechanism with the transfer of a heavy cluster using the coupled channel method. Another goal of the study was to clarify the effects of the coupling of the reaction (d, t) with collective excitations of the target nucleus.

5.1.1 Experimental procedure and measurement results

The measurements were performed on a deuteron beam with an energy of 14.5 MeV extracted from the isochronous cyclotron U-150M of the Institute of Nuclear Physics (Almaty, Republic of Kazakhstan). The energy spread in the beam was about 150 keV.

The target was a self-sustaining boron film 0.2 mg/cm^2 thick enriched in ^{11}B 98%. The thickness was determined by the energy loss of α particles from a radioactive source with an accuracy of about 8%. Charged particles, products of nuclear reactions, were recorded by a telescope of counters, consisting of two thin (E) silicon detectors with thicknesses from 15 to 50 microns and thick (E) with 1–2 mm thickness. The deuterons and tritons were separated from other charged particles by a two-dimensional analysis system (E – E) using electronics in the CAMAC standard and a processing program implemented on a personal computer. The total energy resolution was determined mainly by the energy spread in the beam.

Typical spectra of deuterons and tritons scattered at an energy of 14.5 MeV from the ^{11}B (d, t) ^{10}B reaction are shown, respectively, in figure 5.1 and 5.2.

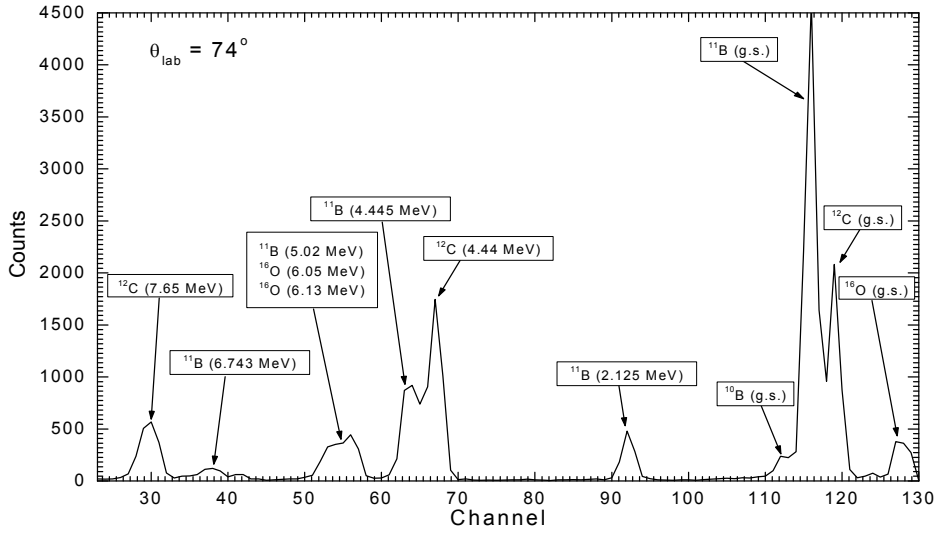

Figure 5.1 – Energy spectrum of scattered deuterons on an ^{11}B target

In the deuteron spectrum (figure 5.1), in addition to the elastic peak, intense transitions to the states of 4.445 MeV ($5/2^-$) and 6.742 MeV ($7/2^-$) are observed, which are members of the rotational band of the ^{11}B ground state (K = 3/2). The levels of 2.125 MeV ($1/2^-$) and 5.02 MeV ($3/2^-$), corresponding to the band K = 1/2, are excited much weaker.

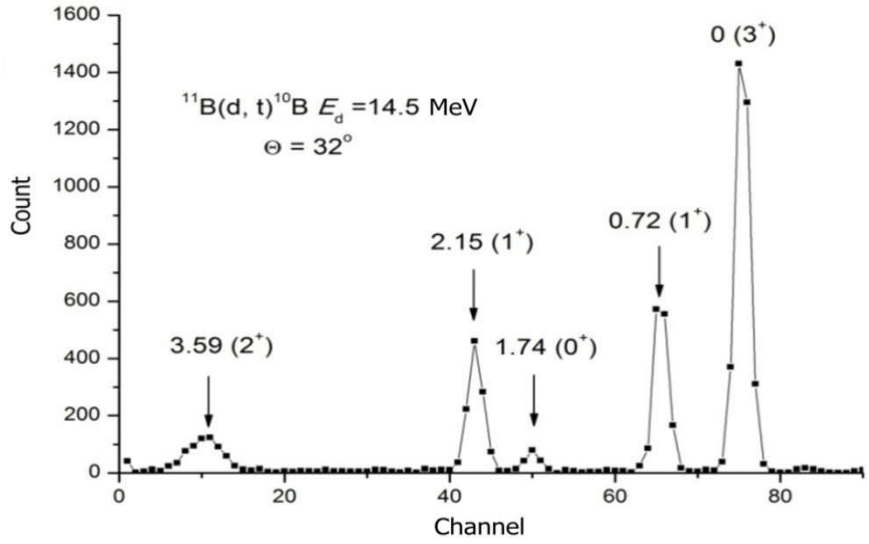

Figure 5.2 – The energy spectrum of tritons from the ^{11}B (d, t) ^{10}B reaction at beam energy of 14.5 MeV, measured at an angle of 32^0

The spectrum of tritons (figure 5.2) contains all previously known [183] states of the ^{10}B nucleus up to an excitation energy of 4 MeV. The strongest of them correspond to the ground (3+) transitions and states with excitation energies of 0.718 MeV (1^+) and 2.15 MeV (1^+). The impurities of carbon and oxygen present in the target interfere with observation due to the large negative reaction energies (Q = – 12.463 and –9.406 MeV, respectively).

The differential cross sections of deuterons and tritons were measured in the range of angles 20-163° in the center of mass system. The beam intensity was controlled in the usual way using a Faraday cup. The error in the current measurement did not exceed 1%. The relative errors of the measured cross sections were determined mainly by the statistics of recorded events and did not exceed 10%. As can be seen from figure 5.3 and 5.6, only in the angular distribution of elastic scattering there is a well-defined diffraction structure. In inelastic scattering and reaction (d, t), it is much weaker.

Errors in the absolute values of cross sections, in addition to statistics, were determined by uncertainties in the thickness of the target (8%), solid angle (2-3%), and current measurement (1%). They amounted to no more than 15%.

5.1.2 Elastic and inelastic scattering analysis by coupled channel method

At the first stage, the task was to find the optimal interaction potentials of deuterons with ^{11}B nuclei necessary for calculating both inelastic scattering and the reaction (d, t). This problem was solved on the basis of the analysis of the elastic scattering measured by us in the framework of the optical model using phenomenological potentials with bulk or surface absorption. In all calculations, r_C = 1.3 fm was assumed. The calculated cross sections were fitted to the experimental data using the SPI-GENOA program [184].

The found potentials and the corresponding volume integrals of the real (J_V /$2A_t$) and imaginary ($J_W/2A_t$) parts normalized to a pair of interacting particles (ApAt) are shown in table 5.1.

It is well known that the volume integral of the nuclear potential characterizes the data much better than the potential itself, since possible minor changes in some parameters can be compensated by changes in others without changing the quality of fitting and the value of the integral. As can be seen from the table, the $J_V/2A_t$ values do not contradict the prediction of the microscopic model and are in the range of 500-600 MeV*fm^3. Despite the equally good description of the elastic scattering experiment, the volume integrals of imaginary potentials vary greatly.

It is known that the ^{11}B core is strongly deformed, as a result of which low-lying states have a pronounced collective nature and form rotational bands. In this case, the description of inelastic scattering is most appropriate for the coupled channel method under the assumption that the interaction following the deformation of the nuclear surface is described by the optical potential V(r,R(θ′)) with a radius parameter R(θ′) depending on the polar angle θ ′ in fixed coordinate system associated with the core. For axial symmetry, the parameter R(θ′), taking into account only quadrupole and hexadecapole deformation (R(θ′)= R_0[1+ β_2 Y_{20}(θ′)+ β_4 Y_{40}(θ′)]). Here β_2 and β_4 are the parameters of the quadrupole and hexadecapole deformations.

Table 5.1 – Optical potentials used in the calculations of deuteron scattering on ^{11}B nuclei at beam energy of 14.5 MeV

№	V, MeV	r_V, Fm	a_V, Fm	W, MeV	r_W, Fm	a_W, Fm	r_C, Fm	$J_V/2A$, MeV*Fm^3	$J_W/2A$, MeV*Fm^3	χ^2/N
1	83.47	1.15	0.9	S25.6	1.916	0.354	1.3	594	385	11.1
2	72.21	1.15	0.9	V22.0	1.216	0.81	1.3	514	157	14.0
3	111.5	0.904	1.04	S10.6	1.779	0.505	1.3	648	202	8.3

In the calculations, we neglected the effects of mixing the ground state bands (K = 3/2) and the band starting from the level of 2.125 MeV (1/2$^-$) (K = 1/2). This is justified by the fact that transitions between states with different K are weak. Studies of ^{3}He scattering by ^{11}B [185] have shown that the band mixing model does not improve the description of the experimental data and does not significantly change the values extracted from the analysis of deformation parameters.

The calculations were carried out according to the FRESCO program [130, p. 177] using the potentials shown in table 5.1. A comparison of the calculated cross sections with experimental data is shown in figure 5.3. In the connection diagram shown in the inset, only quadrupole transitions were taken into account (L = 2), since according to [21, p. 064315], the ^{11}B core has no pronounced hexadecapole deformation. Since the quadrupole moment ^{11}B is large, reorientations of the spins of the ground (3/2$^-$) and excited (5/2$^-$ and 7/2$^-$) states were also included in the bond scheme. The analysis showed, however, that the effects of reorientation do not play a significant role. It can be seen that the calculations well reproduce the pronounced diffraction structure of elastic scattering and the almost structureless nature of the

angular distributions for excited states over the entire range of angles. The strain β_2 was a free parameter and was determined from the best description of the experimental cross sections. The average value for calculations with the potentials of table 5.1 turned out to be $\beta_2 = 0.80 \pm 0.2$. The obtained value is consistent with the results of other studies where the scattering of protons ($\beta_2 = 0.77$) [186], ^{3}He ($\beta_2 = 0.5$) [185, p. 83], and α particles ($\beta_2 = 0.6$) [21, p. 1303; 187] was analyzed.

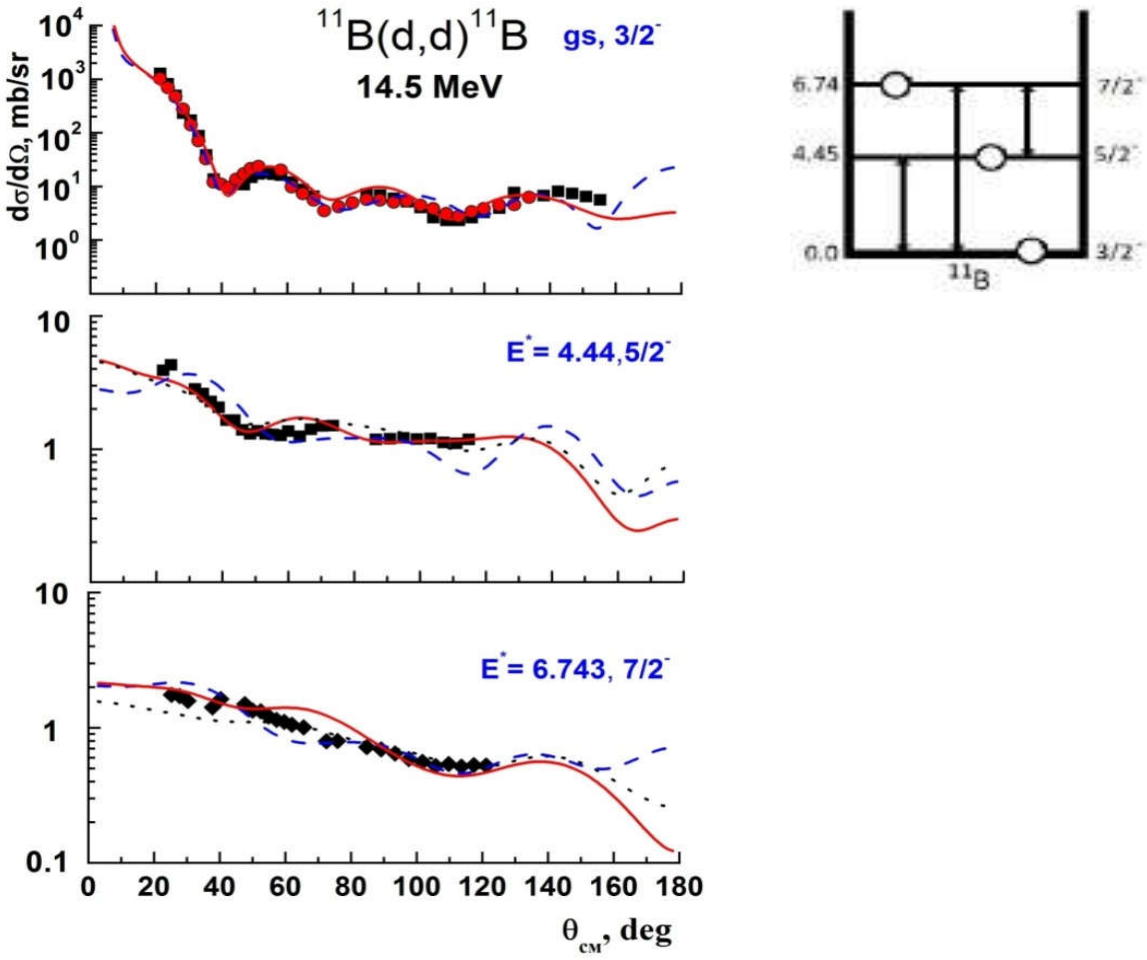

Red and black dots - correspond to two series of measurements of elastic scattering cross sections. Solid red, dashed blue, and dotted black curves - calculation by the coupled channel method with potentials 1, 2, and 3 from table 5.1, respectively. The inset shows the communication scheme used in the calculations

Figure 5.3 – Angular distributions of elastic and inelastic scattering of deuterons on ^{11}B nuclei for members of the rotational band of the ground state (K = 3/2): 0.0 ($3/2^-$) – 4.445 ($5/2^-$) – 6.74 ($7/2^-$) measured at a deuteron energy of 14.5 MeV (points)

5.1.3 Analysis of the reaction (d, t) by the method of coupled channels reaction

The angular distributions of tritons from the reaction (d, t) corresponding to transitions to the ground (3^+) and excited states of the ^{10}B nucleus with excitation energies E_x = 0.718 MeV (1^+), 1.74 MeV (0^+, T = 1), and 2.15 MeV (1^+), were analyzed by the method of coupled reaction channels using the FRESCO

computational program [130, p. 177]. In addition to the direct neutron capture mechanism in the reaction (d, t), the calculations took into account the exchange mechanism with the transfer of the ^{8}Be– (d, ^{10}B) heavy cluster, both in a single-stage process and in a two-stage process with sequential transfer of α-particles. The corresponding diagrams are shown in figure 5.4.

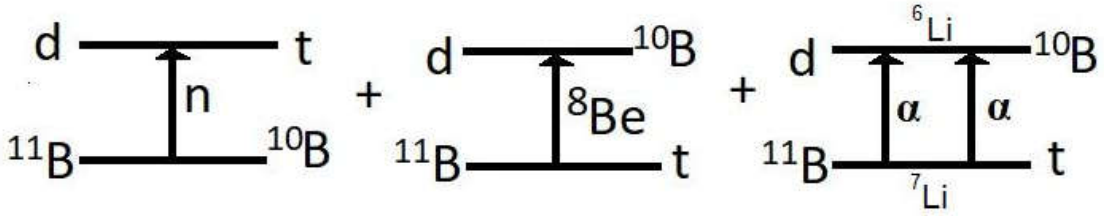

Figure 5.4– Diagrams taken into account in the calculation of the reaction cross sections (d, t) by the method of coupled reaction channels

When calculating the cross sections of the exchange mechanism, only a rough estimate is possible, since a heavy cluster can be transferred not only in the ground state, but also in excited states. In this case, the spectroscopic amplitudes are unknown with sufficient accuracy, which introduces large uncertainties in the calculations. For a rough assessment of the contribution of this mechanism, ^{8}Be transfer was taken into account only in the ground (0^{+}) state.

In addition, taking into account that the boron nuclei are strongly deformed and the lower states $3/2^{-}$, $5/2^{-}$, $7/2^{-}$^{11}B of a collective nature, the transitions between them were included in the bond scheme when calculating the reaction cross sections (d, t). The calculations were carried out with the quadrupole strain parameter β_2, found in the analysis of scattering with excitation of the 4.44 MeV ($5/2^{-}$) and 6.74 MeV ($7/2^{-}$) states of the ^{11}B nucleus. The analysis showed that the effects of the reorientation of state spins do not play a significant role and practically do not affect the shape of the angular distributions and the cross sections. The importance of taking into account the collective nature of nuclear states in the description of nucleon transfer was noted earlier in the study of the ^{11}B (α, t) ^{12}C reaction [182, p. 38]. Thus, the coupled-channel analysis included elastic scattering ^{11}B + d, reactions with the transfer of the neutron and the ^{8}Be heavy cluster, and excited states of the ^{11}B nucleus with quadrupole transitions $3/2^{-}$ - $5/2^{-}$, $5/2^{-}$– $7/2^{-}$, $3/2^{-}$-$7/2^{-}$ (figure 5.5).

The differential cross sections for the transmission reactions were calculated in the post-representation of the distorted wave method with accurate consideration of the finite radius of interaction built into the FRESCO program. The distortions in the input (^{11}B + d) and output (^{10}B + t) channels were calculated with potentials 1 and 2 from table 5.2. The potential 3 taken from [2, p. 30] took into account the interaction between the ^{6}Li and ^{7}Li nuclei in the intermediate channel when calculating the two-stage sequential transfer mechanism α particles.

The wave functions of bound states were calculated with the real Woods-Saxon potential with geometric parameters r_0 = 1.25 fm and a_0 = 0.65 fm. Depths were chosen such that the necessary cluster binding energy was obtained.

Since the theoretical values of the spectroscopic amplitudes of the clusters in the boron nuclei are unknown, they were assumed to be equal to unity. The spectroscopic amplitudes of the neutron capture reaction for the ^{11}B nucleus were considered free parameters and were determined from a comparison of theoretical and experimental cross sections. All SA values used in the calculations are shown in table 5.3. Their theoretical values calculated in [94, p.300; 173, p. 10] are also given there.

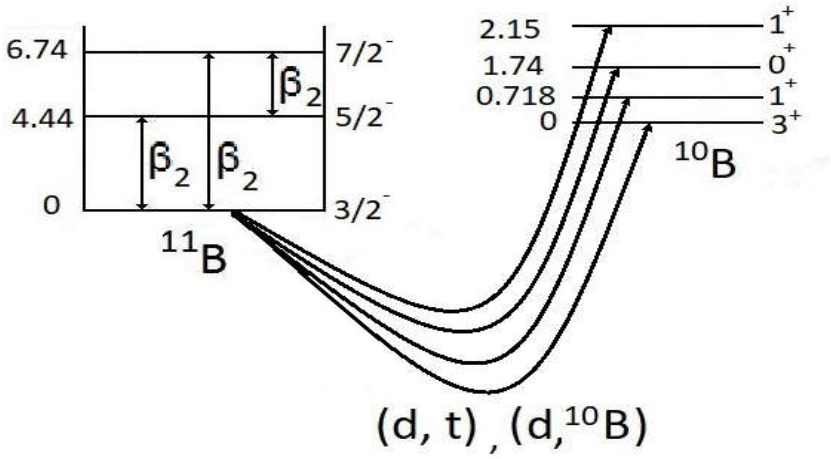

The scheme includes a neutron capture reaction with transitions to the ground and excited states of the ^{10}B nucleus and an exchange mechanism with the transfer of the ^{8}Be heavy cluster to the transition to the ground state

Figure 5.5 – The bond scheme used in the calculations of the ^{11}B (d, t) ^{10}B reaction

Table 5.2 –Optical potentials used in the calculations of the ^{11}B (d, t) ^{10}B reaction at an energy of 14.5 MeV

№	$A+a$	V, MeV	r_V, fm	a_V, fm	W, MeV	r_W, fm	a_W, fm	r_C, fm	Ref.
1	^{11}B+d	83.47	1.15	0.90	D23.6	1.916	0.35	1.3	[pres.work]
2	^{10}B+t	138.0	0.85	0.704	2.98	2.06	0.72	1.4	[2, p. 35]
3	^{6}Li+^{7}Li	109.0	1.13	0.50	23.0	1.206	0.45	1.9	[2, p. 35]

As the spectroscopic amplitudes (SA) of the neutron in the tritium nucleus (t → d + n) and α particles in the ^{6}Li and ^{7}Li nuclei, we took their theoretical values calculated in the framework of the translation-invariant shell model (TISM) [94, p.300].

A comparison of the calculated cross sections with the experimental data is shown in figure 5.6. The calculated cross sections quite well reproduce the nature of the angular distributions for transitions to the lower states of the ^{10}B nucleus at spectroscopic amplitudes from table 5.3. According to the selection rule due to the conservation of angular momentum, for the 1+ state at excitation energies of 0.718 MeV and 2.15 MeV, two values j = 1/2 and j = 3/2 are possible. Theory [94, p.300] predicts that in the first case j = 1/2 dominates, and in the other, j = 3/2. The analysis

showed that the shape of the angular distributions is practically independent of *j*. Therefore, all calculations for the lower states of the ^{10}B nucleus were performed for j = 3/2, except for the state of 0.718 MeV, for which the angular momentum was set equal to j = 1/2. As can be seen from table 5.3, the spectroscopic amplitudes extracted from the analysis for the lower states of the ^{10}B nucleus are in good agreement with theoretical predictions.

Table 5.3 – Spectroscopic amplitudes used in the calculations of the ^{11}B (d, t) ^{10}B reaction at an energy of 14.5 MeV

System	E_x, MeV	J^π,T	nL_j	SA	Theory prediction
$t \rightarrow d + n$	0.00	$1/2^+$,1/2	$1S_{1/2}$	1.23	1.23 [94, p. 300]
$^{10}B \rightarrow ^{11}B - n$	0.00	3^+,0	$1P_{3/2}$	1.15	1.05 [173, p.10]
	0.718	1^+,0	$1P_{3/2}$	0.59	0.27 [173, p.10]
			$1P_{1/2}$		0.44 [173, p.10]
	1.74	0^+,1	$1P_{3/2}$	1.46	0.80 [173, p.10]
	2.15	1^+,0	$1P_{3/2}$	0.95	0.68 [173, p.10]
			$1P_{1/2}$		0.26 [173, p.10]
$^{10}B \rightarrow d + ^8Be$	0.00	3^+, 0	$1D_2$	1.0	none
$^6Li \rightarrow d + \alpha$	0.00	1^+, 0	$2S_0$	1.06	1.06 [94, p. 300]
$^{10}B \rightarrow ^6Li + \alpha$	0.00	3^+, 0	$1D_2$	1.0	none
$t \rightarrow ^{11}B - ^8Be$	0.00	$1/2^+$, 1/2	$2P_1$	1.0	none
$^7Li \rightarrow ^{11}B - \alpha$	0.00	$3/2^-$, 1/2	$2S_0$	1.0	none
$t \rightarrow ^7Li - \alpha$	0.00	$1/2^+$, 1/2	$2P_1$	1.09	1.09 [94, p. 300]

In order to evaluate the possible contribution to the reaction (d, t) of the exchange mechanism with the transfer of the ^{8}Be heavy cluster and the two-stage process with the sequential transfer of α particles, calculations were performed for the transition to the ground (3^+) state of the ^{10}B nucleus. The results are shown in figure 5.6 by dashed (^{8}Be transfer) and dash-dot (serial transfer of α-particles) curves. It was believed that ^{8}Be is transmitted in the ground 0^+ state. It can be seen that the cross sections for both mechanisms are approximately three orders of magnitude smaller than the experimental values, so that metabolic processes do not play a significant role in the reaction (d, t).

To evaluate the effect of nuclear deformation on the reaction cross sections (d, t), calculations were performed with reaction bonds turned off with quadrupole transitions between the states of the $3/2^-$, $5/2^-$, and $7/2^-$ nuclei of ^{11}B. The result is shown in figure 5.6 dashed curves. It can be seen that taking into account the non-sphericity of the nucleus smoothes the diffraction structure of angular distributions and improves agreement with experiment in the range of medium and large angles.

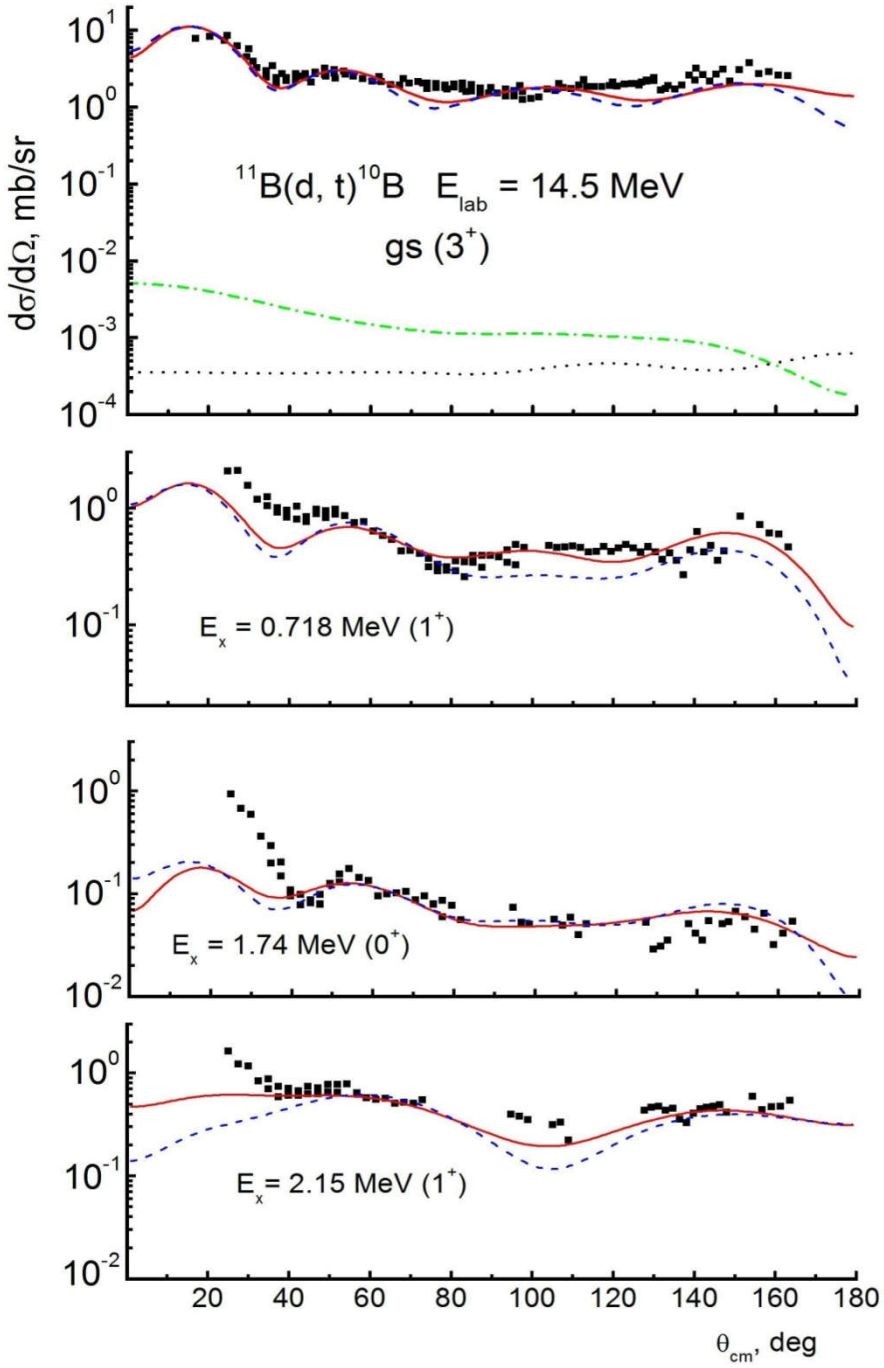

Points are experimental sections. Solid curves – calculation by the method of coupled reaction channels. The dashed curves show the calculated cross sections with disabled reaction (d, t) bonds with the excited states of the ^{11}B nucleus. To transition to the ground state of the ^{10}B nucleus, the dashed curve is the cross section calculated in the case of the exchange mechanism of transfer of the ^{8}Be heavy cluster, the dash–dot curve is the calculation for the two-stage mechanism with sequential transfer of α particles (figure 5.4)

Figure 5.6 – Angular distributions of tritons from the ^{11}B (d, t) ^{10}B reaction for transitions to the ground (3$^+$) and excited 0.718 MeV (1$^+$), 1.74 MeV (0$^+$), 2.15 MeV (1$^+$) states of the ^{10}B nucleus

5.2 Scattering and reaction (α, t) in the interaction of α-particles with ^{11}B nuclei at an energy of 40 MeV

The scattering of α particles on ^{11}B nuclei was previously studied at an energy of 25 MeV with excitation of the state of 4.445 MeV ($5/2^-$) [42, p. 318; 98, p.90]. Differential cross sections for transitions to other states were measured at higher beam energies from 40 to 65 [21, p. 1303; 108, p. 778]. When analyzing the measured angular distributions, with the exception of [21, p. 1303], the optical model and the distorted wave method were used. It should be noted, however, that the ^{11}B nucleus, which belongs to the nuclei of the middle of the p shell, has an extremely high quadrupole deformation [3, p. 313]. Therefore, it is quite natural that the low-lying states of this nucleus are interpreted as members of two rotational bands (K =$3/2^-$ and K =$1/2^-$): 0.0 MeV ($3/2^-$) - 4.445 MeV ($5/2^-$) - 6.742 MeV ($7/2^-$) and 2.125 MeV ($1/2^-$) - 5.02 MeV ($3/2^-$). This is confirmed by strong quadrupole transitions between these states [188]. In this case, when describing the scattering, the channel coupling effects become significant, which is the main reason for the failure of the distorted wave method. Without taking them into account, it is impossible to achieve an acceptable description of the experimental data. Under these conditions, the most appropriate method of analysis becomes the method of coupled channels. In addition, its use allows, in principle, to determine the sign of deformation. Thus, the results of studies of the scattering of α particles at energies of 40 and 50 MeV [21, p. 1303] and ^{3}He at energies of 17.5 and 40 MeV [185, p. 83], where the analysis was performed by the coupled channel method, unambiguously indicate the preference of the negative sign. At the same time, in [2, p.30; 8, p. 540; 98, p.90; 105, p. 115] a good description of the measured angular distributions was also achieved with a positive quadrupole deformation.

Although studies of the reaction (α, t) have been carried out for almost fifty years, they are still few of them. Differential cross sections for transitions to the ground (0^+) and excited (E_x = 4.44 MeV, 2^+) states of the ^{12}C nucleus were measured only at energies of 46 MeV [189] and 20-30 MeV [190-193] and mainly in range of angles of the front hemisphere. The cross sections calculated by the method of distorted waves under the assumption of a direct one-step mechanism are in poor agreement with experiment. The coupled channel method improves agreement, but only in the region of the front angles of triton emission [190, p.625; 193, p.592]. The reason for this discrepancy is due to the fact that the direct disruption mechanism at energies up to 30 MeV is apparently not dominant, which is facilitated by the high binding energy of the proton in the α particle and in the ^{12}C nucleus (ε = 19.8 and 15.96 MeV). It can be expected that a decrease in the cross section of the direct proton disruption mechanism will lead to an increase in the contribution of other mechanisms, for example, a composite nucleus and severe disruption. It should also be borne in mind that ^{11}B and ^{12}C nuclei are strongly deformed, therefore, when describing the angular distributions of the reaction (α, t), the collective nature of the states of these nuclei must be taken into account. As was shown in [194, 195], the quadrupole coupling of the main (0^+) and excited (E_x = 4.44 MeV, 2^+) of the states of

the ^{12}C nucleus significantly affects the reaction cross sections (α, t) upon transition to these states.

5.2.1 Experimental procedure and measurement results

The angular distributions of the differential cross sections for the scattering of α particles and tritons from the reaction (α, t) on ^{11}B nuclei were carried out on a beam of α particles with an energy of 40 MeV extracted from the isochronous cyclotron U-150M of the Institute of Nuclear Physics of the Republic of Kazakhstan.

The target was a self-sustaining film from the ^{11}B isotope with a thickness of about 0.2 mg/cm^2 enriched to 98%. The film thickness was determined by the energy loss of α particles from a radioactive source with an accuracy of ~ 8%. Charged particles, products of nuclear reactions, were recorded by a telescope consisting of two silicon detectors: one thin (ΔE) for measuring specific ionization and thick (E) for measuring the energy of a charged product. The thicknesses of the detectors were in the range of 30-100 μm (ΔE) and 1-3 mm (E). The scattered α-particles and tritons were separated from other charged particles by a ΔE-E two-dimensional analysis system using electronics in the CAMAC standard and a processing program implemented on a personal computer. The total energy resolution was about 400 keV and was determined mainly by the energy spread in the cyclotron beam.

Typical spectra of scattered α particles and tritons from the reaction (α, t) are shown in figures 5.7 and 5.8, respectively. There are no strong transitions in the spectra of α particles at excitation energies of ^{11}B above 7 MeV. In addition to elastic scattering, intense transitions to 4.445 MeV (5/2$^-$) and 6.742 MeV (7/2$^-$) states are observed, which are members of the rotational band of the ^{11}B ground state (K = 3/2). The levels of 2.125 MeV (1/2$^-$) and 5.021 MeV (3/2$^-$), related to the K = 1/2 band, are much weaker excited. The levels of 4.445 MeV (5/2$^-$) and 5.021 MeV (3/2$^-$) were not completely separated in our experiment. For their separation, a standard procedure was used with the structure decomposed into two peaks of a Gaussian shape with an energy resolution width.

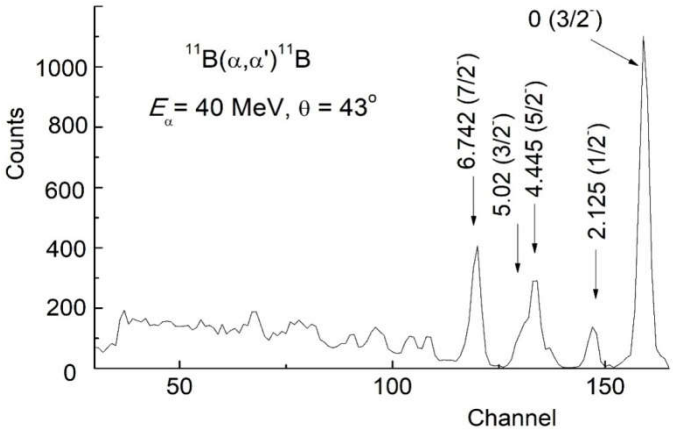

Figure 5.7 – The energy spectrum of α particles measured at an angle of 43^0 scattered on ^{11}B nuclei at a beam energy of 40 MeV

In the spectrum of tritons (figure 5.8), four intense transitions to the ^{12}C state are observed: the ground state (0^+), 4.44 MeV (2^+), 9.64 MeV (3^-) and the 14.08 MeV state (4^+) in the continuous spectrum region. The state of 7.65 MeV (0^+) is weakly excited.

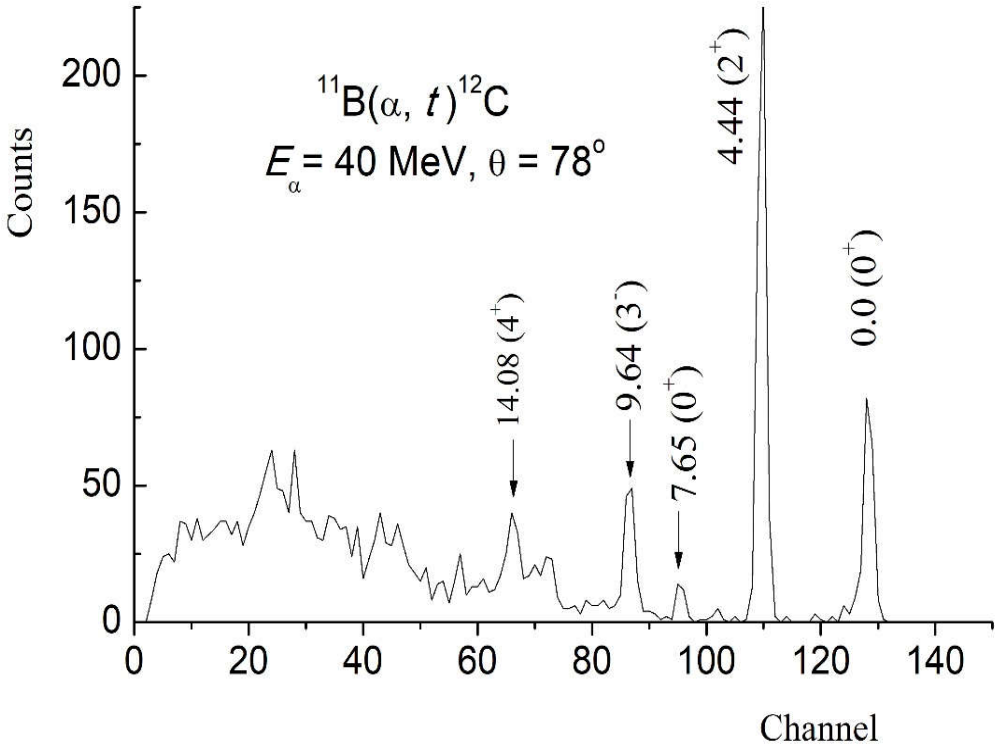

Figure 5.8 – Energy spectrum of tritons from the reaction (α, t) on ^{11}B nuclei measured at an angle of 78° at a beam energy of 40 MeV

The measurements were carried out in the range of angles 10-170° in the laboratory system. The experimental angular distributions of elastic and inelastic scattering are shown in figure 5.9. In all cases, in the region of the angles of the front hemisphere there is a well-defined diffraction structure, which attenuates at angles of more than 90°. It is seen that the cross sections for inelastic scattering oscillate in antiphase with elastic according to the Blair phase rule for levels with parity of the ground state. At the largest angles in the differential cross sections, an increase is observed, which may indicate a contribution to the scattering mechanism of a heavy breakdown.

The angular distributions of tritons from the $^{11}B(\alpha, t)^{12}C$ reaction with transitions to various states of the ^{12}C nucleus are shown in figure 5.10. In contrast to scattering, the diffraction structure in the reaction (α, t) is weakly manifested. Another feature of the measured differential cross sections is their slower decline for excited states compared with the transition to the ground state.

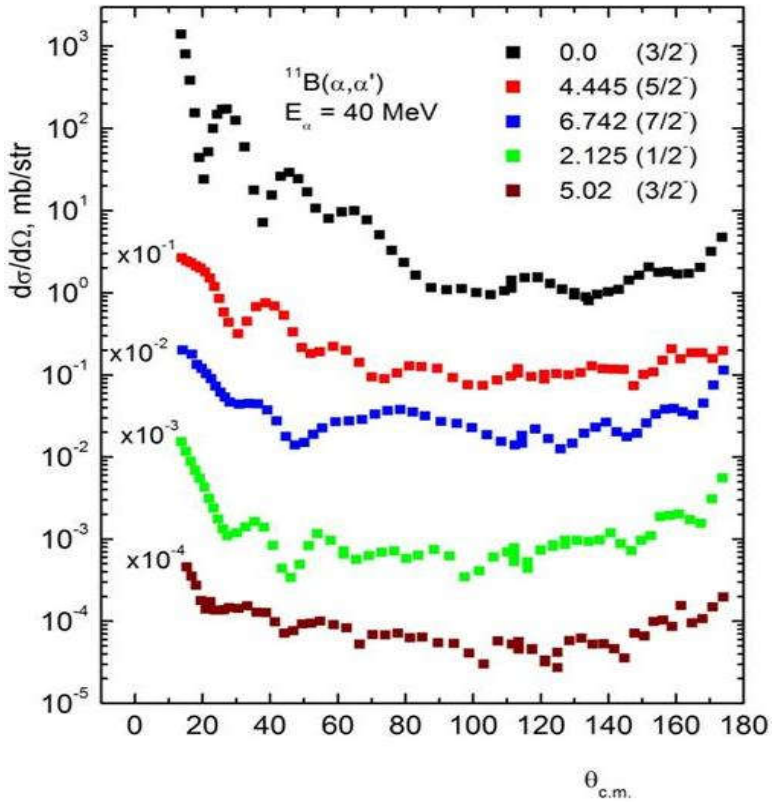

Figure 5.9 – Angular distributions of α particles scattered on ^{11}B nuclei with transitions to the ground and excited states at a beam energy of 40 MeV

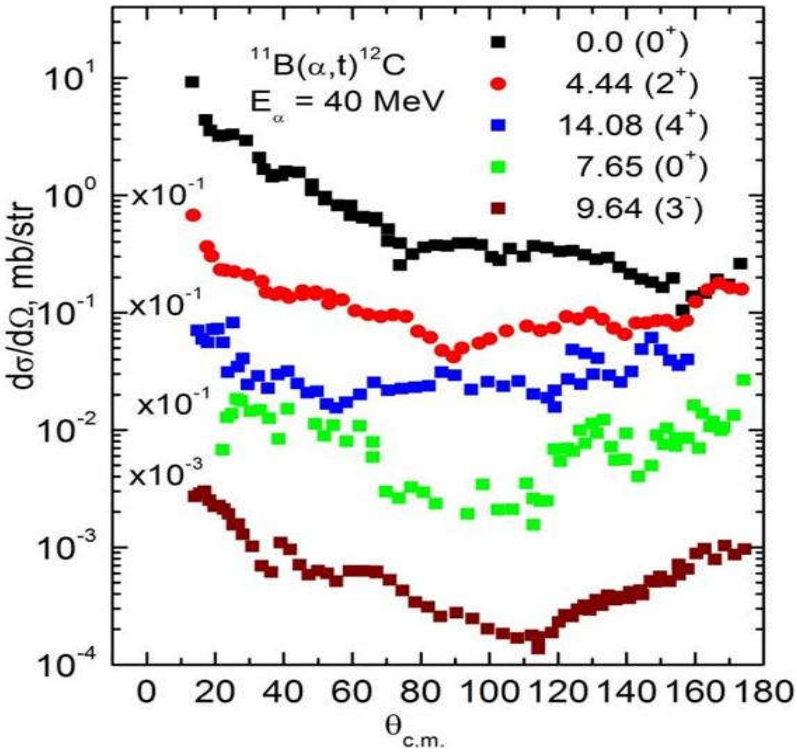

Figure 5.10 – Angular distributions of tritons from the ^{11}B (α, t) ^{12}C reaction, with transitions to different states of the ^{12}C nucleus at a beam energy of 40 MeV

5.2.2 Elastic and inelastic scattering analysis by coupled channel method

In this analysis, we used the previously obtained experimental data [3, p.310; 21, p.1303] on elastic and inelastic scattering of α particles with transition to the states of the rotational band of the ground state of the ^{11}B nucleus: 0.0 MeV ($3/2^-$) – 4.445 MeV ($5/2^-$) - 6.742 MeV ($7/2^-$). The task was to find the optical potential that better describes elastic scattering in the region of large angles. The analysis was carried out in the framework of the optical model using phenomenological potentials with volumetric or surface absorption. In all calculations, the Coulomb radius r_C = 1.3 fm was assumed. The calculations were performed using the SPI-GENOA program [184].

The found potentials corresponding to it volume integrals of the real (J_V/4A) and imaginary (J_W/4A) parts, normalized to a pair of interacting particles, are given in table 5.4.

Table 5.4 – Optical potentials used in calculating the scattering of α particles on ^{11}B nuclei at a beam energy of 40 MeV

№	*A+a*	*V*, MeV	r_V, fm	a_V, fm	*W*, MeV	r_W, fm	a_W, fm	r_C, fm	$J_V/4A$, MeV*fm^3	$J_W/4A$ MeV *fm^3
1	^{11}B+α	163.6	1.022	0.830	40.91	0.978	0.791	1.3	427	93
2	^{11}B+α				35.91*					
3	α+α	92.0	1.14	0.60	1.0	1.14	0.600	1.14		

Since the ^{11}B nucleus is strongly deformed and low-lying states are rotational in nature, the calculations by the coupled channel method are most adequate for describing scattering data. In such calculations, it is assumed that the interaction, following the deformation of the nuclear surface, is described by the optical potential V (r, R(θ′)) with the radius parameter R(θ′) dependent on the polar angle θ′ in the fixed coordinate system associated with the core. In the case of axial symmetry, the parameter R(θ′) contains only the quadrupole — β_2 and hexadecapole — β_4 deformations.

In our calculations, we neglected the effects of mixing the ground state bands (K = 3/2) and the band starting from the level of 2.125 MeV ($1/2^-$) (K = 1/2). This is justified by the fact that transitions between states with different K are weak. Studies of ^{3}He scattering by ^{11}B [185, p. 83] have shown that the band mixing model does not improve the description of the experimental data and does not significantly change the values extracted from the analysis of deformation parameters.

The calculations were carried out using the FRESCO program [130, p. 177] using the potential found by their analysis of elastic scattering and listed in table 5.4. In this case, to reconcile the cross sections calculated at large angles with the measured ones, the value of the imaginary potential depth was reduced by 5 MeV. A comparison of the calculated cross sections with the experimental data is shown in figures 5.11 and 5.12. It can be seen that the calculation well describes the experimental cross sections in the entire range of angles. An exception is the range of

angles of 70-100° for the transition to the 6.742 MeV ($7/2^-$) state, where theoretical cross sections do not reproduce the broad maximum observed in the experiment. In the communication schemes shown in the insets of figures 5.11 and 5.12, only quadrupole transitions (L = 2) were taken into account, since according to [21, p.1303], the ^{11}B nucleus does not have a pronounced hexadecapole deformation. Since the quadrupole moment ^{11}B is large, the reorientation effects of the spins of excited states ($3/2^-$, $5/2^-$ and $7/2^-$) were taken into account in the coupling scheme. The analysis showed that the effects of reorientation do not play a significant role. The strain β_2 was a free parameter, which was determined from the best description of the experimental cross sections. Calculations showed that $\beta_2 = 0.545$ satisfies this condition. Figures 5.11 and 5.12 show sections calculated with both a negative (solid curves) and a positive (dashed curves) sign of deformation. It can be seen that a negative sign is preferable. The obtained value of β_2 is consistent with the conclusion of [21, p.1303] and the results of other works, where proton scattering ($\beta_2 = 0.77$) [196] and ^3He ($\beta_2 = -0.5$) [185, p.83] were analyzed.

The calculations by the coupled channel method with the optical potential from table 5.4 give a fairly good description of the measured differential cross sections at large angles without taking into account the contribution of other mechanisms to the scattering process. Nevertheless, we estimated the probable contribution to the scattering of the heavy ^7Li cluster transfer mechanism: ^{11}B (α, ^{11}B) α. It is well known that at large angles of the cross section of the cluster transfer mechanism (C = A-a) in the reaction A (a, A) a, indistinguishable from scattering, in principle, it can significantly exceed the cross section of purely potential scattering. In the case of scattering of α particles by ^{11}B, the relatively small dissociation energy of the ^{11}B nucleus by ^7Li and the α particle (ε = 8.664 MeV) and spectroscopic amplitudes of the ^7Li + α configuration close to unity contribute to the increase in the contribution of this mechanism [21, p.1303]. Taking this mechanism into account is complicated, however, in comparison with the transfer of a light cluster (d, t, ^3He, α), a heavy cluster can be transmitted not only in the ground, but also in excited states for which spectroscopic amplitudes are not known with sufficient accuracy.

Differential cross sections calculated by the coupled reaction channel method using the FRESCO program taking into account the exchange mechanism of ^7Li cluster transfer are compared with experimental data for state transitions of the ^{11}B ground state band (K = 3/2): 0.0 ($3/2^-$) - 4.445 ($5/2^-$) - 6.74 ($7/2^-$) in figure 5.13. The calculations were performed taking into account the finite radius of interaction in the post-representation of the distorted wave method using the optical potentials from table 5.4 for the ^{11}B + α system and for the interaction between alpha-partial cores (α + α) ^{11}B cores in the input and output channels. Cluster (^7Li + α) wave functions of the bound states of the ^{11}B nucleus were calculated with the Woods-Saxon real potential, the geometric parameters of which were $r_0 = 1.25$ fm and a = 0.65 fm. The potential depth was chosen so that the desired cluster binding energy was obtained.

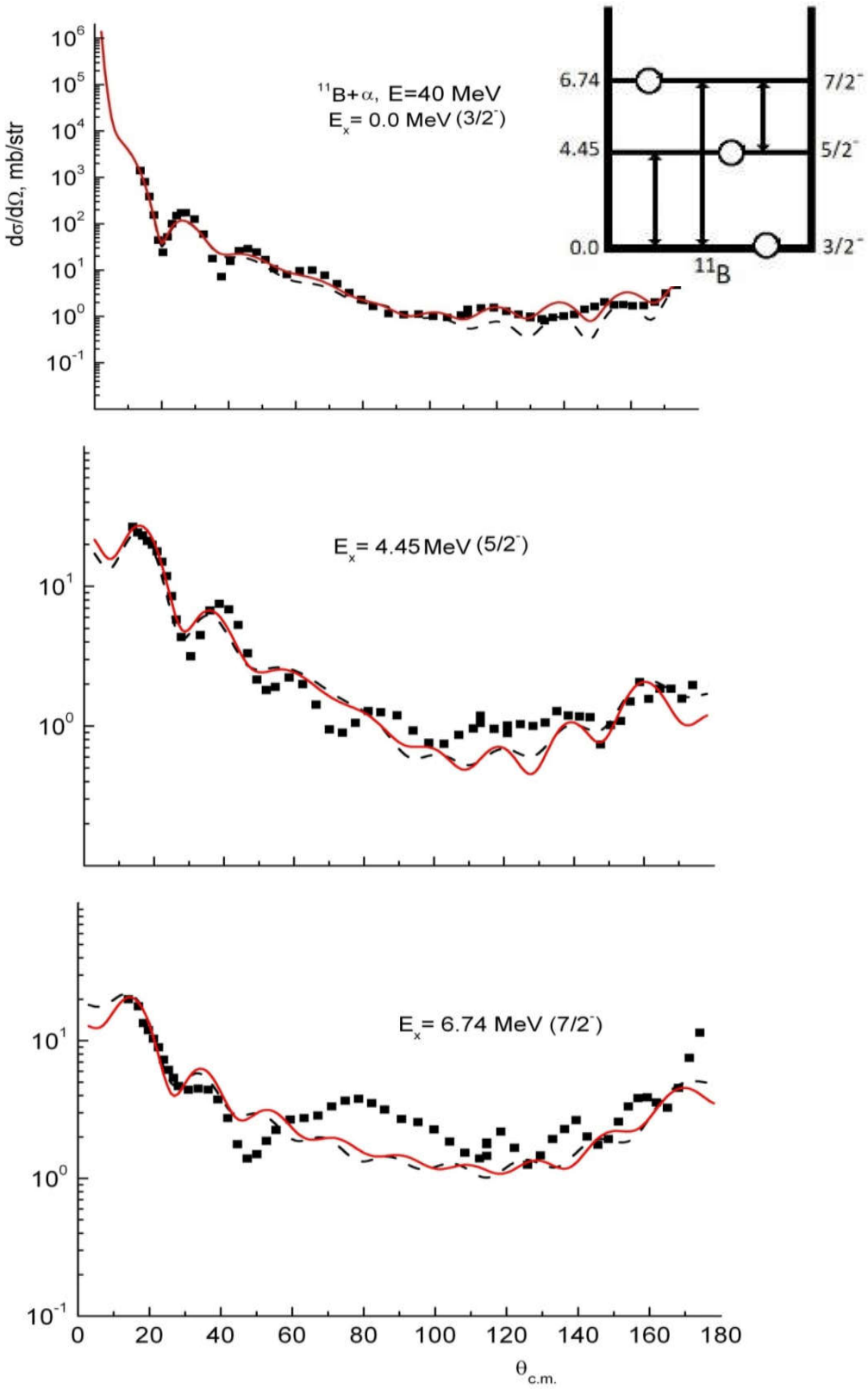

Solid red and dashed black curves are coupled-channel calculations with strain parameters β_2 = -0.545 and β_2 = +0.545, respectively, and with optical potentials from table 5.4.–The inset shows the communication scheme used in the calculations

Figure 5.11 - Angular distributions of elastic and inelastic scattering of α particles on ^{11}B nuclei for members of the rotational band of the ground state (K = 3/2): 0.0 (3/2$^-$) - 4.445 (5/2$^-$) - 6.74 (7/2$^-$), measured at an energy of 40 MeV (points)

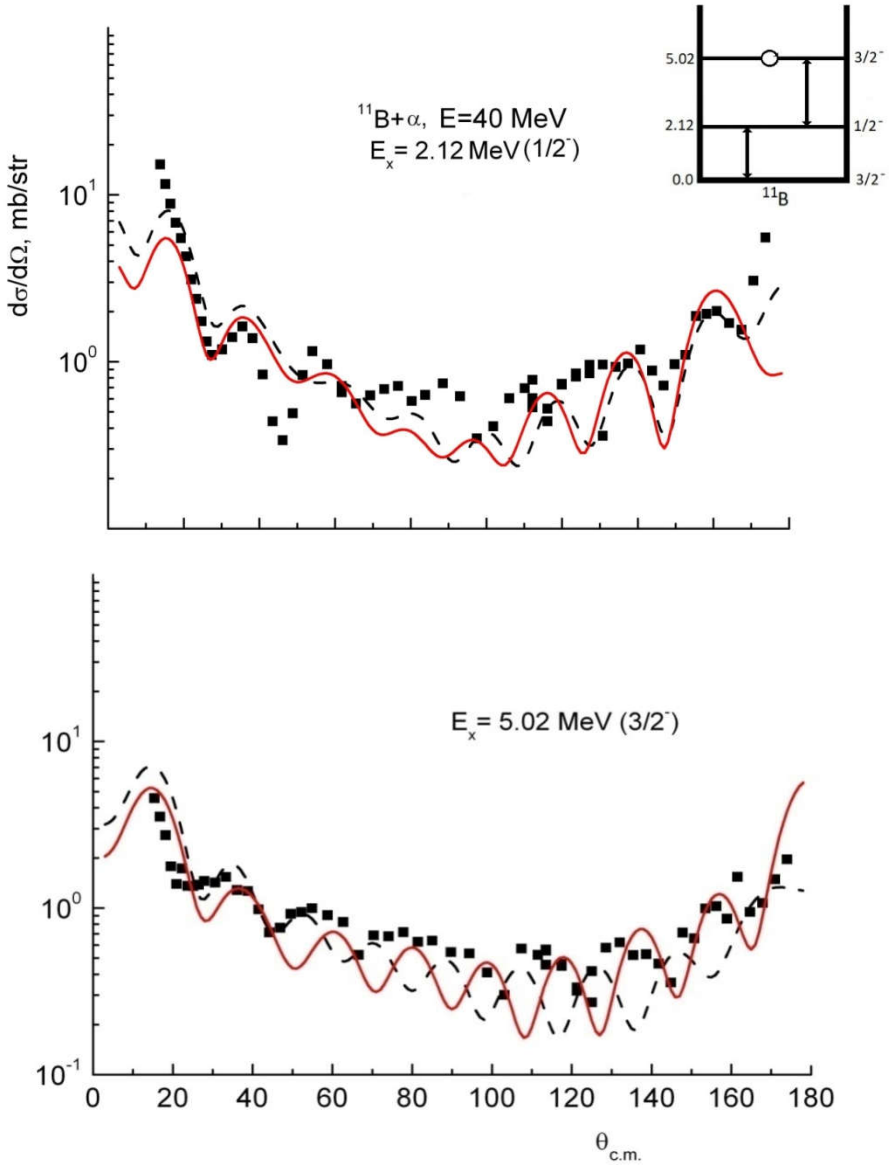

The designations of the curves are the same as in figure 5.11

Figure 5.12 – Angular distributions of elastic and inelastic scattering of α particles on ^{11}B nuclei for members of the rotational band (K = 1/2): 2.12 (1/2$^-$) - 5.02 (3/2$^-$), measured at an energy of 40 MeV (dots)

The number of nodes of the wave function (N) was determined from the equality 2N + L = 4, where L is the angular orbital moment of the relative motion of the clusters. For evaluative calculations, we took into account only ^{7}Li transfer in the ground state, and the spectroscopic amplitude was assumed to be unity. The calculated angular distributions for the mechanism of picking up the ^{7}Li cluster are shown in figure 5.13 by dashed curves. The total cross sections determined by the coherent addition of the scattering and transmission amplitudes of the heavy cluster are shown in the figure 5.13 by solid red curves. It can be seen that the exchange mechanism does not play a significant role.

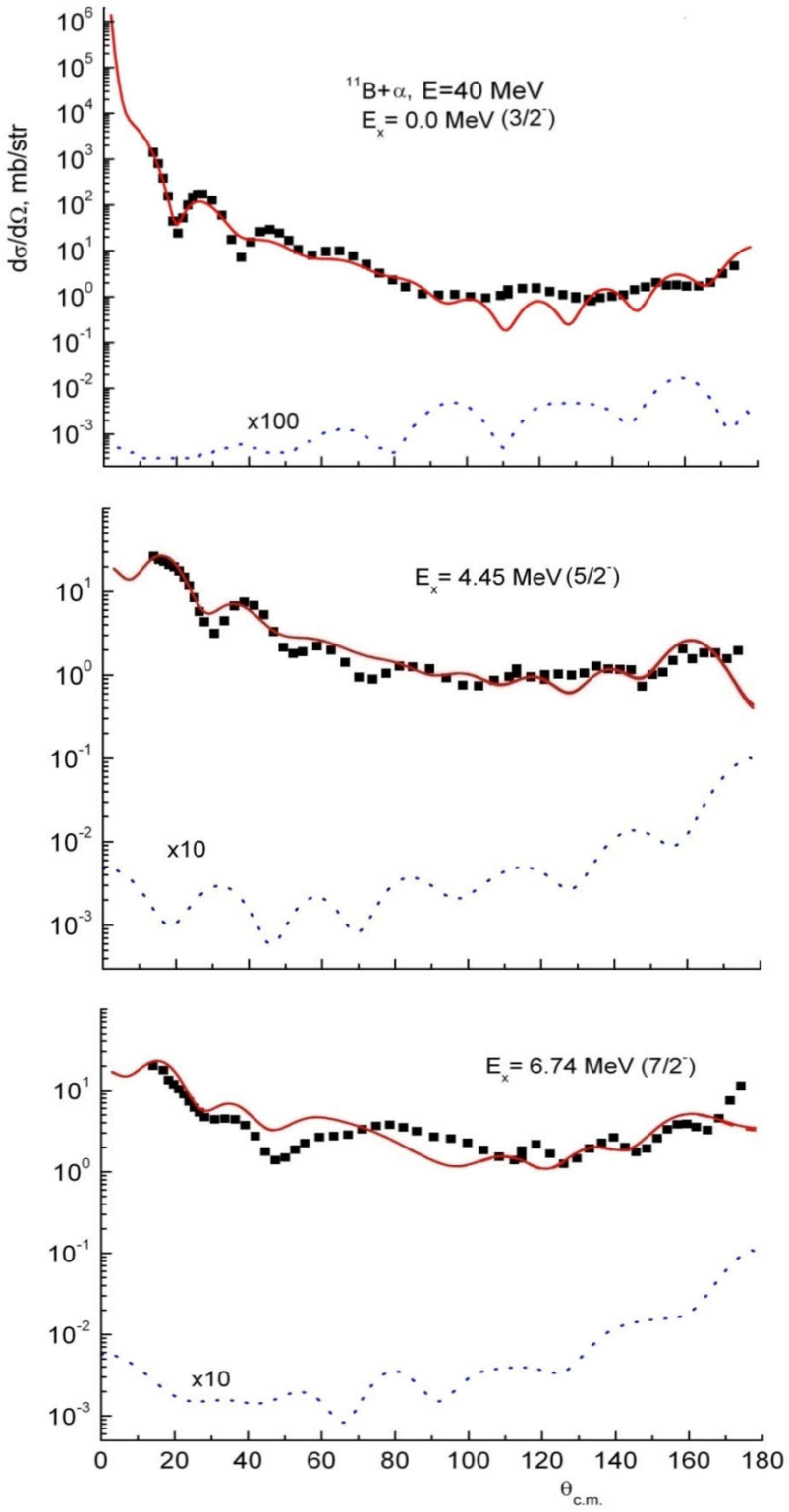

Dotted curves are cross sections calculated for the ^{7}Li heavy cluster transfer mechanism and multiplied by a coefficient of 100 (ground state) and 10 (excited states). The solid curves are the result of the coherent addition of the scattering amplitudes and the exchange mechanism

Figure 5.13 – Angular distributions of elastic and inelastic scattering of α particles on ^{11}B nuclei for members of the rotational band of the ground state (K = 3/2): 0.0 (3/2$^-$) - 4.445 (5/2$^-$) - 6.74 (7/2$^-$), measured at an energy of 40 MeV (points)

5.2.3 Analysis of the reaction ^{11}B (α, t) ^{12}C by the method of coupled reaction channels

The angular distributions of the differential cross sections of the reaction (α, t) with transition to the ground (0+) and excited states of the ^{12}C nucleus with energies E_x = 4.44 MeV (2^+), 7.65 MeV (0^+), 9.64 MeV (3^-), and 14.08 MeV (4^+) were analyzed by the method of coupled reaction channels according to the FRESCO program. In addition to the direct process of proton transfer in the reaction (α, t), the calculations took into account the exchange mechanism of heavy stall with the transfer of ^8Be nucleus. For a rough assessment of the role of the latter mechanism, we limited ourselves to the transfer of ^8Be in the ground state. All the transitions noted above caused by the reactions (α, t) and (α, ^{12}C) were included in the coupled channels scheme. Taking into account the fact that the ^{12}C nucleus is strongly deformed, the quadrupole and octupole transitions between the levels of this nucleus, as well as transitions associated with the reorientation of the spins of the excited states 2^+, 3^- and 4^+, were also included in the scheme. The analysis showed that the effects of reorientation do not play a significant role. The importance of taking into account the collective nature of nuclei in describing the reaction (α, t) was noted earlier in [194, p. 2077; 195, p. 243]. The connection diagram used in the calculations by the method of coupled reaction channels is shown in figure 5.14. In the calculations of the relations between the levels, a rotational model with fixed lengths of the quadrupole and octupole strains δ_2 = -2.1 and δ_3 = 1.8 Fm was used. With the mean square radius of the real part of the channel potential ^{12}C + t, with which the calculations were made, equal to $\langle r^2 \rangle^{1/2}$ = 3.242 fm, the average radius determined by the relation $R = \sqrt{5/3}\langle r^2 \rangle^{1/2}$ is R = 4.184 fm, which corresponds to strain parameters β_2 = - 0.50 and β_3 = 0.43. This is close to previously known results obtained from the analysis of scattering of protons and α particles on ^{12}C nuclei with excitation of 4.44 MeV (2^+) states (β_2 = 0.47 ± 0.05) and 9.64 MeV (3^-) (β_3 = 0.35 ± 0.06) [197-203].

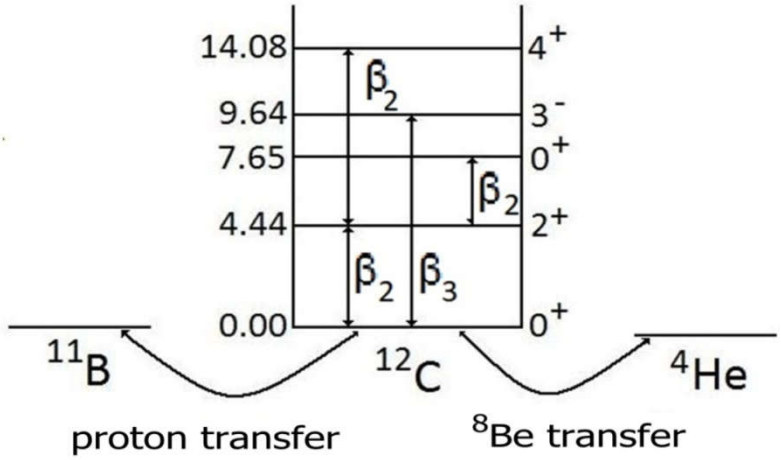

Figure 5.14 – The bond scheme used in the calculations of the reaction ^{11}B (α, t) ^{12}C

For the input and output channels, we used the optical potentials shown in table 5.5. The calculations were performed by the distorted wave method built into the FRESCO program with accurate consideration of the final interaction radius in the post representation. For the core – core ^{11}B + t and t + ^{4}He interactions, the potentials 7 and 8 from table 5.5 were used. The wave functions of the bound states of the ^{11}B + p, t + p, ^{4}He + ^{8}Be and t + ^{8}Be systems were calculated with the Woods-Saxon real potential, geometric whose parameters were r_0 = 1.25 fm and a = 0.65 fm. Depths of potentials were chosen such that the desired cluster binding energy was obtained.

Table 5.5 – Optical potentials used in the calculations of the reaction (α, t) on ^{11}B nuclei at a beam energy of 40 MeV

№	*A*+*a*	*V*, МэВ	r_V,Fm	a_V,Fm	*W*,MeV	r_W,Fm	a_W,Fm	r_C,Fm	Reference
1	^{11}B+α	163.6	1.022	0.830	30.0	0.978	0.791	1.3	[pres.work]
2	^{12}C+*t*	148.6	0.67	0.851	3.95	2.67	0.403	1.3	[pres.work]
					+6.81*				
3		133.3	1.13	0.686	15.6	1.75	0.76	1.13	[197,p.561]
4		121.2	1.10	0.800	14.1*	1.268	0.787	1.4	[198,p.3]
5		152.2	1.4	0.5	23.0	1.36	1.04	1.4	[199,p.97]
6		115.2	1.13	0.75	5.84	1.55	0.70	1.4	[200,p.153]
					+9.62*				
7	^{11}B+^{3}He	115.3	1.071	0.856	13.30	1.794	0.719	1.07	[201,p.545]
8	α+^{3}He	106.6	1.57	0.70	10.65	1.52	0.700	1.60	[202,p.201]

Spectroscopic amplitudes (SA) for the configurations α → t + p and ^{12}C (0+) → ^{11}B + p were taken from [94, p.310], where they were calculated in the framework of the translation-invariant model of shells. The remaining values were determined by fitting the calculated angular distributions to the experimental data. The SAs used in the calculations are shown in table 5.6.

Table 5.6 – Spectroscopic amplitudes used in the calculation of the reaction ^{11}B (α, t) ^{12}C

System	E_x,MeV	J^π	SA
α→*t*+*p*	0.00	0^+	1.91
^{11}B→*t*+^{8}Be	0.00	$3/2^-$	1.0
^{12}C→^{11}B +*p*	0.00	0^+	-1.7
	4.44	2^+	1.0
	7.65	0^+	1.0
	9.64	3^-	0.7
	14.08	4^+	0.9
^{12}C→ α + ^{8}Be	0.00	0^+	0.82
	4.44	2^+	1.0
	7.65	0^+	1.0
	9.64	3^-	1.0
	14.08	4^+	1.4

To describe the experimental cross sections, it was important to find the optimal optical interaction potential in the output channel $^{12}C + t$. We tested five potentials. They are shown in table 5.5 under numbers 2-6. A comparison of the calculated cross sections with the experimental ones for the transition to the ground state of the ^{12}C nucleus is shown in figure 5.15.

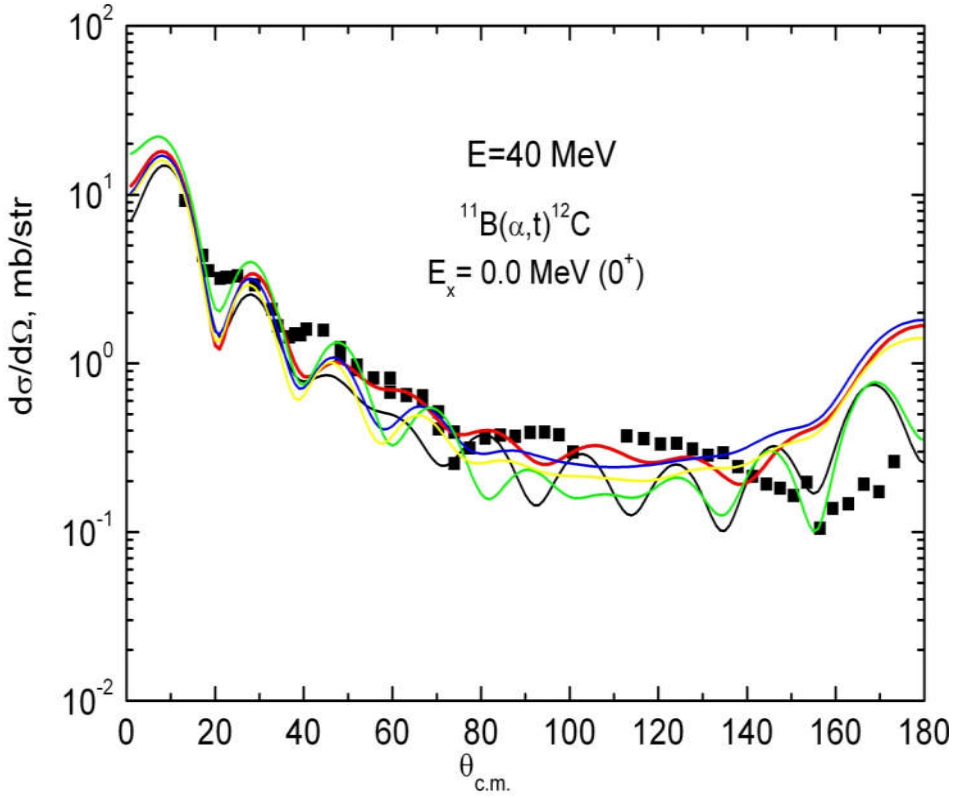

Points are measured sections. Black, red, blue, green, and yellow curves are calculated sections with potentials 2, 3, 4, 5, and 6 from table 5.5, respectively

Figure 5.15– Comparison of the cross sections calculated by the coupled reaction channel method for various optical potentials of the $^{12}C + t$ system with the experimental reaction data (α, t) with the transition to the ground state of the ^{12}C nucleus

As can be seen from the figure 5.15, the potential of the output channel strongly affects the cross sections at large angles, and the best result is given by potential 3 from table 5.5. All further calculations were made with it.

Figures 5.16 and 5.17 show a comparison of the calculated results with the measured reaction cross sections (α, t) with the transition to the ground and excited states of the ^{11}B nucleus with energies E_x = 4.44 MeV (2^+), 7.65 MeV (0^+) (figure 5.16) and 9.64 MeV (3^-), 14.08 MeV (4^+) (figure 5.17). Two reaction mechanisms were taken into account in the calculations: proton transfer and heavy disruption with ^8Be nucleus transfer in the ground state.

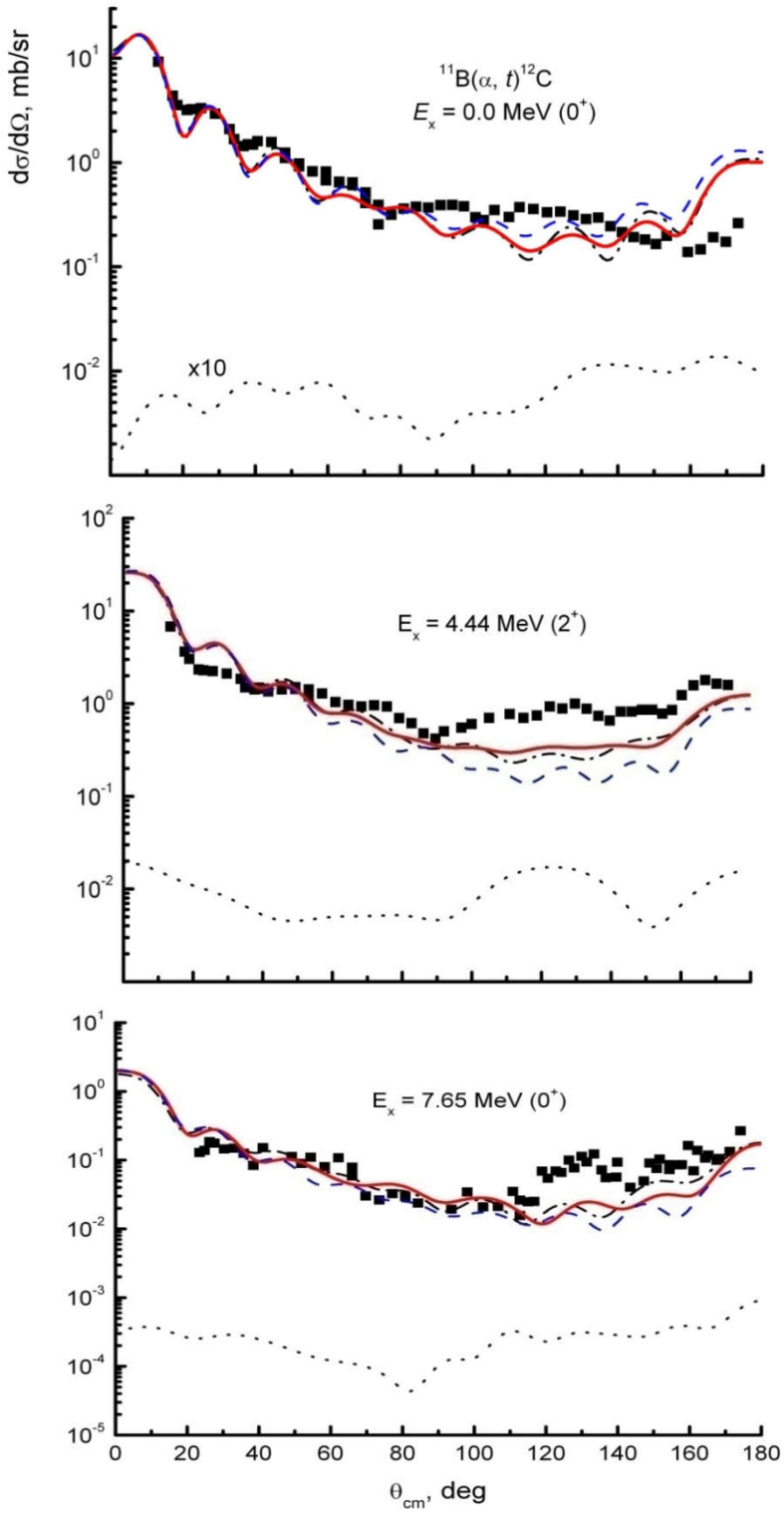

Squares are experimental points. Curves: dash-dotted black – calculation of the direct mechanism (α, t) with proton transfer, dotted black - heavy disruption (α, ^{12}C) with ^{8}Be cluster transfer in the ground state, solid red – coherent sum of the direct and exchange mechanisms. The dashed curves show the calculation of disconnected bonds due to deformation of the ^{12}C nucleus

Figure 5.16– Angular distributions of tritons from the ^{11}B (α, t) ^{12}C reaction corresponding to transitions to the ground (0$^+$) and excited states with energies E_x = 4.44 MeV (2$^+$) and E_x = 7.65 MeV (0$^+$) of the ^{12}C nucleus

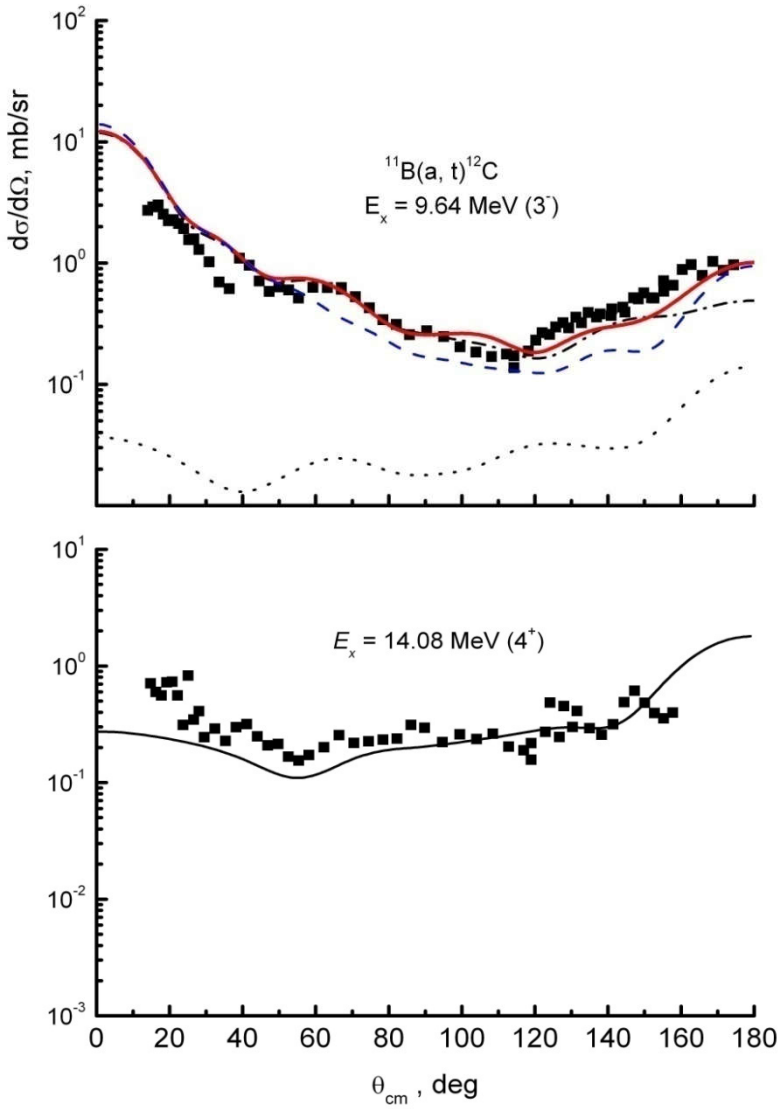

Squares are experimental points. For level 9.64 (3^-), the designations of the curves are the same as in figure 5.16. The solid curve for level 14.08 (4^+) is the calculation of the mechanism of severe disruption (α, ^{12}C) with the transfer of the ^{8}Be nucleus in the ground state

Figure 5.17– Angular distributions of tritons from the ^{11}B (α, t) ^{12}C reaction corresponding to transitions to the excited states of the ^{12}C nucleus with energies E_x = 9.64 MeV (3^-) and E_x = 14.08 MeV (4^+)

The calculated cross sections for direct proton transfer and heavy disruption are shown in the figures in black dot-and-dot and dotted curves, respectively. Their coherent sum for all transitions, with the exception of the transition to the state with E_x = 14.08 MeV (4^+), corresponds to solid red curves. It can be seen that the contribution of heavy disruption is quite small and is noticeable only at large angles. To assess the role of nuclear deformation on the reaction cross sections (α, t), calculations were performed with disconnected bonds between the states: 0.0 MeV (0^+) - 4.44 MeV (2^+), 0.0 MeV (0^+) - 9.64 MeV (2^+), 7.65 MeV (0^+) - 4.44 MeV (2^+) (blue dashed curves in the figures). It can be seen that taking into account the non-

sphericity of the ^{12}C nucleus and the relations between excited states due to it have little effect on the reaction cross sections at small angles, but strongly affect the cross sections and improve agreement with experimental data in the backward hemisphere.

A special case is the transition to the 14.08 MeV state (4^+). A direct mechanism with proton transfer to the 1p shell with excitation of level 4 is forbidden by the selection rules. Its formation is possible only due to other mechanisms. This level can be excited by the exchange of a heavy ^8Be cluster, through a composite core, or in multi-stage processes. Figure 5.17 shows the calculation of the mechanism of severe disruption (α, ^{12}C) with the transfer of the ^8Be nucleus in the ground state (black solid curve). It can be seen that the heavy disruption mechanism reproduces well the experimental cross sections for a reasonable spectroscopic amplitude of the $^{12}C \rightarrow \alpha + ^8Be$ configuration.

Thus, a comparison of the calculated cross sections with the experimental data shown in figures 5.16, 5.17 shows that, at an α-particle energy of 40 MeV, the dominant process of formation of the ground (0^+) and excited states with energies of 4.44 MeV (2^+), 7.65 MeV (0^+) and 9.64 MeV (3^-) is the direct mechanism of proton transfer in the reaction (α, t), and the transition to the 14.08 MeV state (4^+) is carried out by the mechanism of heavy disruption. However, it should be noted that the diffraction structure in the experimental angular distributions is somewhat less noticeable than it appears in the calculated cross sections. This can be explained by the contribution of two-step processes unaccounted for by us, for example, ^{11}B (α, ^5He) ^{10}B (^5He, t) ^{12}C. The mechanism of the formation of a compound nucleus does not play a significant role, as was shown earlier in [204].

Summury of chapter 5

At an energy of 14.5 MeV, elastic and inelastic scattering of deuteron ^{11}B nuclei with the excitation of low-lying states of 0.0 MeV ($3/2^-$), 4.445 MeV ($5/2^-$) and 6.74 MeV ($7/2^-$), as well as the reaction (d, t) with transitions to the ground (0^+) and excited states with energies of 0.718 MeV (1^+), 1.74 MeV (0^+, T=1) and 2.15 MeV (1^+). The analysis of experimental angular distributions was carried out by the method of coupled reaction channels in the framework of the collective model and direct mechanisms with neutron capture and with the transfer of heavy clusters. The calculations were carried out using the FRESCO program. From the scattering analysis, the optical potentials of the ^{11}B + d system were found, with which a good description of the experimental cross sections for elastic and inelastic scattering in the full range of angles was obtained, and the quadrupole deformation parameter β_2 = 0.80 ± 0.2 was extracted in accordance with the results obtained from proton scattering, α -particles and ^3He.

Assuming the reaction (d, t) to be the direct mechanism of neutron capture, it is possible to fairly well describe the angular distributions for transitions to the ground (0^+) and excited states with energies of 0.718 MeV (1^+), 1.74 MeV (0^+, T = 1), and 2.15 MeV (1^+) ^{10}B nucleus. Spectroscopic amplitudes extracted from the analysis are consistent with the theoretical predictions of the shell model. The possible contribution to the reaction of the exchange mechanism of the transfer of the heavy

^{8}Be cluster in the reaction ^{11}B(d,^{10}B)t, which is physically indistinguishable from the reaction (d, t), is estimated. It was shown that both single-stage (with ^{8}Be transfer) and two-stage (with sequential transfer of α-particles) mechanisms do not play a significant role at a deuteron energy of 14.5 MeV.

It was found that the deformation of the ^{11}B nucleus significantly affects the reaction cross sections (d, t). Taking into account non-sphericity smooths the diffraction structure of angular distributions and improves agreement with experiment in the range of medium and large angles.

At an energy of 40 MeV, elastic and inelastic scatterings of α-particles on ^{11}B nuclei were investigated with the excitation of low-lying states belonging to the two rotational bands with $K = 3/2$ and $K = 1/2$: 0.0 MeV (3/2) – 4.445 MeV (5/2) – 6.74 MeV (7/2) and 2.125 MeV (1/2) – 5.02 MeV (3/2). The analysis of the experimental angular distributions was carried out via the coupled channels method within the framework of the collective model using the FRESCO program. The calculations reproduce quite well the experimental cross-sections in the full angular range with the optical potential found for the system ^{11}B+$\alpha$and with the parameter of quadrupole deformation $\beta_2 = 0.545$. An indication is obtained of the preference of the negative sign of the quadrupole deformation, which is consistent with the results of the analysis of the scattering of protons, α-particles and ^{3}He.An estimation was made of the probable contribution to the scattering process of the exchange mechanism of the ^{7}Li heavy cluster transfer in the ^{11}B(α,^{11}B)αreaction, which is physically indistinguishable from the scattering process. The differential cross-sections for the scattering and the exchange process were calculated by CCR using the FRESCO code with exact account of the finite-range interaction in the *post*-representation of DWBA which was incorporated in the code. It was shown that the exchange mechanism does not play an important role in thescattering of α-particles on ^{11}B nuclei at the energy of 40 MeV.

The differential cross sections of tritons from the ^{11}B (α, *t*) reaction were measured with transitions to the ground (0^+) and excited states at energies E_x = 4.44 MeV (2^+), 7.65 MeV (0^+), 9.64 MeV (3^-) and 14.08 MeV (4^+) of the ^{12}C nucleus in the full angular range at the energy of α-particles of 40 MeV. The analysis of the measured differential cross sections was carried out within the framework of the coupled reaction channels method using the FRESCO program. In addition to the direct transfer of the proton in the reaction (α, *t*), the exchange mechanism with the ^{8}Be cluster was also taken into account. It was established that a direct proton transfer mechanismisthe dominant process in the (α, *t*) reaction with formationof the ground (0^+) and excited states of the ^{12}C nucleus at energies of 4.44 MeV (2^+), 7.65 MeV (0^+) and 9.64 MeV (3^-), and the contribution of the exchange mechanismis rather small and itis noticeable only at large angles at the particle energy of 40 MeV. An exception is the transition to the14.08 MeV (4^+)state. The selection rules prohibit the direct transfer of a proton into 1*p*-shell with excitation of the 4^+ level. The analysis showed that only the exchange mechanism with the ^{8}Be transfer makes possible to reproduce the experimental cross sections for this state.

It is shown that the nonsphericity of the ^{12}C nucleus and the resulting couplings between the excited states have little effect on the (α, *t*) reaction cross sections in the angular region of the forward hemisphere, but it strongly affects on the cross sections at large angles. The considering these couplings improve agreement with the experimental data.

The analysis of the angular distributions of the (α, t) reaction shows that the diffraction structure appeared in the experiment is less noticeable than in the angular distributions calculated in the framework of the coupled reaction channels method. This can be explained by the contribution of the two-step processes, for example ^{11}B (α, $^{5}He)^{10}B$ (^{5}He, *t*)^{12}C,which was not considered in the current paper, and it can lead to the blurringof the diffraction structure.

CONCLUSIONS

This dissertation presents the results of a study of the interaction of deuterons and α - particles on the nuclei of light charged particles, in particular, elastic and inelastic scattering of ^{3}He ions and α - particles on ^{7}Li and ^{11}B nuclei at energies of 7-10 MeV/nucleon. The main results of the work performed are presented and published in the following works [148, p.52; 149, p. 6; 152, p. 942; 155, p. 5; 182, p. 38; 187, p. 1850094, 205-217].

Self-sustaining targets were made from enriched ^{7}Li and ^{11}B isotopes with thicknesses of 150 - 300 μg/cm^{2}. The characteristics of the surface-barrier VPE GaAs detector are established.

The differential cross sections for elastic and inelastic scattering of ^{7}Li (d, d) ^{7}Li were measured at an energy of E_d = 14.5 MeV in the range of angles from 18^{o} to 128^{o} with a step of 2^{o}.

From the analysis of experimental data on the elastic scattering of ^{7}Li (d, d) ^{7}Li in the framework of OM, the optimal parameters of optical potentials are found that satisfactorily describe the angular distributions in the full angular range.

The differential cross sections ^{7}Li(*d*, *t*)^{6}Li reaction with transition to the ground (1^{+}) state of the ^{6}Li nucleus have been measured in the angular range 18^{o}-122^{o} (lab) at the deuteron beam with the energy 14.5 MeV. The differential cross sections of the reaction ^{7}Li(*d, t*)^{6}Li with transitions to the ground (1^{+}) and excited (E_x = 2.186 MeV, 3^{+}) states of the ^{6}Li have been measured in the angular range 8^{o}-169^{o} (lab) at the deuteron beam energy of 25 MeV.

The experimental angular distributions were analyzed in the framework of the coupled reaction channels (CRC) method, with taking into account the exchange mechanism in the process ^{7}Li(*d*,^{6}Li)*t* with *α*-particle transfer. It was shown, that the channel coupling affects the triton emission cross sections only at the angles greater than 40^{o}. In the main maximum region of the angular distributions for the ^{7}Li(*d, t*) ^{6}Li reaction, the CRC and the DWBA give an equivalent description of the experimental data. It was established that the mechanism of the one-step neutronpick-up dominates at the angles up to 40^{o}, and that the reaction occurs on the surface of a nucleus.

The values of SF for ^{7}Li → ^{6}Li + *n* and ^{7}Li → ^{6}Li* + *n* systems were obtained by comparison of the calculated angular distributions with experimental data. The results are close to the theoretical predictions.

At an energy of 14.5 MeV, elastic and inelastic scattering of deuterons on ^{11}B nuclei with excitation of low-lying states of 0.0 MeV ($3/2^{-}$), 4.445 MeV ($5/2^{-}$) and 6.74 MeV ($7/2^{-}$), as well as the reaction (d, t) with transitions to the ground (0^{+}) and excited states with energies of 0.718 MeV (1^{+}), 1.74 MeV (0^{+}, T = 1), and 2.15 MeV (1^{+}). From the scattering analysis, the optical potentials of the ^{11}B + d system were found, with which a good description of the experimental sections of elastic and inelastic scattering in the full range of angles was obtained, and the value of the quadrupole strain parameter $\beta_2 = 0.80 \pm 0.2$ was extracted in accordance with the results obtained from scattering of protons, α particles and ^{3}He.

Assuming a direct neutron capture mechanism in reaction (d, t), it is possible to describe fairly well the angular distributions for transitions to the ground (0^+) and excited states with energies of 0.718 MeV (1^+), 1.74 MeV (0^+, T = 1), and 2.15 MeV (1^+) ^{10}B nucleus. Spectroscopic amplitudes extracted from the analysis are consistent with the theoretical predictions of the shell model. The possible contribution to the reaction of the exchange mechanism of the transfer of the heavy ^{8}Be cluster in the reaction ^{11}B (d, ^{10}B) t, which is physically indistinguishable from the reaction (d, t), is estimated. It was shown that both single-stage (with ^{8}Be transfer) and two-stage (with sequential transfer of α-particles) mechanisms do not play a significant role at a deuteron energy of 14.5 MeV.

The differential cross sections of tritons from the ^{11}B (α, *t*) reaction were measured with transitions to the ground (0^+) and excited states at energies E_x = 4.44 MeV (2^+), 7.65 MeV (0^+), 9.64 MeV (3^-) and 14.08 MeV (4^+) of the ^{12}C nucleus in the full angular range at the energy of α-particles of 40 MeV. In addition to the direct transfer of the proton in the reaction (α, *t*), the exchange mechanism with the ^{8}Be cluster was also taken into account. It was established that a direct proton transfer mechanismisthe dominant process in the (α, *t*) reaction with formationof the ground (0^+) and excited states of the ^{12}C nucleus at energies of 4.44 MeV (2^+), 7.65 MeV (0^+) and 9.64 MeV (3^-), and the contribution of the exchange mechanismis rather small and it is noticeable only at large angles at the particle energy of 40 MeV. An exception is the transition to the14.08 MeV (4^+) state. The selection rules prohibit the direct transfer of a proton into 1*p*-shell with excitation of the 4^+ level. The analysis showed that only the exchange mechanism with the ^{8}Be transfer makes possible to reproduce the experimental cross sections for this state.

REFERENCES

1 Hodgson P.E. The nuclear optical model // Rep. of Progress in Physics. –1971. – Vol. 34. – P. 765-819.

2 Perey C.M., Perey F.G. Compilation of phenomenological optical–model parameters 1954–1975 // Atomic Date and Nucl. Date Tables. –1976. –Vol. 17. –P. 2-101.

3 Баррет Р., Джексон Д. Размеры и структура ядер / пер. с англ. – Киев: “Наукова думка“,1981. –419 с.

4 Гриднев К.А., Оглоблин А.А. Аномальное рассеяние назад и квазимолекулярная структура ядер // ЭЧАЯ. –1975. –Т. 6, вып. 2. –С. 393-434.

5 Теплов И.Б., Зеленская Н.С., Лебедев В.М. и Спасский А.В. Обратные максимумы сечения в ядерных реакциях и обменные процессы // ЭЧАЯ. –1977. –Т. 8, вып. 4. –С. 669-816.

6 Зеленская Н.С., Теплов И.Б. Метод искаженных волн в реакциях со сложными частицами // ЭЧАЯ. –1979. –Т. 11, вып. 2. –С. 342-410.

7 Брагин В.Н., Буртебаев Н., Дуйсебаев А.Д., Иванов Г.Н. Роль обменных эффектов в упругом рассеянии α–частиц и ионов ^{3}He на ядрах ^{6}Li // Ядерная Физика. –1986. – Т. 44, вып. 2. – С.198-203.

8 Буртебаев Н., Дуйсебаев А., Иванов Г.Н., Сакута С.Б. Эффекты обмена тритонным кластером в неупругом рассеянии ^{3}He на ядрах ^{6}Li // Ядерная физика. –1995. – Т. 58, № 4. – С. 540-547.

9 Буртебаев Н., Дуйсебаев А., Дуйсебаев Б.А., Иванов Г.Н., Сакута С.Б. Упругое и неупругое рассеяние α–частиц на ядрах ^{6}Li и ^{7}Li при энергии 50 МэВ: роль обменных эффектов в аномальном рассеянии на большие углы // Ядерная физика. –1996. – Т. 59, № 1. – С. 29-37.

10 Burtebaev N., Burtebayeva J.T., Glushchenko N.V., Rusek K., Kliczewski S. Effects of t– and α–transfer on the spectroscopic information from the $Li^{6}(He^{3},d)Be^{7}$ reaction // Nuclear Physics A. – 2013. –Vol. 909. – P. 20-35.

11 Burtebaev N., Sakuta S.B., Burtebayeva J.T., Trzcińska A., Wolińska–Cichocka M. The channel coupling and triton cluster exchange effects in ^{3}He scattering on ^{6}Li nuclei //Acta Physica Polonica B. –2014. –Vol. 45, № 9. –P. 1853-1863.

12 Буртебаев Н., Артемов С. В., Дуйсебаев Б. А., Керимкулов Ж. К., Куранов С. Б., Сакута С. Б. Рассеяние дейтронов на ядрах ^{6}Li при энергии 25 МэВ // Ядерная физика.– 2010.– Т. 73, № 5.– С. 746-756.

13 Сакута С. Б., Буртебаев Н., Артемов С. В., Ярмухамбетов Р. Связь каналов и механизм обмена α–частичным кластером в рассеянии дейтронов на ядрах ^{6}Li // Ядерная Физика. –2012. – Т. 75, №7. – С. 840-852.

14 Bingham H.G., Zander A.R., Kemper K.W., Fletche N.R. Elastic scattering of deuterons by ^{6}Li and ^{7}Li at 8.0–12.0 MeV // Nuclear Physics A. – 1971. – V.173. – P.265-272.; Zander A.R., Kemper K.W., Fletcher N.R. Measurement and direct reaction analysis of the reactions ^{7}Li(d, t) ^{6}Li and ^{7}Li(τ, α) ^{6}Li // Nucl. Phys. A. – 1971.–Vol. 173. –P. 273.

15 Werby M.F., Edwards S. Study of Neutron and Alpha-Particle Transfer Mechanisms in the ^{7}Li(d,t)^{6}Li Reaction // Phys. Rev. –1973. –Vol. C8. – P. 978.

16 Levine S.H., Bender R.S., McCruer J.N.Angular Distributions of Deuteron-Induced Reactions in Lithium // Phys. Rev. –1955. –Vol.97. –P.1249.

17 Hamburger E.W., Cameron J.R. Study of Some Reactions of 14.8-MeV Deuterons with the Lithium Isotopes // Phys. Rev. –1960.–Vol. 117. –P. 781.

18 Gulamov I.R., Mukhamedzhanov A.M., Nie G.K. Method for selecting peripheral reactions dominated by the pole mechanism: Analysis of (d,t) reactions on 1p-shell and ^{19}F nuclei // Phys. Atom. Nucl. –1995. – Vol. 58. – P. 1689–1789.

19 Ogloblin A.A.On the mechanism of the (d,t) reaction // Nucl. Phys. –1963. – Vol. 47. – P. 408.

20 Slobodrian R.J. Stripping with 28-Mev Deuterons // Phys. Rev. –1962. – Vol.126. – P. 1059.

21 Burtebaev N., Baktibayev M.K., Duisebaev B.A., Peterson R.J., Sakuta S.B. Scattering of alfa–particles on ^{11}B nuclei at energies 40 and 50 MeV // Physics of Atomic Nuclei.–2005. –Vol. 68, № 8. – P. 1303-1367.

22 Navrátil P., Ormand. W.E. Ab initio shell model with a genuine three–nucleon force for the *p*–shell nuclei // Physical Review. – 2003. – Vol. 68. –P. 034305.

23 Nishioka H., Saito S., Yasuno M. Structure study of 2α + *t* system by the orthogonality condition model // Progress of Theoretical Physics. – 1979. – Vol. 62. – P. 424.

24 Kanada–En'yo Y. Negative parity states of ^{11}B and ^{11}C and the similarity with ^{12}C // Physical Review. – 2007. – Vol.75. – P.024302.

25 Yamada T., Funaki Y. $\alpha + \alpha + t$ cluster structures and ^{12}C(0^{+}_{2}) – analog states in ^{11}B // Physical Review. – 2010. – Vol. 82. – P. 064315.

26 Yamaguchi H., Hashimoto T., Hayakawa S., Binh D.N., Kahl D., Kubono S., Wakabayashi Y., Kawabata T., Teranishi T. α resonance structure in ^{11}B studied via resonant scattering of ^{7}Li + α // Physical Review. – 2011. –Vol. 83. – P. 034306.

27 Kawabata T., Akimune H., Fujita H., Fujita Y., Fujiwara M., Hara K., Hatanaka K., Itoh M., Kanada–En'yo Y., Kishij S., Nakanishi K., Sakaguchi H., Shimbara Y., Tamiie A., Terashima S., Uchida M., Wakasa T., Yasuda Y., Yoshida H.P., Yosoi M. $2\alpha+t$ cluster structure in ^{11}B // Physics Letters B. – 2007. – Vol. 646. – P. 6.

28 Uegaki E., Okabe S., Abe Y., Tanaka H. Structure of the excited states in ^{12}C // Progress of Theoretical Physics. – 1977. – Vol. 262. – P. 57.

29 Tohsaki A., Horiuchi H., Schuck P., Röpke G. Alpha cluster condensation in ^{12}C and ^{16}O // Physical Review Letters. – 2001. – Vol. 87. – P. 192501.

30 Kanada–En'yo Y. The structure of ground and excited states of ^{12}C // Progress of Theoretical Physics. – 2007. – Vol. 655. – P. 177.

31 Зеленская Н.С., Теплов И.Б., Ющенко Т.А. Описание обратных максимумов сечения с учетом обменных процессов // Ядерная физика. –1977. – Т. 26, вып.1. – С. 61-68.

32 Eck J.S., Thompson W.J., Eberhard K.A., Schiele J., Trombik W. Systematics of backward–angle elastic alpha scattering // Nucl. Phys. A. – 1975. – Vol.255, № 1. –P. 157–172.

33 Grotowski K. Effects of cluster structure on nuclear scattering // Radial Shape of Nuclei. – Invited Papers Proc. Intern. Conf., Cracow. –1976. –P.239-273.

34 Дмитриева Т.А., Лебедев В.М., Матусевич В.А. Исследование обратного рассеяния d,^{3}He и α–частиц на легких ядрах в предположении механизма срыва тяжелой частицы // Изв. АНСССР. –1977, сер.физ. –Т.41, № 1. –С.143-146.

35 Wit M. J. Schiele, Eberhard K. A., and Schiffer J. P.Back-angle elastic alpha scattering from ^{89}Y and ^{90,91,94} Zr // Phys. Rev. C. – 1975. – Vol. 12, № 6. –P. 1447-1451.

36 Булкин В.С., Горпинич О.К., Дубар Л.В., Немец О.Ф., Полянский В.Н., Слюсаренко Л.И., Стрюк Ю.С., Токаревский В.В. Рассеяние α-частиц с энергией 27,2 МэВ на ядрах изотопов хрома // Изв. АН, сер. физ. – 1981. – Т. 45. – С. 2163.

37 Igo G., Lorentz W., Schmidt–Rohr U. Elastic scattering of 11.8–MeV deuterons from several elements // Phys.Rev. –1961. –Vol.124, № 3. – P. 832–835.

38 Morsch H.P., Breuer H. Anomalous ^{3}He scattering in the Ca region // Nucl. Phys. –1973. –Vol. 208, № 2. –P. 255-260.

39 Cage M.E., Clough D.L.,Cole A.J., England J.B.A., Pyle G.J., Rolph P.M., Watson L.H., Worledge D.H. The elastic scattering of 32 MeV ^{3}He particles from ^{56,60,62,64}Ni, ^{63,63}Cu, ^{64,66,68}Zn // Nucl. Phys. A. –1972. –Vol. 183, № 3. – P.449-471.

40 Kondo Y., Sinobu Nagata, Shigeo Ohkubo, Osamu Tanimura. Backward, angle anomaly in alpha–nucleus scattering and parity–dependent optical model // Progr. Theor. Phys. –1975. –Vol.53. – P. 1006-1021.

41 Gaul G., Lüdecke H., Santo R., Schmeing H., Stock R. Effects of α–particle correlations in elastic α–scattering // Nucl. Phys. A. –1969. –Vol.137, № 1. –P. 177-192.

42 Taylor R.B., Fletcher N.R., Davis R.H. Elastic scattering of 4-20 MeV α–particles by ^{9}Be // Nucl. Phys. – 1965. – Vol.65, № 2. – P.318–328.

43 Денисов А.Е., Колалис Р.П., Садовский В.С., Феофилов Г.А. Рассеяние α–частиц с энергией 24 МэВ на ^{10}B и ^{11}B // ЯФ. –1976. –Т. 24, вып. 2. – С. 249-253.

44 Кузнецов Б.И., Чернов И.П., Овсянникова Р.Е. Обратное рассеяние α–частиц на ^{12}C и ^{13}C // ЯФ. –1973. –Т. 18, вып. 5. –С. 950- 953.

45 Bolta J.M. et al. Elastic scattering of.20.1–22.3 MeV α–particles by ^{14}N // Anales de Fisica Y Quimica A. –1967. –Vol. 63, № 1. –P.35-40.

46 Oeschler H., Fuchs H., Schroter H. Study of enhanced backward α–scattering of nuclei with A = 12–18 // Nucl. Phys. A. –1973. –Vol. 202, № 3. –P. 513-529.

47 Takeda M., Kato S., Yamazaki T. Elastic scattering of alpha particles by ^{20}Ne and ^{24}Mg // J. Phys. Soc. Japan. –1971. –Vol. 31, № 3. –P. 625-631.

48 Budzanowski A. Jarczyk L., Kamys B., Kapuścik A.Mechanism of α–particle scattering from ^{28}Si nuclei // Nucl. Phys. A. –1976. –Vol. 265, № 3. –P. 461- 478.

49 Антропов А.Е., Васильев С.Н., Зарубин П.Р., Орлов Б.Н. Упругое и неупругое рассеяние α–частиц на большие углы на ядрах оболочки 2s– 1d // Изв. АН СССР, сер.физ. –1974. –Vol. 38, № 10. – С. 2175-2185.

50 Bingham H.G., Zander A.R., Kemper K.W., Fletcher N.R. Elastic scattering of deuterons by ^{6}Li and ^{7}Li at 8.0–12.0 MeV // Nucl. Phys. A. –1971. –Vol. 173, № 2. –P. 265-272.

51 Матусевич В.А., Соловьев В.А., Чернов И.П. Обратное рассеяние дейтронов на легких ядрах // ЯФ. –1972. –Т. 15, вып. 4. – С. 670-672.

52 Матусевич В.А., Чернов И.П., Козырь В.В. Обратное рассеяние ^{3}He на изотопах углерода // ЯФ. –1976. –Т.23, вып. 4. –С.697-701.

53 Fortune H.F., Gray T. J., Trost W. and FletcherN. R. Elastic and inelastic scattering of ^{3}He by ^{12}C, 12.0–18.0 MeV // Phys. Rev. –1968. –Vol. 173, № 4. – P. 1002-1010.

54 Давыдов В.В., Новацкий Б.Г., Оглоблин А.А., Сакута С.Б, Степанов Д.Н., Чуев В.И. Взаимодействие ионов ^{6}Li и^{7}Li с легкими ядрами // ЯФ. –1968. – Т. 7, вып. 4. –С.758–769.

55 Bohn H., Eberhard K. A., Vandenbosch R., Bernhardt K. G., Bangert R., and ChanY.-d. Back–angle anomalies in ^{6}Li scattering from ^{40}Ca and ^{44}Ca // Phys. Rev. C. –1977. –Vol. 16, № 2. –P.665-675.

56 Fulmer G.B., Hensley D. C., Hafele J. C., Foster C. C., O'Fallon N. M., Edison W. W. and Gronemeyer S. A. Back–angle ^{3}He and α–particle elastic scattering from ^{27}A1 // Phys. Rev. C. –1976. –Vol.13, № 3. – P. 937-943.

57 Brink D., Grabowski J., Vogt E. On the anomalous large–angle scattering of α–particles // Nucl. Phys. A. –1978. –Vol. 309, № 2. –P. 559-580.

58 Delbar Th., Grégoire Gh., Paic G., Ceuleneer R., Michel F., Vanderpoorten R., Budzanowski A., Dabrowski H., Freindl L., Grotowski K., Micek S., Planeta R., Strzalkowski A. and EberhardK. A. Elastic and inelastic scattering of alpha particles from ^{40,44}Ca over a broad range of energies and angles // Phys. Rev. C. –1978. –Vol. 18, № 3. –P.1237-1248.

59 Ogloblin A.A., Glukhov Yu.A., Trzaska W.H., Dem'yanova A.S., Goncharov S.A., Julin R., Klebnikov S.V., Mutterer M., Rozhkov M.V.,Rudakov V.P., Tiorin G.P., Khoa Dao T., Satchler G.R. New measurement of the refractive elastic ^{16}O+^{12}C scattering at 132, 170, 200, 230, and 260 MeV incident energies // Phys. Rev. C. – 2000. – Vol. 62, № 4. – P.044601.

60 Nicoli M.P., Haas F., Freeman R.M., Szilner S., Basrak Z., Morsad A., Satchler G.R., Brandan M.E. Detailed study and mean field interpretation of ^{16}O+^{12}C elastic scattering at seven medium energies // Phys. Rev. C. – 2000. – Vol. 61, № 3. – P.034609.

61 Gutbrod H.H., Bock R., Von Oertzen W., Schlotthauer–Voos U.C. Elastic and inelastic scattering of ^{16}O by ^{12}C at forward and backward angles // Z. Phys. A. – 1973. – Vol. 262, № 5. – P. 377-392.

62 Ursula C., Von Oertzen W., Bock R. Optical–model analysis of the elastic scattering of complex nuclei at low energies // Nucl. Phys. A. – 1969. – Vol. 135, № 1. – P. 207-224.

63 Гриднев К. А., Родионова Е. Е., Фадеев С. Н. Анализ рассеяния $^{16}O+^{12}C$ и $^{16}O+^{16}O$ в широком диапазоне энергий // Вестник СПбГУ.– 2007. – сер. 4, вып. 4. – С. 49.

64 Hamada Sh., Burtebayev N., Gridnev K.A., Amangeldi N. Analysis of alpha–cluster transfer in $^{16}O+^{12}C$ and $^{12}C+^{16}O$ at energies near Coulomb barrier // Nucl. Phys. A.–2011.–Vol. 859. – P. 29-38.

65 Гриднев К.А., Буртебаев Н., Мальцев Н.А., Амангельды Н., Хамада Ш. Изучение реакции $^{16}O + ^{12}C$ В широком диапазоне энергий // Известия РАН, сер. физ. –2011. –Т.75, № 7. –С. 1016-1018.

66 Гриднев К. А., Родионова Е. Е. Распределение плотности α –частиц в ядре ^{16}O // Материалы международной конференции “Ядро–2008. Проблемы фундаментальной ядерной физики. Разработка ядерно–физических методов для нанотехнологий, медицинской физики и ядерной энергетики”.– М.:Наука, 2008. – С. 264.

67 Stock R., Jahnke U., Hendrie D.L., Mahoney J., Maguire C.F., Schneider W.F.W., Scott D.K., Wolschin G. Contribution of alpha cluster exchange to elastic and inelastic $^{16}O+^{20}Ne$ scattering // Physical Review C. – 1976. – Vol.14, № 5. – P. 1824-1831.

68 Kondo Y., Robson B. A., Smith R. Resonant structures in the $^{16}O+^{20}Ne$ system // Nuclear Physics A.–1983.–Vol. 410. – P. 289-316.

69 Gao C., Kondo Y., Robson B.A. Analysis of resonant structures in the $^{16}O+^{20}Ne$ system using a deep optical potential and LSNO model // Nuclear Physics A. – 1991. – Vol. 529. – P. 234-242.

70 Jarczyk L., Okołowicz J., Strzałkowski A. Large angle elastic scattering of ^{9}Be ions on carbon isotopes // Nuclear Physics A.–1979.– Vol. 316. – P. 139-145.

71 Bodek, M., Jarczyk L, Kamys B, Porebska M, Sromicki J., Strazalkowski A., Hugi M., Lang J., Muller R., Ungricht E. and BalzerD. Nuclear reactions in the $^{13}C+^{9}Be$ system at c.m. energies around 11.6 MeV // J. Phys. G: Nucl. Phys.–1980.– Vol. 6. –P. 1017-2024.

72 Barbadoro A., Segato G.F., Taffara L., Gabrielli I., Bruno M. α– transfer contribution to $^{9}Be+^{13}C$ elastic and inelastic scattering // Phys. Rev. C.–1990.–Vol. 41. –P. 2425-2428.

73 Wozniak G. J., Stahel D. P., Cerny Joseph, and Jelley N. A. (α, ^{8}Be) reaction in the 1p shell // Phys. Rev. C. –1976. –Vol. 14. –P. 815.

74 Motobayashi T., Kohno I., Ooi T., and Nakajima S. α–transfer reactions between light nuclei // Nucl.Phys. A. –1979. –Vol. 331. –P. 193.

75 Kurath D. Alpha–Structure Amplitudes for the lp Shell // Phys. Rev. C. – 1976. –Vol. 14. –P. 815.

76 Marquardt N., Hoppe W., and Siegel D. Excitation of the highly-excited rotational band in 24Mg by 10B + 14N // Phys. Rev. C. – 1977. –Vol. 16. –P. 2291.

77 Hoppe W., Klauß E., Sprengel D., Drevermann J., Isenbügel R., Buttlar H.V., Marquardt N. $^{10}B + ^{14}N$ AND $^{12}C + ^{12}C$ reaction data near molecular resonances // Lecture Notes in Physics. Resonances in Heavy Ion Reactions. –1982. –Vol. 156. – P.135-136.

78 Cormier T.M. and Fulton B.R. Structure in the excitation functions of the $^{12}C(^{12}C,^{10}B)$ and $^{12}C(^{12}C,^{11}B)$ reactions // Phys. Rev. C. –1980. –Vol. 22. – P. 565.

79 Boyarkina A.N. Structure of 1p–Shell Nuclei. –Moscow: Moscow State University, 1973. –P.150.

80 Takai H., Koide K. Bairrio A., Nuevo Jr., and Dietzsch O. α–transfer contribution to $^{10}B+^{14}N$ elastic scattering // Phys. Rev. –1988. –Vol. C 38. – P. 741.

81 Rudchik A.T. Rudchik A.T., Herashchenko O.V., Kemper K.W., Rusek K., Szczurek A.^{15}N elastic and inelastic scattering by ^{11}B at 84MeV // Nucl. Phys. A. – 2015. –Vol. 939. –P. 1.

82 Goldberg V.Z., Gridnev K.A., Hefter E.F., Novatskii B.G. Exchange effects in the scattering α–particles and deuterons by ^{6}Li // Phys.Lett. B. –1975. –Vol. 58. – P.405.

83 Bernas M., De Vries R., Harvey B.G., Hendrie D., Zisman M.S.Anomaly an α–scattering from ^{6}Li between 35 and 45 MeV // Nucl.Phys. A. – 1975. –Vol. 242. – P. 149-159.

84 Bachelier D., Bernas M., Boyard J.L., Harney H.L., Devries R.Exchange effect in the 166 MeV α–particle elastic scattering on 6Li // Nucl. Phys. A. – 1972. – Vol. 195, № 2. – P.361-368.

85 Kurdyumov I.V., Neudachin V.G., Smirnov Yu.F. Generalized conception of fractional parentage and (α–d) – (^{3}He –t) duality in the ^{6}Li nucleus // Phys. Lett. B. – 1970. –Vol. 31. – P. 426.

86 Вильдермут К., Тан Я. Единая теория ядра. – М.: Мир, 1980. –502 с.

87 Kunz P.D. Computer program DWUCK5 // University of Colorado, Boulder, Colorado , USA (unpublished).

88 Буртебаев Н., Бактыбаев М.К., Дуйсебаев Б.А., Сахиев С.К., Керимкулов Ж.К., Мукашев К.М., Исабекова Г.С. Анализ рассеяния ионов ^{3}He и α–частиц на ядрах^{7}Li, ^{9}Be и ^{11}B при энергиях 10–20 МэВ/нук // Вестник КазНПУ.им. Абая. –2007. – № 1. – С. 49-56.

89 Lovas R.G., Kruppa A.T., Beck R., Dickman F. Fragmentation properties of ^{6}Li // Nucl.Phys. A. –1987. – Vol. 474. – P. 451-456.

90 Albrecht D., Csatlos M., Ero J., Fodor Z., Végh L. Large–angle quasi–free scattering in $^{6}Li(p,pd)^{4}He$ at 670 MeV // Nucl.Phys. A. –1980. –Vol. 338. – P. 477-482.

91 Ent R., Block N.P., Van Hienen J.F.A.,van der Steenhoven G., van den Brand J.F.J., den Herder J. W. A., Jans E., Keizer P.H.M., Lapikás L., Quint E.N.M., de Witt Huberts P.K.A., Berman B.L., Briscoe W.J., Christou C.T., Lehman D.R., Norum B.E. and Saha A. Reactions $^{6}Li(e,ed)^{4}He$ and the α–d momentum distribution in the ground state of ^{6}Li // Phys.Rev.Lett. –1986. – Vol. 57. – P. 2367–2369.

92 Roos P.G., Chrant N.S., Cowley A.A., Goldberg D. A., Holmgren H. D., and WoodyR. Absolute spectroscopic factors from the (p,pα) reactions at 100 MeV at 1p–shell nuclei // Phys.Rev. C. –1977. – Vol. 15. – P.69–74.

93 Smirnov Ju.F., Chlebowska D. Reduced widths for nucleon clusters in shell model // Nucl.Phys. –1961. – Vol. 26. – P. 306-313.

94 Немец О.Ф., Неудачин В.Г., Рудчик А.Т., Смирнов Ю.Ф., Чувильский Ю.М. Нуклонные ассоциаций в атомных ядрах и ядерные реакций многонуклонных передач. –Киев, «Наукова Думка». –1988.-с.488.

95 Дмитриева Т.А., Лебедев В.М., Маркман В.Г., Спасский А.В., Теплов И.Б. Изучение механизма реакции (α,t) на ядрах ^{6,7}Li^{10,11}Ви^{13}C // Изв. АНСССР, сер.физ. –1974. –Т.38, № 12. – С. 2567-2573.

96 Jarczyk L., Kamys B., Rudy Z. Triton and Helium transfer in ^{10}B(α,^{7}Li)^{7}Be reaction at E_{lab}=91.8 MeV // Z. Physik A. –1985. –Vol. 322. –P. 221-225.

97 Abele H., Hauser H.J., Korber A., Leitner W., Neu R., Plappert H., Rohwer T., Staudt G., Welte S., Walz M., Eversheim P.D., Hinterberger F. Measurement and folding –potential analysis of the elastic α–scattering on light nuclei // Z. Physik A. – 1987. –Vol. 326. – P.373-381.

98 Зеленская Н.С., Лебедев В.М., Ющенко Т.А. Использование эйконального приближения для учета искажений в механизме срыва тяжелой частицы // ЯФ. –1978. – Т.28. – С. 90-97.

99 Ott W.R., Weller H.R. A study of ^{15}N by means of the ^{11}B(α,α)^{11}B reaction // Nucl. Phys. A. – 1972. – Vol. 198. – P. 505–514.

100 Schwinn V., Maizle G., Wagner G.J. Proton pick–up from nuclei in the middle of the 1p shell // Z. Physik A. –1975. –Vol. 275. –P. 241-247.

101 Ajzenberg–Selove F. Louritsen. Energy levels of light nuclei A = 5–10 // Nucl.Phys. A. –1974. –Vol. 227. –P. 1-7.

102 Subinit Roy, Chatterjee J.M., Majumdar H., Datta S.K., Banerjee S.R., Chintalapudi S.N. Coupled channel folding model description of α–scattering from ^{9}Be // Phys.Rev. C. –1995. –Vol. 52. – P. 1524-1531.

103 Burtebaev N., Baktybaev M.K., Duisebaev A., Duisebaev B.A., Zhurynbaeva G.S., Sakuta S.B., Peterson R.J. Coupled channel analyses of ^{3}He and α–particles scattering on the ^{6}Li, ^{7}Li, ^{9}Be, ^{10}B, ^{11}B nuclei // Conference Inter. Materials «I Eurasia conference on nuclear science». – Izmir, 2000. – P. 179-180.

104 Sing P.P., Schwandt P. and Yang G.C. Folding model analysis of elastic α–nucleus scattering // Phys. Lett. B. –1975. –Vol. 59. – P. 113–117.

105 Aspelund O., Ingham D., Djaloeis A., Kelleter H. and Mayer–Böricke C. Investigation of the quadrupole deformation of ^{11}B by means of inelastic helion scattering // Nucl. Phys. A. –1974. –Vol. 231. – P. 115-119.

106 Geoffrion B., Marty N., Morlet M., Tatischeff B. and Willis A. Diffusion élastique et inélastique des protons de 155 MeV sur^{6}Li, ^{7}Li, ^{11}B et ^{14}N// Nucl. Phys. A. –1968. –Vol. 116.–P. 209–233.

107 Burtebayev N., Kerimkulov Zh.K., Mukhamejanov Y.S., Alimov D.K., Demyanova A.S., Danilov A.N. Study of scattering of alpha particles from ^{11}B nuclei at 50 and 65 MeV // Reports of the National Academy of Sciences of the Republic of Kazakhstan. – 2016. – Vol.5, № 309. – P. 20 -25.

108 Danilov A. N., Demyanova A. S., Dmitriev S. V., Ogloblin A. A., Belyaeva T. L., Goncharov S. A., Gurov Yu. B., Maslov V. A., Sobolev Yu. G., Trzaska W., Khlebnikov S. V., Heikkinen P., Julin R., Tyurin G. P., Burtebaev N., Zholdybayev T. Study of Elastic and Inelastic ^{11}B +α Scattering and Search for Cluster States of

Enlarged Radius in ^{11}B // Physics of Atomic Nuclei. – 2015. – Vol.78, № 6. – P. 777-793.

109 Suhara T. and Kanada–En'yo Y. Cluster structures in ^{11}B // Phys. Rev. C. – 2012. – Vol.85. – P.054320.

110 Satchler G.R. Introduction to Nuclear Reactions // Oxford Univ. Press. – 1990.–P. 35.

111 Thompson I.J. and Nunes F.M. Nuclear Reactions for Astrophysics: Principles, Calculation and Applications of Low–Energy Reactions // Cambridge Univ. Press. – 2009. – P. 115.

112 Poling J.E., Norbeck E., Carlson R.R. Elastic scattering of lithium by ^{9}Be, ^{10}B, ^{12}C, ^{13}C, ^{16}O, and ^{28}Si from 4 to 63 MeV // Phys. Rev. C. – 1976. –Vol. 13. – P. 648-660.

113 Brueckner K.A. Nuclear saturation and two–body forces. II. Tensor forces // Phys. Rev. – 1954. –Vol. 96, № 2. –P. 508-516.

114 Bethe H.A. Nuclear Many–Body Problem // Phys. Rev. – 1956. –Vol. 103, № 5. –P. 1353-1390.

115 Feshbach H. Unified theory of nuclear reactions I // Ann. Phys. – 1958. – Vol. 15. –P.357-390.

116 Feshbach H. Unified theory of nuclear reactions II // Ann. Phys. – 1962. – Vol.19. – P.287-313.

117 Родионова Е.Е. Квазиклассическое и квантовое описание рассеяния ионов ^{16}O на ядрах ^{12}C и ^{16}O в широком диапазоне энергий: дис. ... канд. физ.–мат. наук:01.04.16/ –СПб., 2008. –66с.

118 Igo G. Optical–Model Analysis of Excitation Function Data and Theoretical Reaction Cross Sections for Alpha Particles // Phys. Rev. – 1959. – Vol. 115. – P.1665.

119 McFadeen L., Satchler G. R. Optical–model analysis of the scattering of 24.7 MeV alpha particles // Nucl. Phys. – 1966. –Vol.84. –P.177.

120 Mohr P. α–nucleus potentials for the neutron–deficient p nuclei // Phys. Rev. C. – 2000. –Vol. 61. – P.045802.

121 Brown G.E. and Rho M. The giant Gamow–Teller resonance // Nucl. Phys. A. – 1981. –Vol.372. – P.397.

122 Khoa Dao T., Satchler G.R., von Oertzen W. Nuclear incompressibility and density dependent NN interactions in the folding model for nucleus–nucleus potentials // Phys. Rev. C. – 1997. –Vol. 56. – P. 954-969.

123 Ring P., Schuck P. The nuclear many body problem. –Springer, 2004. –P. 85.

124 Rowe D.J. Nuclear collective motion: models and theory. – Methuen, 1970. –P. 49.

125 Skyrme T. H. R. The effective nuclear potential // Nucl. Phys. – 1959. –Vol. 9, № 4. –P. 615-634.

126 Yukawa H. On the interaction of elementary particles // Proc. Phys. Math. Soc. Japan. – 1935. –Vol. 17. –P. 48.

127 Khoa D T., von Oertzen W. and Ogloblin A.A. Study of the equation of state for asymmetric nuclear matter and interaction potential between neutron–rich nuclei using the density–dependent M3Y interaction // Nuclear Physics A. – 1996. – Vol. 602. –P.98-132.

128 Satchler G.R. and Love W.G. Folding model potentials from realistic interactions for heavy–ion scattering // Phys. Rep. – 1979. –Vol. 55. –P.183–254.

129 Bethe H. A. Theory of nuclear matter // Ann. Rev. Nucl. Sci.– 1971. –Vol. 21. – P. 93-244.

130 Thompson I.J. Fresco 2.0. – England: Department of physics, University of Surrey, 2006. – P.177.

131 Ньютон Р. Теория рассеяния волн и частиц. – М.: Мир, 1969. – 607 с.

132 Miller W. WKB Solution of Inversion Problems for Potential Scattering // J. of Chem. Phys. – 1969. –Vol. 51. –P. 3631.

133 Nicoli M. P. Phenomenes resonnants et refractifs dans certaines collisions entre ions lourds legers: thesis … doctor of physics / Universite Louis Pasteur. – Strasbourg, 1998. –P. 189.

134 Brandan M. E., McVoyK. W. Rainbow–shift mechanism behind discrete optical–potential ambiguities // Phys. Rev. C. – 1991. –Vol. 43. –P.1140.

135 Brandan M. E., Satchler G. R. Optical potential ambiguities and $^{16}O+^{16}O$ at 350 MeV // Phys. Lett. B. – 1991. –Vol. 256. – P. 311.

136 Knoll J., Schaeffer R. Semiclassical scattering theory with complex trajectories // Ann. Phys. – 1976. –Vol. 97. –P. 307.

137 Арзуманов А. А., Анисимов О.К., Баталин С.С., Волков Б.А., Громов Д.Д., Кравченко Е.Т. Изохронный циклотрон с регулируемой энергией ионов // Известия АН КазССР, сер. физ.-мат. – 1973. –Т.4. – С. 6–15.

138 Исследование структуры легких и средних ядер при больших энергиях возбуждения и механизма ядерных реакций с легкими частицами: отчет о НИР / ИЯФ АН КазССР: рук. Дуйсебаев А.; исполн.: Буртебаев Н., Иванов Г.Н., Канашевич В.И., Кэбин Э.И., Личман В.А., Нечаев Ю.И., Хаймин В.А., Сухаревский В.Г. – Алма-ата, 1980. – 125 с.

139 Гончар В.Ю., Желтоног К.С., Иванов Г.Н., Рыбин С.Н. Прибор для измерения и контроля энергии частиц, ускоренных в циклотроне // Приборы и техника эксперимента. – 1970. –Т.5. –С.30-33.

140 Артемов С.В., Бажажин А.Г., Бактыбаев М.К., Буртебаев Н., Дуйсебаев А., Дуйсебаев Б.А., Зарифов Р.А., Кадыржанов К.К., Караходжаев А.А., Сахиев С.К., Сатпаев Н.К., Саргаскаев А.М., Сейтимбетов А.М. Камера рассеяния для измерения сечений ядерных реакций в предельно малых углах на выведенном пучке изохронного циклотрона У–150М // Известия НАН РК, сер. физ.-мат. – 2006. –Т.6. –С.61-64.

141 Дуйсебаев А.Д., Иванов Г.Н., Рыбин С.Н., Бергер В.Д., Арзуманова З.М., Канашевич В.И., Буртебаев Н.Т. Камера рассеяния для исследования продуктов ядерных реакций на пучке циклотрона // Известия АН Каз. ССР, сер. физ.-мат. – 1983. –Т.2. –С.80-81.

142 Артемов С.В. и др. Измерительно–вычислительный комплекс для исследования ядерных реакций // Приборы и техника эксперимента. – 1996. – Т.1. – С.44-48.

143 Буртебаев Н.Т., Дуйсебаев А.Д., Виноградов А.А., Вонгай А.Д., Акурашов А.А., Манзуров И.Б., Пармонов В.В., Сакута С.Б., Чуев В.И. и др. Система многомерного анализа для исследования ядерных реакций на циклотроне ИЯФ АН КазССР // Известия АН КазССР, сер. физ.-мат. – 1975. – Т.2. – С.65-68.

144 Мишель Ж., Лоржо К., Эспью Б. Программируемые контролеры – пер. с французского. — М.: Машиностроение, 1986. – 187с.

145 Кондратьев Н.А., Адодин В.В., Иванов Г.Н. Интегратор тока на базе прибора Ф–30 // Известия АН КазССР, сер. физ.-мат. – 1986. –Т.4. – С.89-90.

146 Павлов А.Ф., Иванов Г.Н., Канашевич В.И., Мульгин С.И. Интегратор тока // Известия АН КазССР, сер. физ.-мат. – 1985. –Т. 2. – С.88-89.

147 Lise++. http://lise.nscl.msu.edu/lise.html 01.02.2019.

148 Chernykh S.V., Chernykh A.V., Didenko S.I., Baryshnikov F.M., Burtebayev N., Britvich G.I., Chubenko A.P., Guly V.G., Glybin Yu.N., Zholdybayev T.K., Burtebayeva J.T., Nassurlla M., et al. GaAs detectors with an ultra–thin Schottky contact for spectrometry of charged particles // Nuclear Instruments and Methods in Physics Research Section A: Accelerators, Spectrometers, Detectors and Associated Equipment. – 2017. – Vol. 845. – P. 52-55.

149 Пат. Российская Федерация №178710 от 17.04.2018 - Полупроводниковый детектор с внутренним усилением / Черных С.В., Черных А.В., Диденко С.И., Барышников Ф.М., Буртебаев Н, Буртебаева Д., Насурлла М.; заявитель и правообладатель Москва: Нац. Исслед. Технолог. Университет МиСИС. – № 2017146335; заявл. 27.12.2017; опубл. 17.04.2018, Бюл. № 11. – 6 с.

150 Koltsov G.I.,Didenko S. I., Chernykh A. V., Chernykh S. V., Chubenko A. P., Sveshnikov Yu. N. Schottky Contacts to High–Resistivity Epitaxial GaAs Layers for Detectors of Particles and X– or γ–Ray Photons // Semiconductors. – 2012. Vol. 46, № 8. P. 1066-1071.

151 Didenko S.I., Koltsov G.I., Chernykh A.V., Chernykh S.V., Chubenko A.P., Burtebayev N., Burtebayeva J.T., Sakhiev S.K., Morzobayev A.K., Mussaev J.M. Schottky Barriers at Undoped Epitaxial GaAs Films Used For Nuclear Radiation Detectors // Book of Abstracts. International Conference Nuclear Science and its Application. – Tashkent, 2012.– P. 171-172.

152 Chernykh A.V., Chernykh S.V., Didenko S.I., Burtebayev N., Nasurlla Maulen; Nasurlla Marzhan, Britvich G.I., Chubenko A.P., Baryshnikov F.M., Sleptsov E.V. GaAs Schottky Barrier Detectors for Alpha–Particle Spectrometry at Temperatures up to 120° C // Technical Physics Letters. – 2018. – Vol. 44, № 10. – P.942-945.

153 Bespalov V.A.,Vorontsov A. V., Gorbatsevich A. A., Egorkin V. I., Zhigal'skii G. P., Il'ichev É. A., Kulakov A. V., Nalbandov B. G., Pantuev V. S., Rasputnyi V. N., Sveshnikov Yu. N., Shmelev S. S. Electrophysical properties of

GaAs layers and the characteristics of fast particle GaAs detectors // Technical Physics. – 2004. Vol. 49, № 3. – P. 310.

154 Мульгин С.И., Околович В.Н., Русанов А.Я., Суботин М.И. Методика изготовления спектрометрических мишеней из тугоплавких веществ для ядерно–физических исследований // Препринт ИЯФ АН КазССР. – 1985. – №7. – С. 37-38.

155 Zazulin D.M., Burtebayev N., Peterson R.J., Artemov S.V., Igamov S., Kerimkulov Zh.K., Alimov D.K., Mukhamejanov E.S., Maulen Nassurlla, Sabidolda A., Marzhan Nassurlla, Khojayev R. New results for the p-12C radiative capture at low energies // News of the NAS of the RK. Phys.-math. Ser. –2019. – Vol. 4, № 326. –P. 5-13.

156 Burtebayev N., Burminsky V.P., Berger V.D., Dzhazairov-Kakhramanov V.et. al. Universal experimental facility for investigation in the field of radiation physics of solids and physics of atomic nucleus // Presentation of 1. Eurasia conference on nuclear science and its application. – 2000. –P.791–795.

157 Lyons P.B., Toevs J.W., Sargood D.G. Total yield measurements in $^{27}Al(p,\gamma)^{28}Si$ // Nuclear Physics A. – 1969. –Vol. 130. –P. 1-24.

158 Bulter J.W. Table of (p,γ) resonances by proton energy: E = 0.163 – 3.0 MeV // U.S. Naval Research Laboratory. NRL Report. – 1959. –P.5282-5299.

159 Немец О.Ф., Гофман Ю.В. Справочник по ядерной физике. — Киев: Наукова думка, 1975. –416 с.

160 Сакута С.Б., Артемов С.В., Буртебаев Н., Керимкулов Ж.К., Новацкий Б.Г., Степанов Д.Н., Ярмухамедов Р. Роль связи каналов и механизмов с обменом дейтроном в аномальном рассеянии α-частиц на ^{6}Li // Ядерная физика. – 2009. – Т.72, №12. – С. 2046-2055.

161 Goldberg D.A. and Smith S.M., Burdzik G.F. Refractive behavior in intermediate-energy alpha scattering // Phys. Rev. C. –1974. –Vol. 10. –P.1362.

162 Sakuta S.B., Burtebayev N., Burtebayeva D.T., Duisebayev A., Glushchenko N.V., NassurllaM., AmarA., Artemov S.V., Kliczewski S., Piasecki E., Rusek K., Siudak R., Trzcińska A., Wolińska-Cichocka M. The channel coupling and triton cluster exchange effecs in scattering of ^{3}He ions on ^{6}Li nuclei // Acta Physica Polonica B. –2014.–Vol. 45, № 9. –P. 1853-1863.

163 Vereshchagin A.N., Korostova I.N., Sokolov L.S., Tokarevskii V.V., Chernov I.P. Investigation of elastic scattering of deuterons on light nuclei with 13.6 MeV energy // Bull. Russian Academy of Sciences, Physics. – 1969. – Vol.32. – P.573.

164 Matsuki S., Yamashita S., Fukunaga K., Nguyen D.C., Fujiwara N., Yanabu T. Elastic and inelastic scattering of 14.7 MeV deuterons and of 29.4 MeV alpha-particles by ^{6}Li and ^{7}Li // Jap. Phys. Soc. of Jpn. – 1969. – Vol.26.–P.1344-1353.

165 Goldberg D.A. and Smith S.M. Criteria for the Elimination of Discrete Ambiguities in Nuclear Optical Potentials // Phys.Rev.Lett. – 1972. –Vol.29, № 8. – P. 500-504.

166 Abramovich S.N., Guzjovskii B.Ya., Dzyuba B.M., Zvenigorods A.G., Trusillo S.V., Sleptsov G.N. Elastic Scattering of Deuterons by Lithium Isotopes // Izv.Akad.Nauk SSSR, Ser.Fiz. —1976.— Vol.40. — P. 842.

167 Burtebayev N.; Burtebayeva J.T., Duisebayev A., Kerimkulov Z.K., Nassurlla M., Zholdybayev T., Artemov S.V., Karakhodzhayev A.A.,Salikhbayev U.S., Sakuta S.B., Kliczewski S., Piasecki E., Rusek K., Siudak R., Trzcinska A., Wolinska-Cichocka M., Amar A. Mechanism of the Li-7(d,t)Li-6 reaction at 25 MeV energy of deuterons, values of spectroscopic factors and asymptotic normalization coefficients for the Li-7 -> Li-6 + n vertex // Acta Physica Polonica B. –2015.–Vol. 46, № 5. – P.1037-1054.

168 Daehnick W.W. J. D. Childs, and Z. Vrcelj Global optical model potential for elastic deuteron scattering from 12 to 90 MeV // Phys.Rev. C. – 1980. – Vol. 21. – P.2253.

169 Burtebayev N., Nassurlla Marzhan, Nassurlla Maulen, Kerimkulov Zh. K. and Sakuta S. B. Optical Model Potential Parameters for p, d, ^{3}He and Alpha-Particle Scattering on Lithium Nuclei // AIP Conference Proceedings. –2008. – Vol. 1072. – P. 203-208.

170 Burtebayev N., Burtebayeva J.T., Glushchenko N.V., Kerimkulov Zh.K., Amar A., Nassurlla M., Sakuta S.B., Artemov S.V., Igamov S.B., Karakhodzhaev A.A., Rusek K., Kliczewski S. Effects of *t*- and α-transfer on the spectroscopic information from the Li6(He3,d)Be7 reaction // Nucl. Phys. A. –2013. –Vol. 909. – P. 20.

171 Abramovich S.N., Guzhovsky B.Ya., Zherebtsov B.A., Zvenigorodsky A.G. // Yaderno-fisicheskie Konstanty Termoyadernogo Sinteza.– M.: TSNI Iatominform, 1989. – P.271.

172 Basak A.K., Karban O., Roman S., Morrison G.C., Nelson J.M.Scattering and charge-exchange reactions with polarized ^{3}He on lithium isotopes // Nucl. Phys. A.–1981. –Vol. 368. – P. 74-92.

173 Cohen S., Kurath D. Spectroscopic factors for the 1p shell //Nucl. Phys. A. –1967. –Vol. 101. –P. 1-16.

174 Mukhamedzhanov A.M., Clark H.L., Gagliardi C.A., LuiY.-W., Trache L., Tribble R.E., Xu H.M., Zhou X.G., Burjan V., Cejpek J., Kroha V., Carstoiu F. Asymptotic normalization coefficients for $^{10}B\rightarrow{}^{9}Be+p$ // Phys.Rev. C. –1997. –Vol. 56. –P. 1302.

175 Artemov S.V., Bajajin A.G., Igamov S.B., Nie G.K., Yarmukhamedov R. Асимптотические нормировочные коэффициенты ядра для конф-и $^{14}N\rightarrow C+p$ и астрофизический S-фактор радиационного захвата протона // Phys. Atomic Nuclei. –2008. –Vol. 71. –P. 998 – 1025.

176 Blokhintsev L.D., Borbely I., Dolinskii E.I. Ядерные вершинные константы // Fiz. Elem. Chastits i At. Yadra. –1977. –Vol.8. – P.485 – 1189.

177 Artemov, S.V., Zaparov E.A., Nie G.K. Асимптотические нормировочные коэффициенты для легких ядер из реакции передачи протона // Izv. RAN, ser.fiz.–2003. –Vol.67. –P.1577 // Bull. Rus. Acad. Sci. Phys. –2003. – Vol.67.–P. 1741.

178 Tsang M.B., Lee J. and Lynch W.G.Survey of Ground State Neutron Spectroscopic Factors from Li to Cr Isotopes // Phys. Rev. Lett. –2005. –Vol.95. – P. 22501.

179 Titus L.J., Capel P., Nunes F.M. Asymptotic normalization of mirror states and the effect of couplings // Phys. Rev. C. –2011. – Vol. 84. – P. 035805.

180 G.K. Nie, S.V. Artemov. Нейтронный и протонный асимптотический коэффициент симметричных и зеркальных ядер. // Bull. Rus. Acad. of Sci., Physics. –2007. –Vol.71. – P.1762–1805.

181 Fitz W., Jahir R., Santo R. Scattering and pick-up reactions with deuterons on Be, B, C, N and O at 11.8 MeV // Nucl. Phys. A. –1967. – Vol. 101. – P. 449.

182 Burtebayev N., Sakuta S.B., Nassurla Marzhan, Saduev N., Nassurlla Maulen, Sadykov T.Kh., Trzcińska A., Wolińska-Cichocka M., Khojayev R. Mechanism of the $^{11}B(\alpha,t)^{12}C$ reaction at an energy of 40 MeV, role of exchange processes and collective excitations // Eur. Phys.Jorn. A. –2019. –Vol. 55. –P. 38.

183 Tilley D.R., Kelley J.H., Godwin J.L., Millener D.J., Purcell J., Sheu C.G. and Weller H.R.Energy levels of light nuclei A=8, 9, 10 // Nuclear Physics A. –2004. –Vol. 745. –P. 155–362.

184 Perey F. SPI-GENOA. An optical model search code (unpublished).

185 Shahabuddin M.A.M., Webb C.J., and Edwards V.R.W.Elastic and inelastic scattering of 17.5 and 40.0 MeV ^{3}He particles from ^{11}B // Nucl. Phys. A. –1977. – Vol. 284. – P. 83-92.

186 Cavaignac F., Jang S., Worledge D.H.Study of $^{11}B(p, p')$ in a core-hole coupling scheme // Nucl. Phys. A. –1975. –Vol. 243. – P.349.

187 Burtebayev N., Nassurlla Maulen, Nassurlla Marzhan, Saduyev N., Sabidolda A., Zazulin D., Sadykov T.Kh., Sakuta S.B., Trzcińska A., Wolińska-Cichocka M.Scattering of α-particles by ^{11}B nuclei at an energy of 40MeV and role of the exchange mechanism with transfer of ^{7}Li // Int. Journal of Modern Physics E. – 2018. –Vol. 27. –P.1850094.

188 Kelley J.H., Kwan E., Purcell J.E., Sheu C.G. and Weller H.R. Energy levels of light nuclei A=11 // Nuclear Physics A. –2012. –Vol. 880. –P. 88.

189 Siemssen R.H., Dehnhard D. Possible Spin Dependence of Direct Reactions on Light Nuclei // Phys.Rev.Lett. –1967. –Vol. 19. – P. 377.

190 Васильева О.И., Гуревич Г.С., Игнатенко А.В., Лебедев В.М., Орлова Н. В., Спасский А.В., Теплов И.Б., Шахворостова Г.В., Шестакова И.К. Угловая зависимость плотности состояния 2+; 4,43 МэВ ядра ^{12}C в реакции $^{10}B(\alpha,d\gamma)^{12}C$ и $^{11}B(\alpha,t\gamma)$ ^{12}C при E_α =30МэВ // Ядерная физика. –1989. –Vol.49. – P. 625.

191 Васильева О.И., Лебедев В.М., Орлова Н. В., Спасский А.В., Теплов И.Б., Фатеева Л.Н., Шахворостова Г.В., Эль-Камхави А.Х. Восстановление спин тензоров матрицы плотности состояния 2^{+}; 4,43 МэВ ядра ^{12}C в реакциях $^{10}B(\alpha, d\alpha)^{12}C$ и ^{11}B $(\alpha, t\gamma)^{12}C$ при E_α=30 МэВ // Изв. АН СССР, сер.физ. –1987. – Vol.51. –P. 88.

192 Васильева О.И., Лебедев В.М., Спасский А.В., Теплов И.Б., Фатеева Л.Н. Исследование реакции (α, d) и (α, t) на ядрах $^{10,11}B$ при E_α=30 МэВ // Изв. АН СССР, сер.физ. –1983. –Vol. 47. – P. 2248.

193 Ignatenko A. V., Lebedev V. M., Spasskii A. V. Energy-dependence of the angular-correlation functions in the reactions ^{10}B(alpha, d-gamma)^{12}C and ^{11}B(alpha,t-gamma)^{12}C in the region Eα = 21-25 MeV // Yad.Fiz. – 1988. – Vol. 48, №. 4. – P. 592–595.

194 Galanina L.I.,Zelenskaya N.S. Effect of spin-orbit interaction on the features of intermediate-energy nuclear reaction involving moderately heavy ions // Phys.Atomic Nuclei. – 1998. – Vol.61. – P.2077–2084.

195 Балашова О.Ю., Зеленская Н.С., Овчинникова А.А. Dynamic deformation of C-12 in reactions induced by alpha-particles // Ядерная физика. – 1991. –Vol.53, № 2. –P. 243-248.

196 Cavaignac J.F., Jang S., Worledge D.H. Study of ^{11}B(p,p′) in a core-hole coupling scheme // Nucl. Phys. A. –1975. –Vol. 243. –P. 349.

197 Keaton P.W., D.D. Armstrong, L.R. Veeser, H.T. Fortune, N.R. RobersonCross-section and polarization measurements for the^{12}C(t,p)^{14}C reaction // Nucl. Phys. A. –1972. – Vol. 179. – P.561-568.

198 Fujisawa T., et al., Yamaji S., Matsuda K., Motonaga Sh., Yoshida F., Sakaguchi H., and Masu K.The Elastic and Inelastic Scatterings of 3He from 12C at 24.0, 29.2, 34.7 and 39.6 MeV // Phys. Soc. Japan. –1973. –Vol.34. – P. 5.

199 Singh N., R.N. Singh, N. De Takacsy, S.I. Hayakawa, R.L. Hutson, J.J. KraushaarMulti-step processes in the ^{12}C(^{3}He, α)^{11}C reaction // Nucl. Phys. A. –1973. –Vol. 205. – P.97-120.

200 Hutson R.L., R.L. Hutson, S. Hayakawa, M. Chabre, J.J. Kraushaar, E.T. BoschitzPolarization of^{3}He elastically scattered by^{12}C and the ^{3}He spin-orbit optical potential // Phys. Lett. B. –1968. – Vol.27. –P.153-155.

201 A.J. Buffa, M.K. BrusselElastic scattering of^{3}He from^{9}Be,^{10}B,^{11}B,^{24}Mg,^{25}Mg,^{26}Mg and^{27}Al // Nucl. Phys. A. – 1972. – Vol. 195. – P.545-558.

202 Dunnill F., Gray T.J., Fortune H.T., Fletcher H.P.Optical parameters for the elastic scattering of ^{3}He by ^{4}He // Nucl. Phys. A. –1967. –Vol. 93. –P. 201-208.

203 Kelley J.H., Purcell J.E. and Sheu C.G. Energy levels of light nuclei A = 12 // Nucl. Phys. A. –2017. – Vol. 968. –P. 71.

204 Балашова О.Ю., Богданова Н.А., Зеленская Н.С., Овчинникова А.А., Теплов И.Б. The role of linear mechanisms and the nuclear-component mechanism in the reaction B-11(alpha-t1)C-12 // Bull. Russian Academy of Sciences, Physics. – 1990. – Vol.54, №8. – P.1649-1654.

205 Burtebayev N.,Kerimkulov Zh.,Bakhtybayev M.,Hamada Sh., Mukhamejanov Y.S., Nassurlla M., Alimov D.,Morzabayev A., Janseitov D.M., Trzaska W. Investigation of the elastic and inelastic scattering of ^{4}He from ^{11}Be in the energy range 29–50.5 MeV // Nuclear Physics and Astrophysics Conference. IOP Conf.Series: – Journal of Physics: Conf.Series. – 2018. – Vol.940. – P.012034.

206 N. Burtebayev, Zh.K. Kerimkulov, Maulen Nassurlla, J.T. Burtebayeva, Marzhan Nassurlla, S.B. Sakuta, T. Suzuki, K. Rusek, A. Trzcińska, M. Wolińska-Cichockae Study of the ^{7}Li (d, t)^{6}Li reaction at the energy of 14.5 MeV // Acta Physica Polonica B. – 2019. – Vol.50, № 3. – P.703-709.

207 Chernykh A.V., Chernykh S.V., Baryshnikov F.M., Didenko S.I., Burtebayev N., Britvich G.I., Kostin M.Yu., Chubenko A.P, Nassurlla Marzhan, Nassurlla Maulen, Kerimkulov Zh., Zholdybayev T., Glybin Yu.N. and Sadykov T.Kh Characterization and simulation of fast neutron detectors based on surface-barrier VPE GaAs structures with polyethylene converter // Journal of Instrumentation. – 2016. – Vol.11. – P.C12005.

208 Nassurlla Maulen, Burtebayev N., Mukhashev K.M., Nassurlla Marzhan, Khojayev R.A. Temperature dependence of the energy resolution of a gallium arsenide detector // Bulletin of KazNU, Recent Contributions to Physics. –2018. – Vol.67, № 4. – P.85-92.

209 Nassurlla Maulen, Burtebayev N., Kerimkulov Zh.K., Suzuki T., Sakuta S.B., Nassurlla Marzhan, Khojayev R. Investigation of deuteron scattering on ^{7}Li nuclei at energy of 14.5 MeV // News of The NAS of RK series physico-mathematical. –2018. –Vol.6, № 3. – P.15-22.

210 Burtebayev N., Kerimkulov Zh.K., Nassurlla Maulen, Burtebayeva J.T., Nassurlla Marzhan, Sakuta S.B.,Suzuki T., Artemov S.V., Ergashev F., Karakhozhaev A.A., Rusek K., Trzcińska A., Wolińska-Cichockae M. Study of the ^{7}Li(d, t)^{6}Li reaction at the energy of 14.5 MeV // Book of abstract Zakopane Conference of Nuclear Physics, "Extremes of the Nuclear Landscape". – Zakopane, 2018. –P.170.

211 Chernykh S.V., Chernykh A.V., Baryshnikov F.M., Burtebayev N., Britvich G.I., Kostin M.Yu., Chubenko A.P., Nassurlla Marzhan, Nassurlla Maulen, Kerimkulov Zh., Zholdybayev T., Glybin Yu.N., Sadykov T.Kh., Kazakova Yu.V.Didenko S.I. Self-biased fast neutron detector based on VPE GaAs surface-barrier sensor with polyethylene converter // Book of Abstracts of 19 th International Workshop on Radiation Imaging Detectors iWoRID. – Krakov, 2017. – P.76.

212 Burtebayev N., Nassurlla Maulen, Kerimkulov Zh.K., Burtebayeva D.T., Mukhamedzhanov E.S., Nassurlla Marzhan, Suzuki T., Sakuta S.B. Study of the deuteron scattering on ^{7}Li nuclei // DREB2018 - 10th International Conference on Direct Reactions with Exotic Beams. – Matsue, 2018. – P.18.

213 Burtebayev N., Burtebayeva J.T., Kerimkulov Zh.K., Mukhamedzhanov E.S., Nassurlla Marzhan, Nassurlla Maulen, Zholdybayev T.K., Alimov D.K., Suzuki T., Sakuta S.B. Study of the deuteron scattering on ^{11}B nuclei // XXXVI Mazurian Lakes Conference on Physics». – Piaski, 2017. – P.218.

214 Насурлла Маулен, Буртебаев Н., Сакута С.Б., Керимкулов Ж.К., Буртебаева Д.Т., Алимов Д.К., Мухамеджанов Е.С., Насурлла Маржан, Сабидолда А., Ходжаев Р. Исследование реакции (d,t) на ядрах ^{11}B при энергии 14,5 МэВ // II Международный научный форум «Ядерная наука и технологии». – Алматы, 2019. – С.43.

215 Burtebayev N., Nassurlla Maulen, Nassurlla Marzhan, Saduyev N., Sabidolda A., Zazulin D., Sakuta S.B., Trzcińska A., Wolińska-CichockaM. Рассеяние α-частиц на ядрах ^{11}B при энергии 40 МэВ и роль обменного механизма с передачей ^{7}Li // II Международный научный форум «Ядерная наука и технологии». – Алматы, 2019. – С.50-51.

216 Alimov D.K., Burtebayev N., Nassurlla Marzhan, Nassurlla Maulen, Burtebayeva J. Study of the V-W-Ambiguity when Choosing the Optical Potentials from Scattering of α-Particles on ^{10}B and ^{11}B Nuclei // Book of Abstracts of the Ninth International Conference «Modern Problems of Nuclear Physics and Nuclear Technologies". – Tashkent, 2019. – P. 56.

217 Burtebayev N., Nassurlla Maulen, Nassurlla Marzhan, Saduyev N., Sabidolda A., Zazulin D., Sakuta S.B., Trzcińska A., Wolińska-Cichocka M. Scattering of α-Particles by ^{11}B Nuclei and Role of the Exchange Mechanism with Transfer of Heavy Particle // Book of Abstracts of the Ninth International Conference «Modern Problems of Nuclear Physics and Nuclear Technologies". – Tashkent, 2019. – P. 58.